AMERICAN UNIVERSITY OF BEIRUT

A FREQUENCY AGILE TRANSMITTER DESIGN FOR COGNITIVE RADIO APPLICATIONS IN THE TV BAND

by
MOHAMAD YOUSSEF ABOU SHAHINE

A dissertation
submitted in partial fulfillment of the requirements
for the degree of Doctor of Philosophy
to the Department of Electrical and Computer Engineering
of the Faculty of Engineering and Architecture
at the American University of Beirut

Beirut, Lebanon
December 2015

AMERICAN UNIVERSITY OF BEIRUT

A FREQUENCY AGILE TRANSMITTER DESIGN FOR
COGNITIVE RADIO APPLICATIONS IN THE TV BAND

by
MOHAMAD YOUSSEF ABOU SHAHINE

Approved by:

_____

Dr. Ali Chehab, Professor   Chairman of Committee
Electrical and Computer Engineering

_____
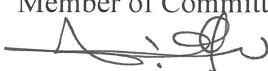
Dr. Karim Kabalan, Chairperson   Advisor
Electrical and Computer Engineering

_____

Dr. Joseph Costantine, Assistant Professor   Member of Committee
Electrical and Computer Engineering

_____

Dr. Youssef Nasser, Senior Lecturer   Member of Committee
Electrical and Computer Engineering

_____

Dr. Mohamad Rammal, Professor   Member of Committee
Lebanese University

iii

Dr. Christos G. Christodoulou, Professor   Member of Committee
University of New Mexico, Albuquerque, NM, USA

Dr. Mohammed Husseini, Research Scientist   Member of Committee
Beirut Research and Innovation Center

Dr. Ali Ramadan, Assistant Professor   Member of Committee
Fahd Bin Sultan University

Date of thesis defense: [December 10, 2015]

iv

AMERICAN UNIVERSITY OF BEIRUT

DISSERTATION RELEASE FORM

Student Name: Abou Shahine, Mohamad Youssef

◯ Master's Thesis   ◯ Master's Project   ⊗ Doctoral Dissertation

☒   I authorize the American University of Beirut to: (a) reproduce hard or electronic copies of my thesis, dissertation, or project; (b) include such copies in the archives and digital repositories of the University; and (c) make freely available such copies to third parties for research or educational purposes.

☐   I authorize the American University of Beirut, **three years after the date of submitting my thesis, dissertation, or project,** to: (a) reproduce hard or electronic copies of it; (b) include such copies in the archives and digital repositories of the University; and (c) make freely available such copies to third parties for research or educational purposes.

_____   Feb 4, 2016

Signature   Date

ACKNOWLEDGMENTS

AN ABSTRACT OF THE DISSERTATION OF

Mohamad Youssef Abou Shahine for   Doctor of Philosophy
                                     Major: Electrical and Computer Engineering

Title: A Frequency Agile Transmitter Design for Cognitive Radio Applications in the
       TV Band

With the growth of mobile data applications and the development of communication systems, the spectrum is becoming very scarce. To ease congestion and boost speeds, cognitive radio (CR) is currently seen as a major solution. It is expected to be the key player in the new wireless technologies. It is one of the most capable techniques to efficiently utilize the spectrum and intelligently share the wireless resources. In a CR network, unlicensed users (secondary users) are allowed to access spectrum bands licensed to primary users, while avoiding interference with them. One of the main motivating factors attributing to the growth of work in CR is the current worldwide digital transition of the TV broadcasting band which resulted in abundant of vacant spectrum. TV white spaces (TVWS) refer to these unused portions of the spectrum in the TV band. These unused TV white spaces are an attractive target for cognitive radio applications, since they operate at an easy to use frequency, and have good propagation characteristics, improved communication quality, better building penetration, and lower energy consumption.

A radio front-end transmitter is a complete system used to transmit radio signals on a certain carrier frequency. In cognitive radio, there is an important need for reconfigurable Radio Frequency (RF) front end transmitter that can be set to steer to any band and tune to a channel of any bandwidth. The main challenge in building this transmitter is the ability in designing linear and spectrally-agile components and architectures. This is because cognitive radio transmitters are required to operate in any unoccupied channel of the frequency range.

In this dissertation, an RF front-end design for frequency-agile transmitter for cognitive radio system applications in the TV band is investigated. The transmitting antenna and the broadband power amplifier are completely examined, in order to come up with developed designs suitable for several cognitive radio applications in the TV band. Concerning the transmitting antenna design, different techniques employed in designing antennas for cognitive radio application in the TV band are studied. Three antenna designs with reduced dimensions and compact size suitable for cognitive radio applications in the TV band are designed. Two printed microstrip reduced-size monopole antennas and one Planar Inverted F Antenna (PIFA) are proposed. These

antennas operate in the upper part of the UHF band with approximately 2.5 dB transmission gains and omnidirectional patterns. A novel design of a reconfigurable compact planar spiral monopole antenna suitable for TVWS applications is also designed. Frequency reconfigurability is reached by inserting a tunable inductor on the spiral monopole and modifying its inductance. The antenna can operate at different bands in UHF range. These bands range between 15 to 20 MHz which is suitable for TVWS applications. In the design of the power amplifier, several techniques and different classes are surveyed. However, to come with the most efficient design with a respectable output power and a linear operation in the TV band, a high efficiency Doherty power amplifier is designed. A class AB power amplifier is firstly implemented, and then the Doherty amplifier has been designed following the previous class AB scheme for the main amplifier and a class C scheme for the peak one. This amplifier attains a high efficiency with a proper power and an operating frequency bandwidth between 550 and 1000 MHz which make it suitable for TV band applications. The other components will be investigated in future in order to finalize a cognitive radio tunable transmitter design suitable for communicating in the TV white spaces and can be used by different cognitive radio applications in the TV band.

CONTENTS

Chapter

Appendix

ILLUSTRATIONS

Figure

xiv

TABLES

Table

CHAPTER 1

INTRODUCTION AND THESIS OBJECTIVES

1.1 Introduction

The development of communication systems and the need for higher data rates have led to the scarcity of the radio frequency (RF) spectrum. This is due to the static frequency allocation which has caused a large portion of the spectrum to be underutilized. The current approach for spectrum allocation is based on assigning a specific band to a particular service. This is displayed in the Federal Communication Committee (FCC) frequency allocation chart shown in Fig. 1.1, where it indicates a high degree of system spectrum utilization [1].

With the increasing demand for efficient operation of radio frequency devices with limited resources, such as energy and frequency spectrum, cognitive radio [2-4] is thought to be a drastic solution. Cognitive radio (CR) is one of the most promising techniques to efficiently utilize the spectrum and intelligently improve communication efficiency. In a CR network, unlicensed users (secondary users) are allowed to access spectrum bands licensed to primary users, while avoiding interference with them. This intelligent radio permits the secondary user to sense the spectrum, identify the free portions or the ones with reduced primary activity, and transmit on the best available channel. On the other hand, if the primary user restarted transmission, the secondary user jumps off into a different band, or alters its transmission power level or modulation

scheme, while staying in the same frequency band, so that the interference level is suppressed.
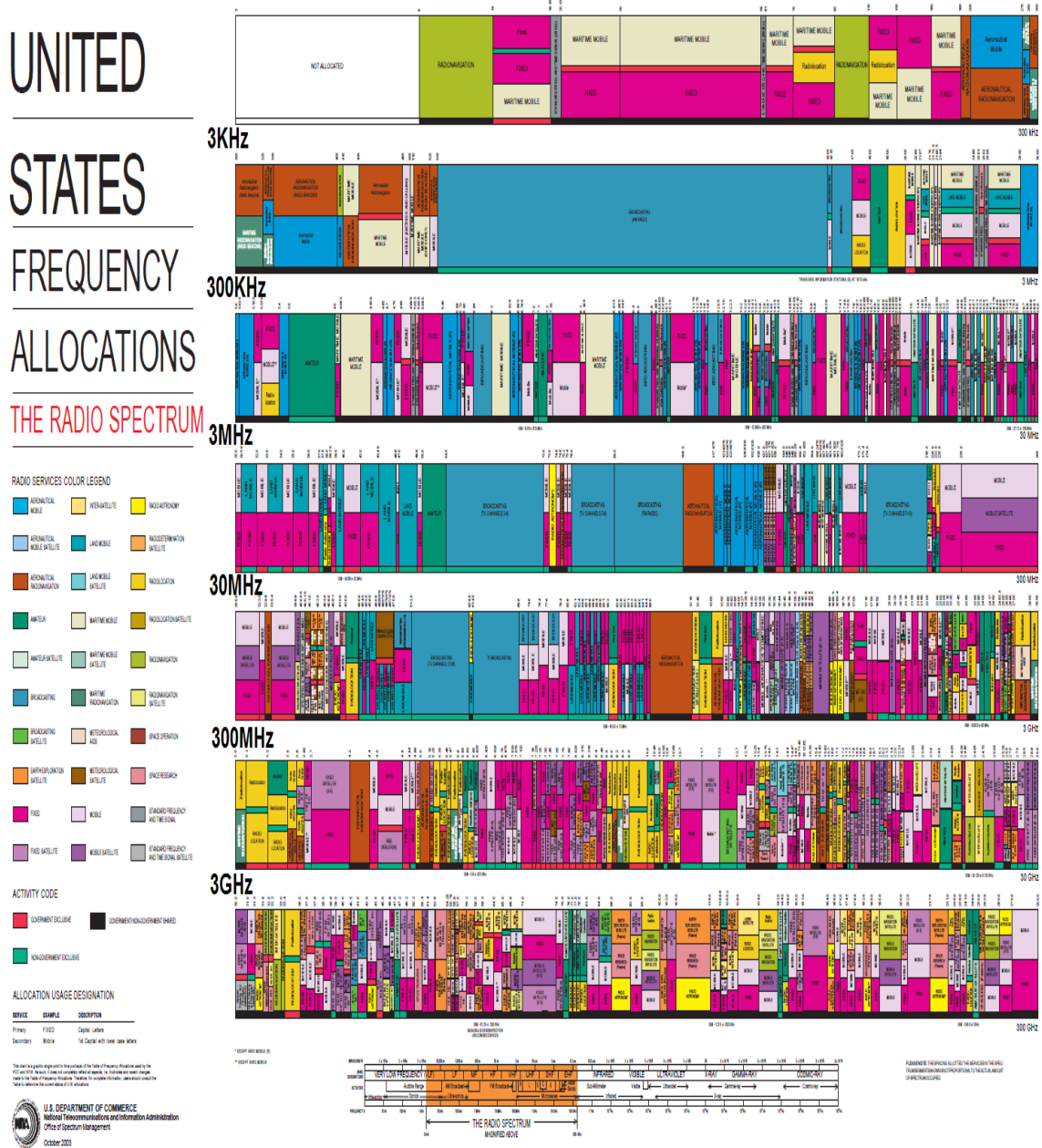
Fig. 1.1: The US spectrum allocation chart [1]

CR, built on a software radio platform, is an intelligent radio capable of independent reconfiguration by learning from and adapting to the communication

environment. Hence, a CR should fulfill two main requirements: cognitive capability and reconfigurability [5]. The cognitive capability identifies, through the interaction with the environment, the spectrum portions that are available in a specific moment and place. These available spectrum portions are called spectrum holes or white spaces. The reconfigurability capability makes the system possible to transmit and receive through different frequency values using different access technologies. That allows the CR system to change its parameters to adapt to the environment and to use the best available frequency band.

A crucial step towards efficient spectrum utilization is the one taken by FCC after the digital switchover [6], where FCC authorities investigated the feasibility of CR opportunistically for secondary users (SU) of the TV licensed spectrum. Indeed, broadcast television services operate in licensed channels in the VHF and UHF portions of the radio spectrum. The regulatory rules in most countries prohibit the use of unlicensed devices in TV bands, with the exception of remote control, medical telemetry devices, and wireless microphones [7]. After the digital switchover, a portion of TV analogue channels become entirely vacant due to the current spectrum available bands for digital TV (DTV). These vacant channels in the TV transmission spectrum are so called the TV white spaces (TVWS).

TVWSs are of special interest because of two main reasons: First of all, their propagation characteristics are especially good for wireless communications, reducing propagation losses and hence, increasing coverage especially in rural areas and enhancing building penetration. Secondly, very little and relatively cheap infrastructure is required for their implementation, making them especially suitable for rural and in

development areas or countries. Moreover, as the TV receivers practically require high SNR at the receiver side, the channel sensing and decision on the availability of these bands (8 MHz for TV transmission) become much more interesting within the CR environment.

Secondary operation of cognitive radios in TV bands known as TVWS communications relies on the ability of cognitive devices to successfully detect TV white spaces. They try to reuse these unused channels by adapting their transmission parameters to the environment and to avoid causing interference to the primary users of the TV bands. Hence, new frequency spectrum for unlicensed users or devices is offered. In addition, there will be typically a number of TV channels in a given geographic area that are not being used by DTV stations [7]. A transmitter operating on such locally vacant TV channels at a much lower power level would not need a great separation from co-channel and adjacent channel TV stations to avoid causing interference. Low power devices can therefore operate on vacant channels in locations that could not be used by TV stations due to interference planning. This can be materialized by the secondary operation of cognitive radios in the TV band.

From the applications of TVWSs, there are mainly two principal use cases. The first use case is the local communications system (called "WhiteFi") [8] typically with laptops and handhelds, where a wireless access point will offer access to the Internet using TVWS frequencies [9]. WhiteFi is a UHF white space wireless network which can be self-adapted to operate in the most efficient part of the available white spaces. It has several distinct advantages in comparison to typical WiFi at the ISM bands. WhiteFi networks can cover longer distances than the conventional WiFi networks and their

signals can penetrate concrete obstructions and many types of walls and can serve in many rural areas where heavy topographical challenges exist. In addition, WhiteFi systems can deliver more bandwidth and more throughput in more places to more consumers at lower network costs and lower power consumption. The second use case is the wide area broadband communications especially in rural areas, with fixed antennas mounted on rooftops mainly for mobile communications and satellite communications in addition to other private applications. There are also a range of other innovative uses of TVWS that might appear due to their favorable propagation characteristics such as mobile communications, television broadcasts, wireless microphone transmitters, and medical telemetry devices.

Like any communication device, the cognitive radio needs a transmitter and a receiver. However, unlike software-defined radios (SDRs), cognitive radios (CRs) are expected not only to perform signal transmission and reception, but also to sense the occupancy of any channel in the entire spectrum, and tune to transmit on the vacant channel. These requirements constrain strict issues on antenna design, broadband amplification, frequency synthesizers that provide a carrier frequency from tens of megahertz to about 10 GHz, mixing spurs, and spectrum sensing. Broadband and tunable antennas, multiband amplifiers, RF filters, broadband direct conversion mixers, baseband filters, analog-to-digital converters and digital-to-analog converters (ADCs/DACs) are needed to realize software-defined cognitive radio equipment. These RF components are expected to operate over a wide range of frequencies [10].

In cognitive radio, a reconfigurable radio front-end at the transmitter is needed. The RF front end is generally defined as everything between the digital baseband

system and the antenna. The design of an RF front end transmitter in cognitive radio systems is a critical issue. It should have awareness of the radio environment in terms of band of operation, spectrum usage and vacancy, transmit powers. It should be also programmed to steer to any band and tune to a channel of any bandwidth. Hence, it should be able to adaptively tune system parameters such as carrier frequency and transmit power. Therefore, the ability to design linear, efficient, and spectrally-agile components and architectures in the radio-frequency front-end transmitter is considered a primary technological concern in cognitive radio architectures.

1.2 Thesis Objectives

In cognitive radio communications and systems, it is very important to design and build an RF front-end transmitter working in the TV band. Previous work has been done on building an RF- front-end sensing receiver for cognitive radio applications [11]. A typical block diagram of a CR transmitter, which includes fundamental components for the transmission, is shown in Fig. 1.2. In this system, a baseband frequency is generated from a source and multiplied by another oscillating frequency generated from a tunable local oscillator. This multiplication is required to be performed by a mixer which up-converts the signal to the UHF frequencies. After that, a tunable band pass filter is required to be applied to the resulting signal in order to take off the undesired frequencies that cause interference and operate on the chosen band. Then, the desired signal on this chosen band is required to be amplified using a broadband power amplifier before transmission through the antenna in the final stage of the transmitter.
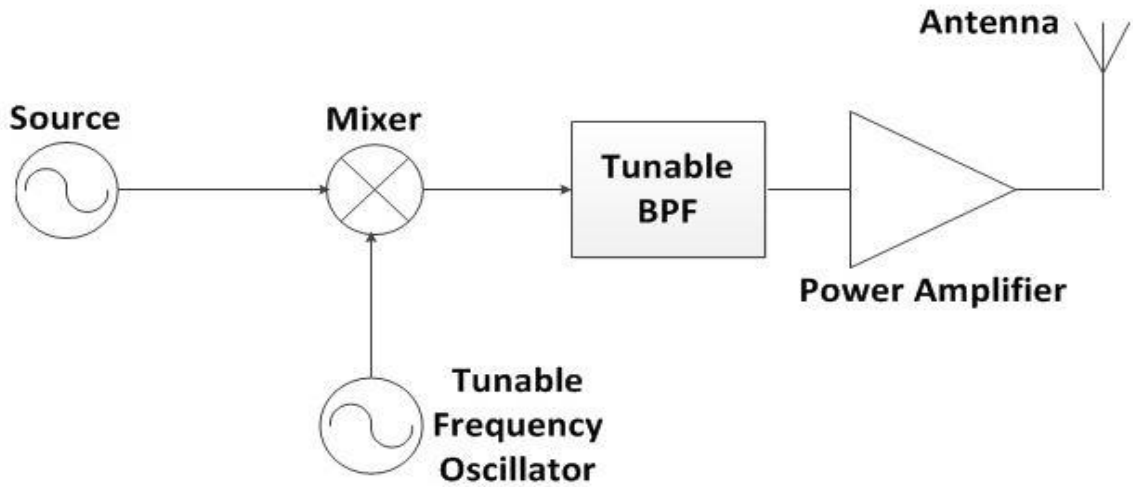
Fig. 1.2: Block diagram of the Cognitive Radio transmitter

Since CR transmitters are required to operate in any unoccupied channel of the TV frequency range, significant problems in a wide variety of RF components such as the antenna, filter, power amplifier, frequency synthesizer and the transmitter circuit, might be arise. This thesis work deals with the design of antennas and power amplifiers required for the CR transmitter. These antennas and amplifiers are designed to meet the TV band standards and are good candidates for cognitive radio applications in the TV band. The main contributions of this work are summarized below:

1. Inspecting and studying different parameters in the design of the antenna component such as the frequency band of operation, the size, and the direction. In addition, reconfigurability which is a main concern in designing transmitting antennas of cognitive radio systems is fully examined.

2. Examining and studying different parameters in the design of the power amplifier component such as linearity, stability, and efficiency. Moreover, a trade-off between the power efficiency of the power amplifier and multiband characteristics

is examined in order to achieve adequate designs of power amplifiers for cognitive radio applications in the TV band.

3. Proposing broadband antenna designs suitable for cognitive radio applications in the TV band. A reduced-size printed monopole antenna, a meander loop monopole antenna and a planar inverted F antenna (PIFA) are implemented in this thesis. A meander structure is used to reduce the size of the antennas for lower band operation. The designed antennas having reduced dimensions operate in the band 700-900 MHz and are suitable for TVWSs applications. The bandwidth and the size of these antennas make them convenient for portable devices such as laptops, notebooks, tablets and mobile phones. In addition, these antennas are good candidates that can be implemented in the CR transmitter system.

4. Investigating and designing a reconfigurable reduced-size planar spiral monopole antenna suitable for TVWS applications. In this antenna, frequency reconfigurability is obtained by inserting a tunable inductor on the spiral monopole and changing its inductance. This designed antenna operates in the higher part of the UHF band (600 - 800 MHz) and is suitable for TVWS applications. Moreover, this antenna can be best employed in the agile CR transmitter system.

5. Proposing and designing advanced power amplifier designs for TV band applications. A class AB power amplifier and a high efficiency Doherty one with operating frequency at 800 MHz were developed and verified for the suitability for TV band applications. The proposed Doherty power amplifier attains higher efficiency, wider bandwidth and an operating frequency bandwidth between 550 and 1000 MHz which make it suitable for TVWS band applications and easily implemented in the cognitive radio transmitter system.

6. Fabricating prototypes of the designed antennas and measuring their response to verify their proper functioning.

1.3   Organization of the Dissertation

The thesis is divided into five chapters. Chapter 2 presents an overview about the different components of the cognitive radio transmitter explaining their importance in the whole system, and reviews the current development and the recent work in all these components. Chapter 3 presents the proposed designs of four different antennas (broadband and reconfigurable) that operate in the TV band and are suitable for TVWS applications. Chapter 4 introduces the proposed designs of an AB power amplifier and a Doherty power amplifier that can be utilized in the transmitter system and can operate in the TV band, and emphasizes their different properties and characteristics. Finally, a conclusion, future work of this thesis, and the thesis-related publications are given in chapter 5.

CHAPTER 2

TRANSMITTER COMPONENTS REVIEW

2.1 Antenna

A transmitting antenna is used to radiate the radio frequency energy of the transmitter output into free space. It can generally be less efficient than the receiving antenna because it is possible to obtain high gains with the use of power amplifiers at the transmitter. If the transmitting antenna efficiency is low, there will be a significant power loss for high power transmitting devices.

In cognitive radio networks, two types of antennas are needed: sensing and communicating antennas. The sensing antenna, which is usually an Ultra-Wide Band (UWB) antenna, is used to sense the spectrum and find the spectrum holes. The communicating antenna, which is usually reconfigurable, is tuned to transmit at the frequencies of these holes.

The first cognitive task preceding any form of dynamic spectrum management is sensing and identifying spectrum holes in wireless environments. Therefore, there is a need to have an omnidirectional radiation pattern antenna which allows users to sense and identify the spectrum holes in wireless environment, transmit and receive independently of their direction. Omni-directional antennas with higher gains are used in cognitive radio networks. However, directional antennas might be also interesting for long range communications. Due to the targeted applications in this thesis, i.e. wireless

fixed broadband access systems such as WhiteFi and cellular and satellite communications, omni-directional compact antennas in the UHF TV band will be prioritized.

The fact that this CR system can be utilized in portable devices leads to an important challenge especially at the TV band [12]. Indeed, the size of the antenna must be small enough so that the antenna can be mounted in these portable devices. Therefore, the trend is to design reduced-size antennas with small and compact sizes.

2.1.1 Recent Work on Broadband Antennas

Different techniques have been used to design broadband antennas transmitting and receiving in TVWSs. The UWB antenna designed for cognitive radio in the UHF TV band reported in [13] presents a wide bandwidth covering the whole TV band. In this design, a quarter-wave cylindrical monopole is implemented with a long copper tube to ensure a relatively large radiating surface. The compact broadband monopole slot antenna, described in [14], exhibits a wide bandwidth ($460 - 1000$ MHz) using a feed-in space and a straight gap. In [15], a coplanar printed monopole antenna for digital television (DTV) in the UHF band (470-862 MHz) application is designed. In this design, a pair of slot lines is adopted in order to minimize the antenna size, providing then a good impedance matching at the UHF band. Moreover, the meander loop monopole and step-shaped ground plane are printed on the same side of a substrate with an area of 15 x 170 mm. In [16], a compact simple folded dipole antenna for DTV signal reception is proposed. This antenna provides a way to control the required bandwidth and impedance matching over the DTV frequency band using narrow

rectangular radiating patches and coupling gap. In [17], an asymmetric fork-like monopole antenna for digital video broadcasting-terrestrial (DVB-T) signal reception for application in the UHF band is presented. The proposed antenna consists of two two-branch strip monopoles on a rectangular ground plane with a concave as shown in Fig. 2.1 achieving a wide bandwidth of 461 MHz (451–912 MHz).
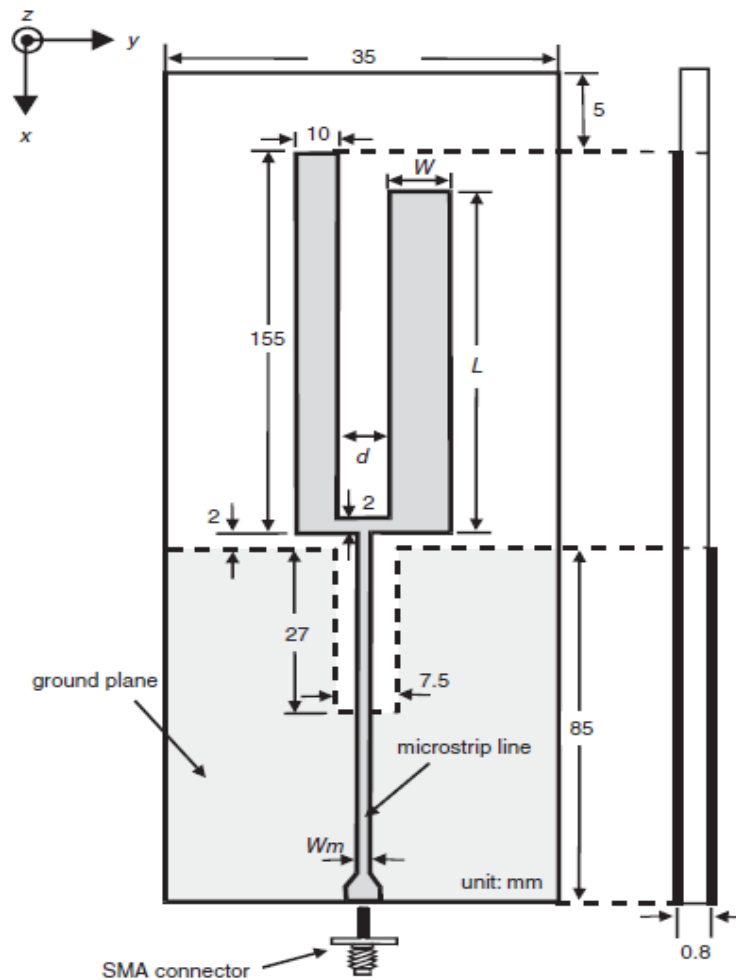
Fig. 2.1: Geometry of asymmetric fork-like antenna [17]

In [18], a novel grating monopole antenna consisting of a grating patch and a rectangular ground plane with a concave used for digital video broadcasting-terrestrial application is presented. The geometry of the antenna is shown in Fig. 2.2.This antenna

exhibits a wideband operating bandwidth which is attained by cutting a notch at the ground pattern opposite to the microstrip line.
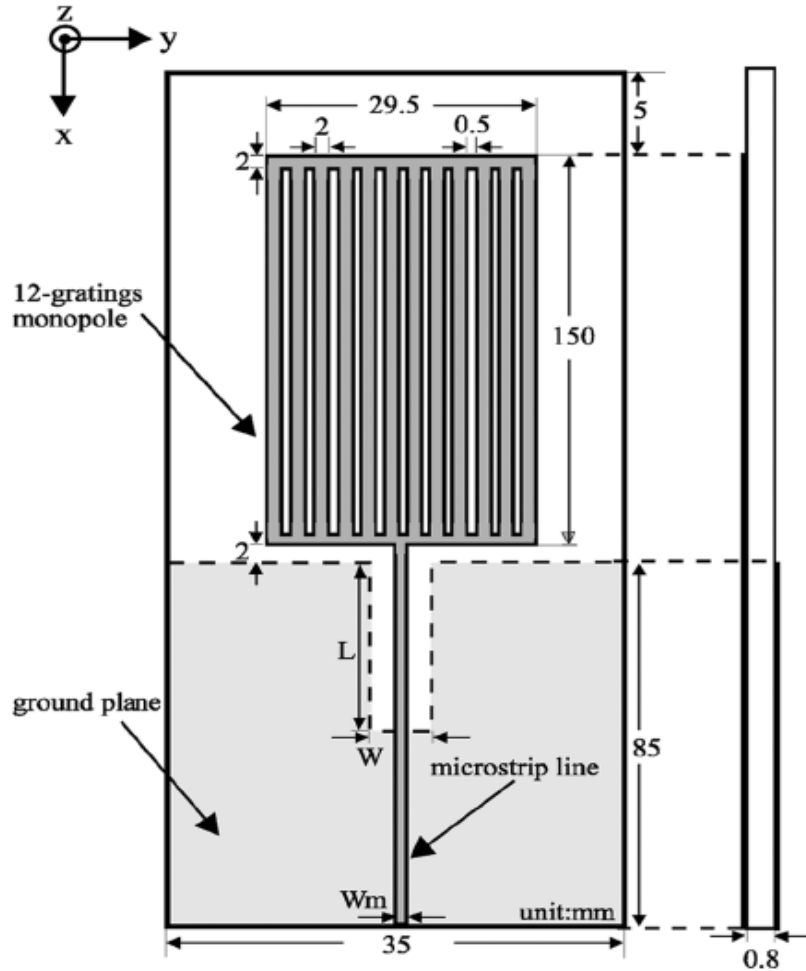
Fig. 2.2: Geometry of the grating monopole antenna [18]

In literature, the surveyed broadband antenna designs are relatively with large dimensions. This makes them difficult to be used in portable devices. Hence, one of our important contributions in this thesis is the proposition of small antenna designs with low complexity and broadband bandwidth as demonstrated in chapter 3.

2.1.2 Recent Work on Reconfigurable Antennas

A key enabler for realization of a cognitive communication system and one of its main challenges is the capability of reconfigurability in the underlying hardware and the associated protocol suite. From the antenna design perspective, the demand for multi wideband antennas which can be easily integrated with the communication system is continuously increasing. Reconfigurable and frequency agile architectures are mostly designed nowadays in order to solve the broad frequency allocation and to reduce the number of functional blocks. Reconfigurability is usually achieved by incorporating switches, variable capacitors, lumped components such as PIN diodes, varactor diodes, MEMS switches, or phase shifters in the topology of the antenna.

Different techniques have been also used to design transmitting reconfigurable antennas for TV band applications. In [19], a frequency-tunable Inverted F-Antenna (IFA) for DVB-H reception is presented. This antenna is suitable for small mobile devices. The operating frequency of this antenna is tuned with a varactor component which loads the IFA element and enables it to resonate at different frequencies. This kind of tunable narrowband antenna is suitable for DVB-H reception, since one channel in a bandwidth of 8 MHz is received at a time. In [20], a reconfigurable meander antenna dedicated to the mobile TV standards DVB-H, T-DMB or DVBSH is introduced. This meander antenna uses PIN diodes inserted in different points of the radiating element to dynamically cover the frequency band needed for these standards with a sufficient bandwidth. The insertion of active components allows compensating the drawback of the small volume of this miniature antenna. The antenna structure and its active elements are shown in Fig. 2.3.
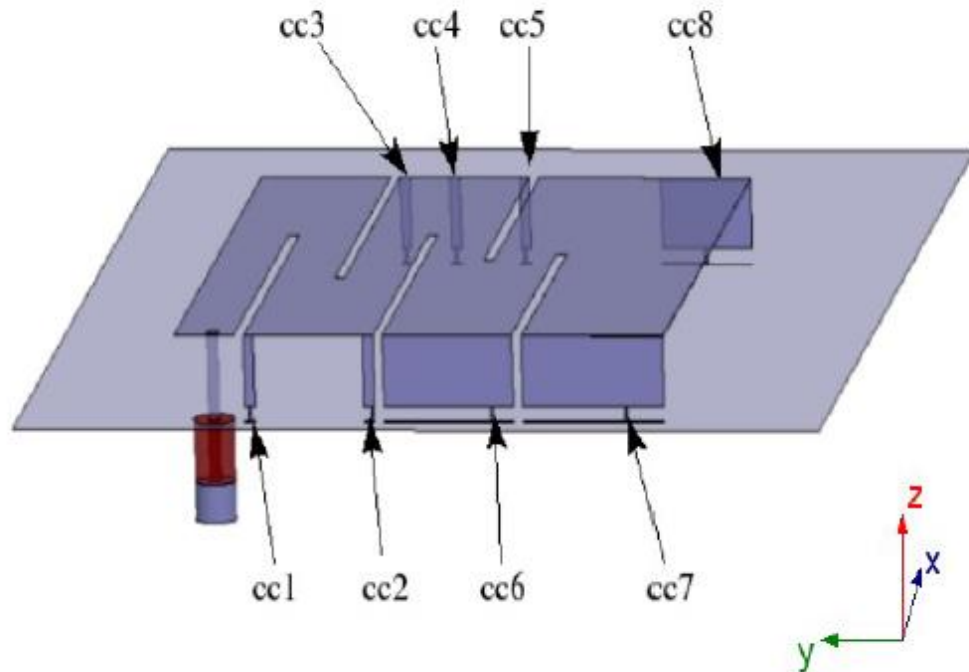
Fig. 2.3: Antenna structure and its active elements [20]

Another miniature antenna for digital TV reception in the UHF band has been designed and implemented in [21]. The concept was based on the commonly known small magnetic loop antenna with inductive feed and capacitive tuning. The size of the antenna is sufficiently small to fit into a USB stick, and the performance is comparable to current low-cost external rod-antennas. In [22], a compact multiband tunable PIFA system using a varactor as an active tuning component is presented covering 88–2175 MHz. The antenna was designed to cover the mobile telephone bands (GSM850, 900, 1800, 1900, UMTS) by controlling the value of the capacitance across the gap in the slotted PIFA. Two broadcast bands, FM radio (76–108 MHz) and mobile television DVB-H (470–702 MHz), were added by designing an appropriate matching circuit into the system as shown in Fig. 2.4.
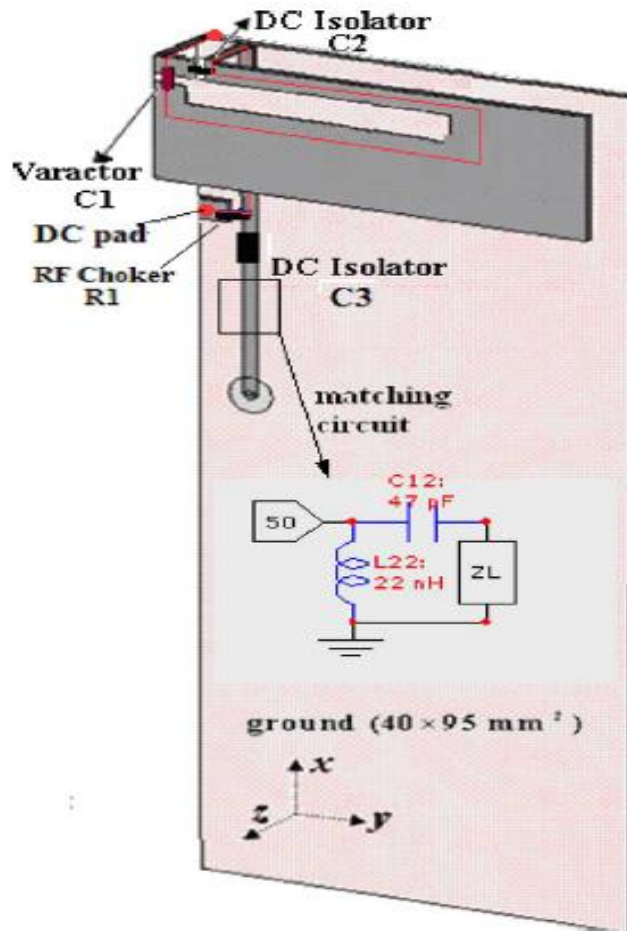
Fig. 2.4: Geometry of the antenna with the implemented matching circuit [22]

From the surveyed reconfigurable antenna designs, we can notice that these antennas are not simple antennas. Some antennas suffer from complexity, others suffer from isolation and biasing techniques, and others suffer from the relatively big size that does not allow the antenna to be mounted in portable devices. The reconfigurable antenna presented later in Chapter 3 of this thesis, which relies on the use of tunable inductors to attain reconfigurability, has a simple structure and a reduced size.

2.2 Broadband Power Amplifier

Power amplifiers are the basic building blocks in electronics communications systems. They convert low-power radio-frequency signals into larger signals of significant power, typically for driving the antenna of a transmitter. For the transmitter design in cognitive radio applications, in order not to interfere with the primary user and operate at multi standard frequency range, a high power gain is required, and thus a broadband linear power amplifier (PA) is desired. It must provide a high output power, simultaneously assuring a high efficiency and linearity behavior.

The power amplifier, however, consumes a large portion of energy in RF circuits during transmission. Consequently, an efficient PA design with high efficiency capabilities is required. As the system requirements vary, the specific constraints on the amplifier design also vary considerably. There are common requirements for nearly all amplifiers, including frequency range, gain flatness, output power, linearity, matching, and stability. Often there are design trade-offs required to optimize any parameter over the other, and performance compromises are usually necessary. Different classes and modes of operation were defined, each achieving certain criteria in such performance metrics. Popular examples are the basic classes such as Class A, B, C, D, E and F PAs. Because of their highly versatile circuit function, PAs have always been the first to benefit from developments in the device and semiconductor technologies, which helped in defining even new techniques for operation like the Doherty amplifiers and Class J PAs to meet the requirements imposed on PAs due to the evolution of new communication systems and standards as CR systems.

When the PA is driven towards saturation, the nonlinear distortion will increase considerably. On the other hand, the highest PA power efficiency is obtained at the saturation point [23]. In fact, there is a trade-off between the power efficiency of the PA and its linearity [24]. The nonlinear behavior of the PA leads to spectral regrowth of its out-of-band output signal, and as a result, to adjacent channel interference (ACI). The ACI power is a nonlinear increasing function of the PA input power [25]. Therefore, it is important to consider the PA nonlinear behavior of the CR transmitter and the resulting ACI power for allocating power in CR networks by noting the interference temperature limits. The CR system design should be aware of the nonlinear behavioral model of the PA and of the other users' constraints in the environment.

2.2.1 Classes of Power Amplifiers

Power amplifiers can be categorized into two major groups: Linear PAs and Nonlinear PAs. Linear PAs are able to generate output power proportional to the input power with a negligible amount of harmonic power generated. On the contrary, non-linear PAs operate near the cut-off region with a significant amount of harmonics generated besides the fundamental signal. The input and output powers are no longer proportional. Furthermore, amplifiers can also be classified into two categories: biasing class and switching class as shown in Fig. 2.5. In biasing class, amplifiers such as Class A, B, AB and C amplifiers are classified based on their quiescent point (bias point) or output Current Conduction Angle (CCA) θ. The angle θ is defined as the fraction of RF input drive signal where non-zero current is flowing through the device [26]. Unlike biasing class, amplifiers in switching class are classified based on the network

configuration connected to the active element, but not the bias level. As suggested by its name, transistors in switching-class act like a switch turning on and off controlled by the input drive signal. Class E and Class F amplifiers are two examples that belong to this class of operation. Class E and Class F amplifiers drew a lot of attention from designers because of their capability to provide high power-added efficiency.

```
                        ┌──────────────────┐
                        │ PA classification │
                        └──────────────────┘
                                 │
              ┌──────────────────┴──────────────────┐
      ┌───────────────┐                     ┌────────────────┐
      │ Biasing Class │                     │ Switching Class │
      └───────────────┘                     └────────────────┘
          Class A                                Class D
          Class AB                               Class E
          Class B                                Class F / inv F
          Class C                                Class G
                                                 Class H
                                                 Class S
```
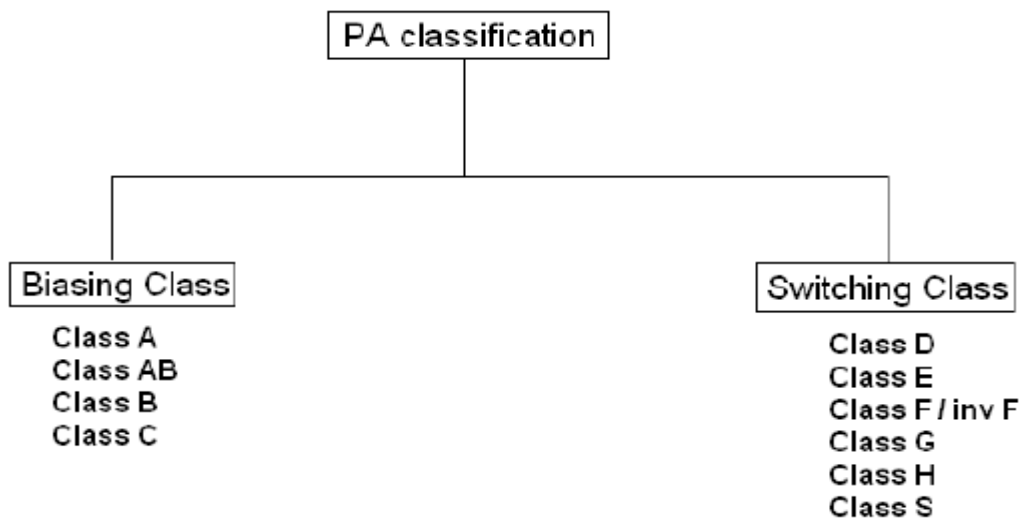
Fig. 2.5: Family tree of PA classification [26]

2.2.1.1 <u>Class A Amplifier</u>

A Class A amplifier is a linear amplifier, which has a conduction angle of 360°. The 360° conduction angle means that the transistor in this class is turned on and conducts over the entire sinusoidal cycle. Most of the small-signal amplifiers are designed in this class because of its simplicity and the best linearity among all classes of amplifiers. Because of the 360° conduction angle of Class A, these amplifiers have the lowest efficiency and are only suitable for low-power applications [26]. The transfer

characteristic of a Class A amplifier and its corresponding voltage and current waveforms are shown in Fig. 2.6 below.
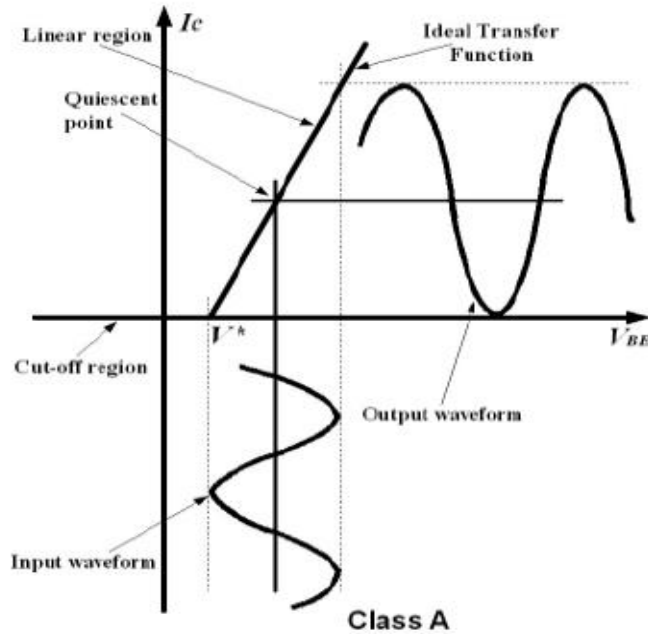
Fig. 2.6: Class A transfer characteristics [26]

2.2.1.2 Class B Amplifier

This class of operation in class B amplifier is lower than that of Class A amplifier and close to deep cut-off region. In Class B, the transistor conducts only on a half-cycle of the input drive signal. This gives Class B amplifiers a CCA of about 180° and also a better efficiency than Class A amplifiers. However, Class B amplifiers have poor performance in term of linearity because of the generation of higher order harmonics. This poor linearity can be improved by using two transistors simultaneously as a Class B push-pull amplifier. In Class B push-pull amplifiers, there is a short period of time that both of the transistors are off at the same time and cross-over distortion is created

[26]. The transfer characteristics of Class B amplifier, the corresponding voltage and current waveforms are shown in Fig. 2.7 below.
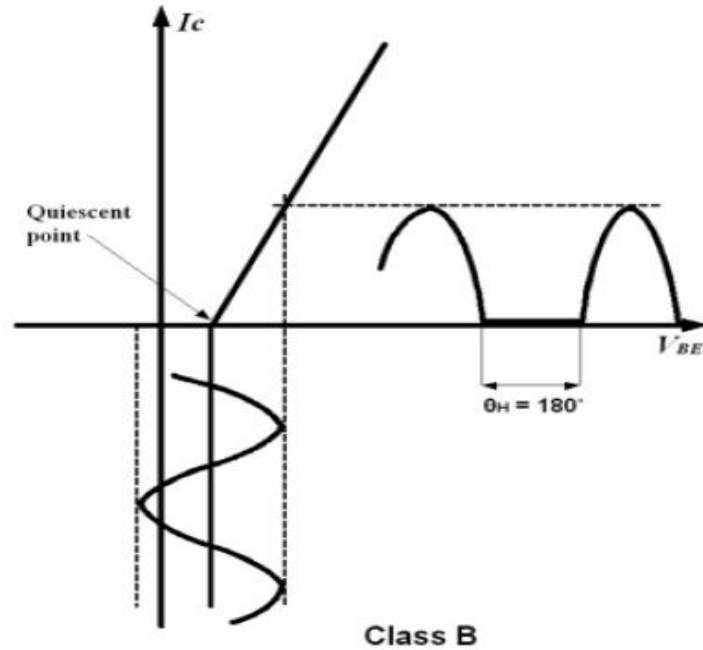
Fig. 2.7: Class B transfer characteristics [26]

2.2.1.3 Class AB Amplifier

A Class AB amplifier is considered as a combination of class A and class B amplifiers in term of linearity and efficiency. The Class AB bias point is between that of Class A and Class B. The efficiency of Class AB amplifiers is usually between that of Class A and that of Class B amplifiers. In Class AB push-pull amplifiers, the cross- over distortion appeared in Class B is reduced so that linearity can be improved [26]. Fig. 2.8 shows the transfer characteristic of a Class AB amplifier and its corresponding voltage and current waveforms.
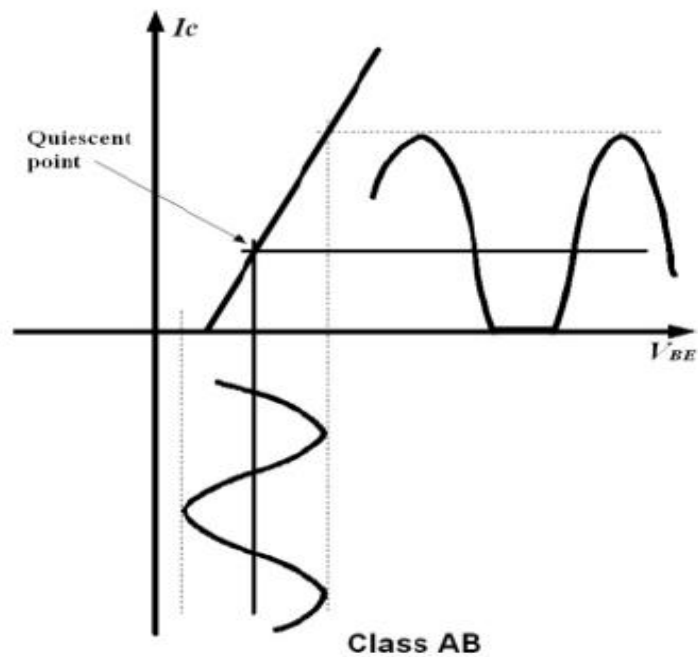
Fig. 2.8: Class AB transfer characteristics [26]

2.2.1.4 <u>Class C Amplifier</u>

A class C amplifier has a conduction angle significantly less than 180°. The transistor is biased such that under steady-state conditions no collector current flows. Linearity of the Class-C amplifier is the poorest of the classes of these amplifiers. The Efficiency of Class-C can approach 85 %, which is much better than either the Class-B or the Class-A amplifier. In order to bias a transistor for Class-C operation, it is necessary to reverse bias of base-emitter junction. External biasing is usually not needed, because it is possible to force the transistor to provide its own bias, using an RF choke from base to ground. One of the major problems with utilizing Class-C in solid-state applications, is the large negative swing of the input voltage, which coincides with the collector/drain output voltage peaks [26]. This is the worst condition for reverse

22

breakdown in any kind of transistor, and even small amounts of leakage current flowing at this point of the cycle have an important effect on the efficiency. For this reason true Class-C operation is not often use in solid-state at higher RF and Microwave frequencies. Fig. 2.9 shows the transfer characteristic of a Class AB amplifier and its corresponding voltage and current waveforms [26].
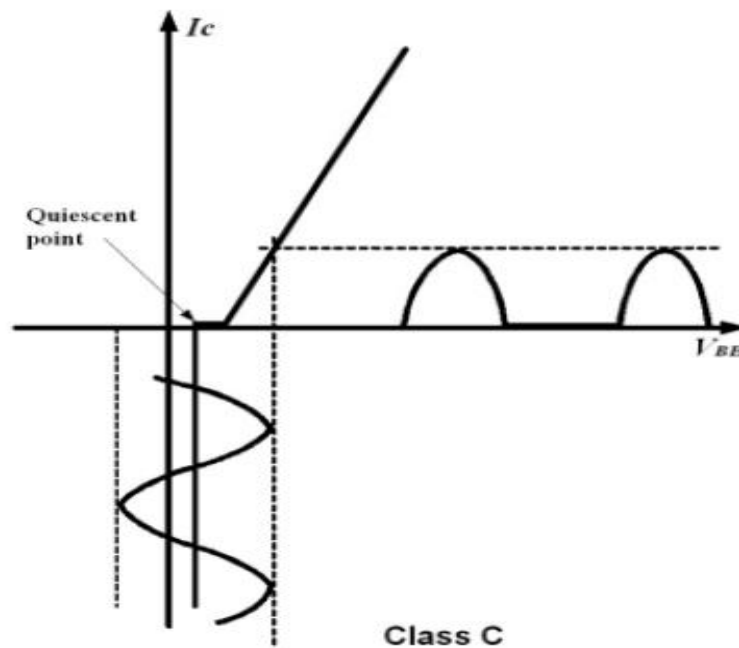
Fig. 2.9: Class C transfer characteristics [26]

2.2.1.5 Class D Power Amplifier

The voltage mode Class D amplifier is defined as a switching circuit that results in the generation of a half-sinusoidal current waveform and a square voltage waveform. Class-D PAs use two or more transistors as switches to generate a square drain-voltage waveform. A series-tuned output filter passes only the fundamental-frequency component to the load.

Class-D amplifiers suffer from a number of problems that make them difficult to realize, especially at high frequencies. First, the availability of suitable devices for the upper switch is limited. Secondly, device parasitics such as drain-source capacitance and lead inductance result in losses in each cycle. If realized, they are common at low RF and audio frequencies. Class-D amplifiers theoretically can reach 100% efficiency, as there is no period during a cycle where the voltage and current waveforms overlap. No real amplifier can be a true Class-D, as non-zero switch resistances and capacitive as well as inductive parasitic elements restrict the shape of drain voltage waveform [26].

2.2.1.6 <u>Class E Power Amplifier</u>

Class-E employs a single transistor operated as a switch. The collector/drain voltage waveform is the result of the sum of the DC and RF currents charging the drain-shunt capacitance Cp which is parallel with transistor internal capacitance. In optimum class E, the drain voltage drops to zero and has zero slope just as the transistor turns on. The result is an ideal efficiency of 100 %, elimination of the losses associated with charging the drain capacitance in class D, reduction of switching losses, and good tolerance of component variation. The transistor behaves as a perfect switch. When it is on, the collector/drain voltage is zero, and when it is off the collector current is zero.

2.2.1.7 <u>Class F Power Amplifier</u>

Class-F boosts both efficiency and output by using harmonic resonators in the output network to shape the drain waveforms. The voltage waveform includes one or

more odd harmonics and approximates a square wave, while the current includes even harmonics and approximates a half sine wave. Alternately, the voltage can approximate a half sine wave and the current a square wave. The required harmonics can be produced by current source operation of the transistor [26]. However, in practice the transistor is driven into saturation during part of the RF cycle and the harmonics are produced by a self-regulating mechanism similar to that of saturating Class-C.

While Class-F requires a more complex output filter than other PAs, the impedances must be correct at only a few specific frequencies. Class-F amplifier designs intentionally square the voltage waveform through controlling the harmonic content of the output waveform. This is accomplished by implementing an output matching network which provides high impedance open circuit to the odd harmonics and low impedance shorts to even harmonics. This results in a squared off (though for Class-F, truly squared) voltage waveform. Class-F amplifiers are capable of high efficiency (88.4% for traditionally defined Class-F, or 100% if infinite harmonic tuning is used). Class-F amplifier design is difficult mainly due to the complex design of the output matching network [26].

2.2.1.8   Doherty Power Amplifiers

Highly efficient and linear power amplifier is a key component in any communication system. However, these PAs require very efficient peak-to-average power ratio (PAPR) Therefore, a power amplifier with high linearity and efficiency is of great importance. The simplest method is to back-off signals form the saturation region to the linear region at the cost of power efficiency. Another may use predistortion

methods or elimination and restoration techniques. However, these techniques which need additional components result in an increase in cost, size, and power dissipation. To meet all these requirements, a Doherty amplifier is the most promising candidate with simple fabrication and high efficiency.

The simplest Doherty amplifier operation can be achieved using two cells with a class-AB biased carrier amplifier cell and a class-C biased peak amplifier cell with respective input matching network and output matching network. It has a high linearity and efficiency across the wideband signal. A classical Doherty power amplifier is shown in Fig. 2.10.
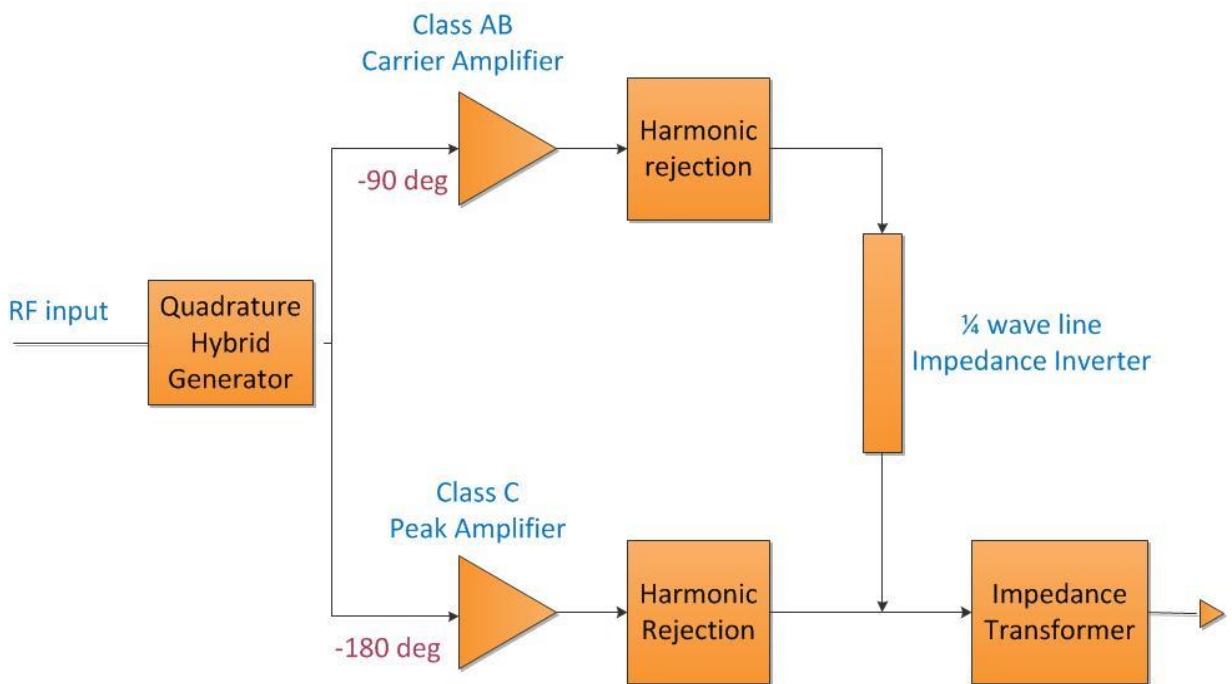
Fig. 2.10: The classical Doherty power amplifier

Moving from left to right in Fig. 2.10, a quadrature hybrid produces two outputs that are 90 degrees out of phase with each other. The 90 degree split is needed because the peaking amplifier output requires a 90 degree delay with respect to the carrier

amplifier in order to be in step with the carrier amplifier output. This is subjected to a 90 degree delay in the quarter wave impedance inverter. After that, the carrier and peaking amplifier modules provide the gain. The output of the carrier amplifier is passed through the quarter wave line, and tied to the output of the peaking amplifier and the impedance transformer.

The DPA operating principle is based on the idea to modulate the load of the carrier device by using a peak device [28]. The peak amplifier loads the signal when the carrier amplifier goes into compression. When the signal is near its average level, the peak amplifier is not operating, yet the carrier amplifier is operating near its compression point, hence operating at its most efficient level. Once peaks appear, the peak amplifier starts to operate and loads the compressing carrier stage, as shown in Fig. 2.11. Once the carrier amplifier is saturated, it will not load the peaking amplifier.
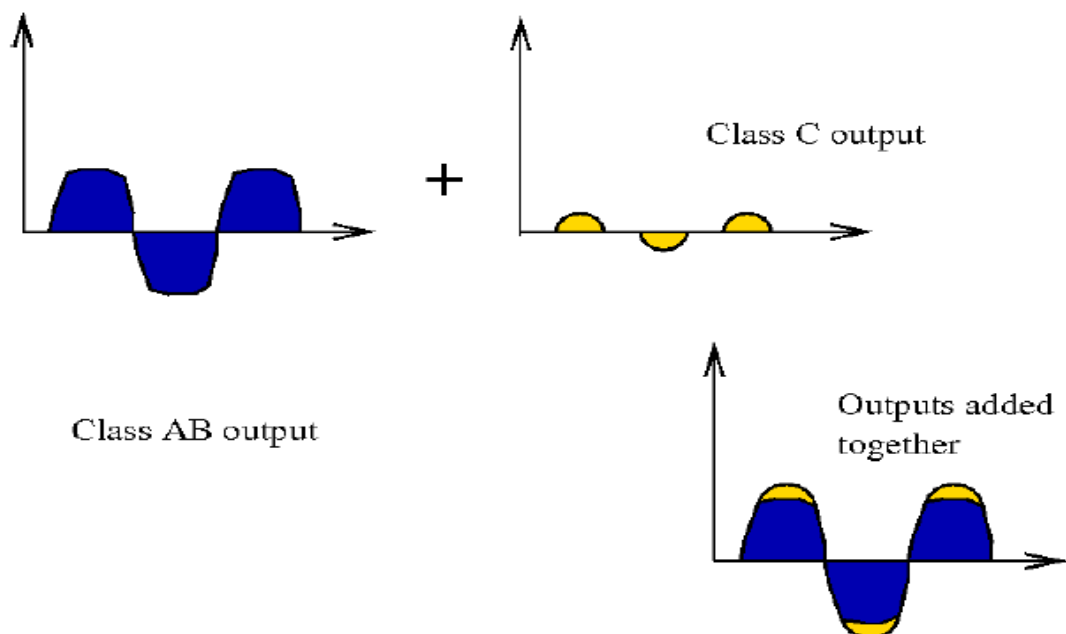
Fig. 2.11: Illustration of the Doherty idea. The class C amplifier loads the signal above the level where class AB compresses [27].

Doherty amplifiers are the best candidates that can provide higher efficiency among all types of amplifiers. Indeed, when the efficiency increases, the battery life of handheld devices such as cellular phones can be extended effectively to satisfy consumers' needs. As more features and hardware are added to cell phones, efficiency improvement becomes one of the major issues for designers. Therefore, Doherty amplifiers are widely used for many applications where RF power amplifier efficiency is important.

2.2.2 Methods of Developing Broadband PASs

There are several methods to develop broadband PAs:

- The traveling-wave and distributed amplifier topologies are widely used for broadband PA development because of the excellent characteristics in terms of bandwidth, gain flatness, and input voltage standing-wave ratio [29-30].

- The multistage LC combination technique is proposed in [31] to develop the GaAs HBT PA for the broadband wireless applications.

- The push-pull PAs can achieve wide bandwidth by using broadband transformers [32-34].

- The shunt-feedback technique and multi-section distributed matching networks are demonstrated to be useful in [35].

- The staggered matching is a viable technique to extend the bandwidth of the millimeter-wave PAs [36].

- The reconfigurable output matching by using PIN diodes to adjust the LC networks is applied in the dual mode broadband InGaP HBT PA at 0.9 and 1.8 GHz [37].

2.2.3 Recent Work on Power Amplifiers

Several works have been proposed in designing PAs for cognitive radio applications. In [38], a broadband PA is demonstrated in InGaAs HEMT technology using load impedance tracking. The power-added efficiency and the 1 dB compression point of the PA are better than 20% and 21.4 dBm, respectively. In [39], a wideband power amplifier for the application of intelligent cognitive radios is proposed. In this PA design, the broadband frequency response is enhanced using transformer matching network and resistive feedback. As shown in Figure 6, series stack topology is used to achieve the broadband load impedance match by discussing the constraints of stack PA in both GaAs and CMOS methods. The main difference between these two PAs is the feed point. In the first one, transformers are employed using RF input at the bottom and ground at the top. In Fig. 2.12(b), the RF feed point is upside-down compared to Fig. 2.12(a). Due to the fact that these two PAs are voltage combined, the total biasing current is controlled by the transistor. To verify the design models, a high-efficiency broadband PA in commercial 0.18 m CMOS process with the best PAE of 30% and the 1 dB compression point of 20 dBm is established. This PA also demonstrates the widest bandwidth performance among CMOS PAs below 10 GHz.
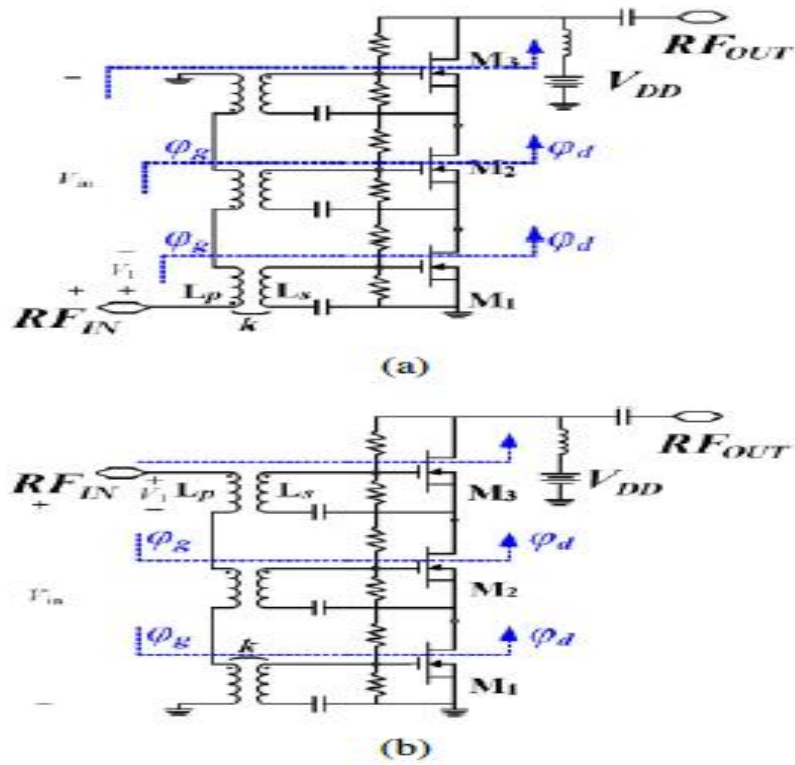
Fig. 2.12: Two kinds of transformer orientations of stack PA. In (a), the transformers

are opposite coupled. (b) the upside-down input fed configuration [39]

In [40], power allocation in cognitive radio networks is studied by considering the

nonlinear effects of the PA on the received signal-to-noise ratio (SNR) at the secondary

receiver and adjacent channel interference (ACI) to the primary receivers. A nonlinear

PA with limited dynamic range and a lower limit on the transmit power is assumed for

the secondary transmitter. The PA needs to be turned off in some fading blocks in order

to control the resulting ACI from the secondary transmitter to the primary receivers. A

high efficient, high power push-pull GaN amplifier for CR applications is reported in

[41]. This PA shows an efficiency of 60-55% from 10 MHz to 650 MHz, for an output

power of 100W and a compressed gain of 19.5dB. By reducing the drain voltage to

30V, the efficiency is about 60 to 70% with an output power of 47 dBm and a power

gain of 18.5 dB. In [42], a class-AB power amplifier was designed for an envelope

tracking (ET) application. As a power device, Cree Gallium Nitride High Electron Mobility Transistor (GaN HEMT) CGH4010F was chosen. The input and output matching networks were designed and simulated with Advanced Design System (ADS) [43]. After some optimization, the amplifier was fabricated and good agreement between the simulation and measurement results was observed. The maximum power added efficiency (PAE) is around 50% with the supply voltage Vsup= 10V and the maximum drain efficiency is around 75% with Vsup= 5V. An output power up to 42 dBm and good linearity of the output voltage with respect to the supply voltage were achieved as shown in Fig. 2.13.
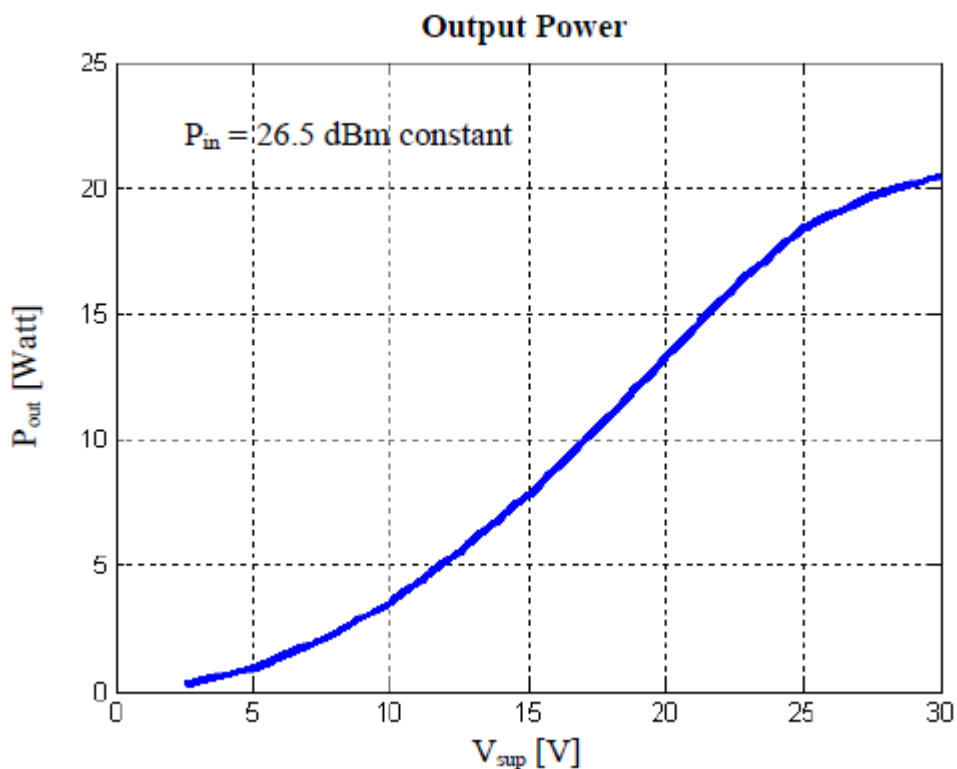
Fig. 2.13: Output power versus drain supply voltage is approximately linear [42]

A class B and a class F power amplifier are described in [44] using a GaN HEMT device. They both were designed to operate at a frequency of 1.7 GHz with the same

bias conditions. The performance of each amplifier was successfully simulated and compared. A class B amplifier was physically implemented and achieved a high power-added-efficiency of 69.2%, 39.9 dBm output power and associated gain of 14.9 dB.

Several works have been also proposed in designing PAs operating in the UHF band. The configuration of a high-power amplifier used for modern radar system operating at UHF band (820MHz – 900MHz) is proposed in [45]. The power amplifier module consists of two stage 90W and 200W amplifier that allows the output to reach up to 1.2kW per block, and even approximate 9.6 kW to the whole transmitter system using the classical power combination method. The design and simulated results were carried out by the microwave engineering professional design software, known as ADS2008 package. The achieved results meet the demand of modern radar transmitter. In [46], the design of a wideband and highly efficient class-E power amplifier are reported in this work. The amplifier can cover the whole UHF broadcast band from 470MHz to 860MHz with an output power of 10W. The PA can achieve better than 70% power added efficiency (PAE) in a fractional bandwidth of 41% or better than 60% PAE in a bandwidth of 54% with 10W output power. A reactance compensation method was used to implement the output matching network as shown in Fig. 2.14. To achieve the required operational bandwidth, a double reactance compensation matching is required. A UHF power amplifier which can be used for small satellites and has 435.2MHz center frequency and an 8 MHz bandwidth is designed in [47]. The power gain is between 15dB and 20dB in this work. In addition, this power amplifier has linear characteristics and is stable in the operating band.
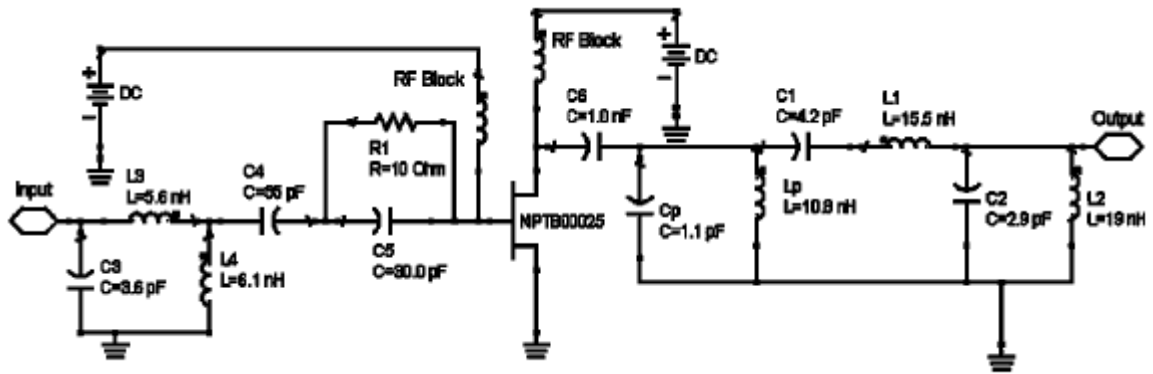
Fig. 2.14: A schematic layout of the PA using the reactance compensation method [46]

Moving to Doherty power amplifiers, several works have been also presented. In [48], a wideband Doherty amplifier is designed and implemented in GaN HEMT technology using simple circuitry. This amplifier was designed to cover a bandwidth of 640 MHz, ranging from 1.5 GHz to 2.14 GHz achieving a 1 dB compression output power of 43.8 dBm (24.1 W), with a maximum power-added efficiency of PAE = 69 % at 1.9 GHz. The designed Doherty amplifier also showed acceptable linearity when characterized with two-tone and single-carrier wideband code-division multiple access (W-CDMA) stimuli. The design, implementation and characterization of a Doherty power amplifier for 3.5GHz WiMAX applications are discussed in [49]. The DPA has been implemented using a commercial GaN HEMT from Cree inc., following a class AB and C scheme for the main and peak amplifiers, respectively. The measured maximum power of the DPA is 22W with a first peak efficiency of 57%, and maximum drain efficiency of 65% at the DPA saturation. Efficiency over the so-called Doherty region does not drop below 55% from saturation to 6 dB input back-off. The gain at the onset of the Doherty region is 8dB. In [50], a theoretical analysis of a DPA employing a Class F PA as a main amplifier has been presented. The proposed theory has been

validated through the realization of a Class F AB-C DPA using GaN HEMT devices. A saturated output power of 35 dBm has been measured with a drain efficiency larger than 45% and almost constant over a 6-dB dynamic output range. In [51], the design, realization and experimental characterization of a GaN-based hybrid Doherty power amplifier for wideband operation in the 3–3.6-GHz frequency range is presented and shown in Fig. 2.15. The design implements a novel and simple approach based on wideband compensator networks. The realized amplifier is based on a packaged GaN HEMT and shows, at 6 dB of output power back-off, a drain efficiency higher than 38% in the 3–3.6-GHz band, gain around 10 dB, and maximum power between 43 and 44 dBm, with saturated efficiency between 55% and 66%.
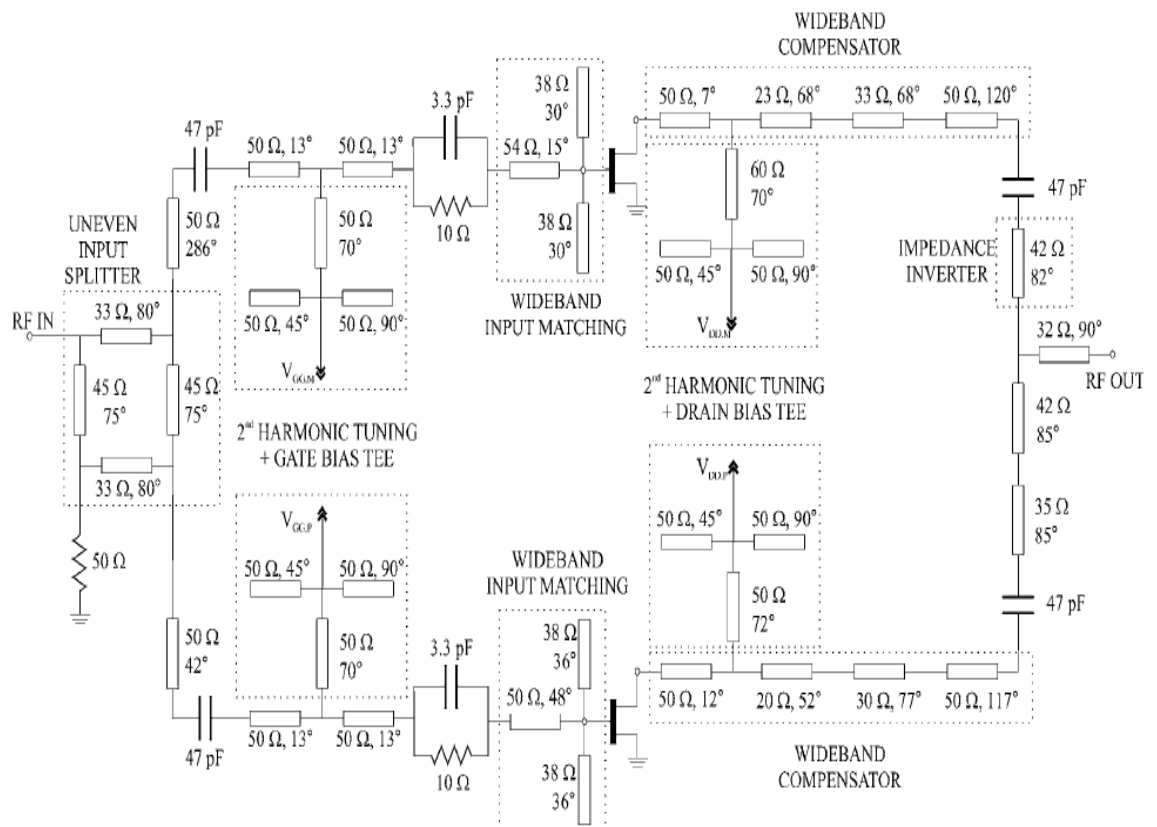
Fig. 2.15: Complete scheme of the Doherty power amplifier in [51]

From the surveyed power amplifier designs, we can notice that some designs suffer from low efficiency and other designs suffer from narrow bandwidth and that the maximum attained efficiency is 70%. Moreover, some designs cannot achieve good linearity and some designs have relatively low gain.

In this thesis, some specifications are mainly desired as the transmitter is required to work in the TV band. The broadband power amplifier is aimed to cover the frequency range from 600 to 900 MHz with linearity, high stability, and high efficiency. Since this amplifier is used in a cognitive radio transmitter that needs high output powers, the gain of the intended power amplifier is required to be high (above 20 dB) with gain flatness over the desired frequency band. Moreover, the input impedance and the output impedance must exactly be 50 ohm. The power amplifier designs reported in Chapter 4 of this thesis satisfy these specifications and attain linearity, higher efficiency, and an operating frequency bandwidth between 550 and 1000 MHz which make it suitable for TV band applications.

2.3   Tunable RF Band Pass Filter

A band-pass filter is a device that passes frequencies within a certain range and rejects (attenuates) frequencies outside that range. Band-pass filters are widely used in wireless transmitters and receivers. In a transmitter, the main function of such a filter is to limit the bandwidth of the output signal to the band allocated for the transmission which prevents the transmitter from interfering with other stations. Well-designed band-pass filters are designed to have the optimum bandwidth and to maximize the

number of signal channels that can exist in a system, while minimizing the interference between signals.

Tunable filters are essential components for reconfigurable front-ends since they allow the use of a single component. Compared to a bank of fixed filters, a tunable filter assures greater functionality, better channel selectivity, reduced size, and lower weight since the same hardware can be employed at multiple bands. However, since they are placed before the power amplifier, they must exhibit very low loss and high linearity, especially in today's crowded RF environments.

There has been significant research on tunable RF band-pass filters in recent years. Tuning can be realized using varactor diodes, ferroelectric devices, PIN diodes, or RF Microelectromechanical systems (MEMS) switched capacitors. A number of MEMS based tunable filters, based on switched capacitors, have been developed [52–55]. A variety of varactors have also been utilized to achieve frequency tuning [56–58]. In addition, the authors in [59] show that open split ring resonators (OSRRs) and open complementary split ring resonators (OCSRRs) can be loaded with varactor diodes in order to implement tunable filters in coplanar waveguide (CPW) technology.

When band pass filters are required to be implemented in CR systems, tunability must be dealt carefully in order to reduce spurious content in the transmitter and limit out-of-band interference in the receiver. Moreover, a wide tuning range is preferred in cognitive radio systems in order to maintain tunability over different bands and several applications.

Primarily, some target specifications are needed when the transmitter is designed to work in the TV band. The filter is aimed to achieve frequency coverage from 600 to

900 MHz. The targeted insertion loss is assumed to be less than 4 dB in order to achieve a small noise figure of the entire system. The dimensions of the filter are required to be small with an impedance of 50 ohm. Moreover, the filter is required to be designed in higher orders (higher than the second order) in order to improve the shape factor and the out-of-band rejection.

2.4 Frequency Mixer

A frequency mixer is a nonlinear electrical device that creates new frequencies from two signals applied to it, as shown in Fig. 2.16. Mixers are widely used to shift signals from one frequency range to another for transmission or further signal processing. This process is known as heterodyning. Frequency mixers are also used to modulate a carrier frequency in radio transmitters.
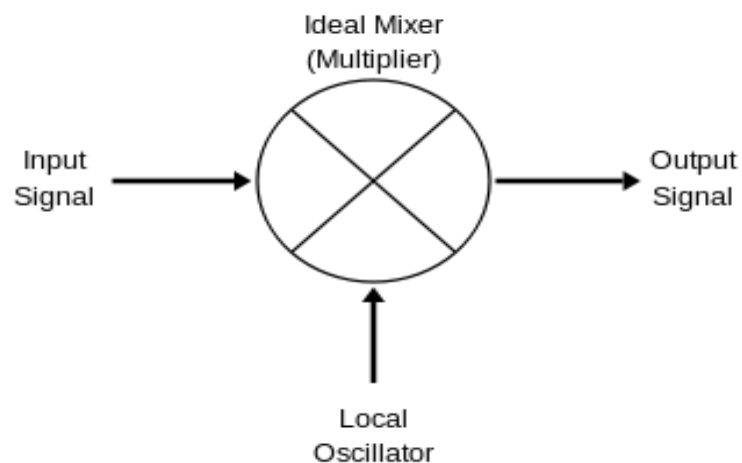
Fig. 2.16: Schematic of a frequency mixer

For complete on-chip solutions, homodyne architectures have been the preferred choice. Homodyne architectures ease the requirements on the IF filter; however, they suffer from a number of issues including flicker noise, dc offsets, and second order non-linearity. Homodyne architectures have gained popularity for moderate to wide bandwidths, especially in SDR applications. Passive mixers have often been the preferred choice for SDR applications due to their lower flicker noise and excellent linearity [60-61].

Taking into consideration that a tunable RF filter does not provide out-of-band rejection as effective as fixed RF filters, and that SDR applications often require more severe out-of-band rejection specifications [61], harmonic reject mixers become necessary. However, subsequent mixing with a square wave up-converts the desired signal, but also causes interference around the LO harmonics. To ease the problem of harmonic mixing, multi-phase harmonic rejection mixers can be employed [62]. Such mixers have been employed in a number of SDR architectures, providing 30–40 dB harmonic rejection. Further harmonic rejection can be obtained using digital correction [61].

In the design of a mixer, there are some key specifications that need to be known. The mixer type, the frequency range, the impedance, the conversion loss, and the noise figure are all important points in designing a frequency mixer. In addition, the anticipated RF input power should be also identified. The intended frequency range is between 600 and 900 MHz and the impedance is 50 ohm. It is required to maintain tolerable noise and low up-conversion loss (about 7 dB) in order to attain a low noise

figure of the entire system. The tunable local oscillator must have enough power to operate the mixer with low conversion loss.

2.5 Tunable Frequency Oscillator

A tunable frequency oscillator is a critical building block for the CR transmitter [63]. The following requirements can be identified for this oscillator:

- Wide-tuning range, such that the oscillator can cover different bands and several applications.
- Excellent tuning, in order to reduce spurious content and limit out-of-band interference.
- Low phase noise, such that the phase noise skirts do not cause up-conversion of spurious signals onto the desired signal.
- Fast-settling behavior, to enable fast band-switching in the SDR.
- Fine-frequency resolution determined by the minimum channel spacing desired.

An oscillator can be designed so that the oscillation frequency can be varied over some range by an input voltage or current. A voltage-controlled oscillator (VCO) is an electronic oscillator whose oscillation frequency is controlled by a voltage input. The applied input voltage determines the instantaneous oscillation frequency. The VCO is widely used in phase-locked loops, in which the oscillator's frequency can be locked to the frequency of another oscillator.

Radio frequency VCOs are usually made by adding a varactor diode to the tuned circuit or resonator in an oscillator circuit. Changing the DC voltage across the varactor changes its capacitance, which changes the resonant frequency of the tuned circuit. Voltage controlled relaxation oscillators can be constructed by charging and discharging the energy storage capacitor with a voltage controlled current source. Increasing the input voltage increases the rate of charging the capacitor, decreasing the time between switching events.

On-chip VCOs are based on two popular architectures: LC tank based and ring based. The LC tank VCOs are usually suitable for low phase noise applications, but suffer from a low tuning range. On the contrary, ring oscillators provide a wide tuning range, but suffer from poor phase noise. In general, ring oscillators are considered to be suitable candidates because of their wide tuning range and their relatively small area which makes them good choices for low cost portable devices.

Generally, the oscillating frequency of a ring oscillator is proportional to the number of stages (N) and the transmission delay of each delay cell stage (TD). The ring oscillator has a large VCO gain variation over the tuning range. In particular, very high gain is often observed in the middle of the tuning range, where the oscillator would suffer from high sensitivity to control voltage imperfections. A linear relationship between the tuning voltage and the oscillating frequency is desirable for wide band systems to guarantee the locking range of the frequency synthesizer.

Different works have been proposed in designing local oscillators for cognitive radio applications and summarized in Table 2.1.

Work	Used Technique	Bandwidth	Phase Noise (dBc/Hz)	Output power (dBm)
[64]	Harmonic Balance (HB) optimization with feedback loop	0.75 GHz – 1.85 GHz	-111.2	5.2
[65]	Adopting a transmission gate in a saturated ring oscillator	20 MHz – 807 MHz	-108	13.42
[66]	Switched-capacitor frequency detector with a negative impedance converter feedback	140 MHz – 1.15 GHz	-93.44	5.56

Table 2.1: Comparison between different oscillators' schemes

Principally, the oscillator target in the CR transmitter system is to achieve frequency coverage from 600 to 900 MHz and tuning ability within this range with an impedance of 50 ohm. The phase noise is targeted to be low (approximately less than -120 dBc/Hz) in order to achieve a small noise figure of the entire system. Moreover, the oscillator must have enough power to operate the mixer with low conversion loss.

2.6   Summary

In this chapter, the main components of the CR transmitter system have been fully examined, explained and related to the CR transmitter design and applications.

Moreover, some of the latest and the most important antenna designs and amplifier designs in addition to the design of oscillators have been reviewed.

The design of antennas for cognitive radio transmission must maintain omnidirectional patterns, high gains, and compact sizes in which they can be mounted in portable devices. The surveyed broadband antenna designs are relatively with large dimensions which makes them hard to be implemented in portable devices. The antenna designs presented later in Chapter 3 of this thesis are small antennas with low complexity and broadband bandwidth. In addition, most the surveyed reconfigurable antenna designs suffer from complexity, isolation and biasing techniques, and relatively big size. The reconfigurable antenna proposed later in Chapter 3 of this thesis has a simple structure and a reduced size and depends on the use of tunable inductors to attain reconfigurability.

The design of power amplifiers for the transmitter design in CR applications must provide high output power, high efficiency and linearity behavior. The best amplifiers that can attain these specifications are Doherty amplifiers. Most of the existing power amplifier designs suffer from low efficiency, narrow bandwidth, bad linearity, and relatively low gain. In Chapter 4 of this thesis, the power amplifier designs reported achieve linearity, higher efficiency, and an operating frequency bandwidth between 550 and 1000 MHz.

CHAPTER 3

PROPOSED ANTENNA DESIGNS

3.1 Introduction

In this thesis, three broadband antennas: a reduced-size printed monopole antenna, a meander loop monopole antenna and a planar inverted F antenna (PIFA) suitable for cognitive radio applications in the TV band are proposed. In addition, a reconfigurable compact spiral monopole antenna is also designed. These antennas are printed with small dimensions and can operate in the frequency band 600 – 900 MHz, with omni-directional patterns and an acceptable gain of about 2.5 dB. The bandwidth and the size of these antennas make them suitable for portable devices such as notebooks, tablets, laptops and mobile phones, and convenient for cognitive radio communicating applications in the TV band.

3.2 Broadband Antennas

3.2.1 Reduced-size Printed Monopole Antenna

A reduced-size printed monopole antenna, shown in Fig. 3.1, is designed on a 76 mm x 44 mm Rogers RO3203 substrate with dielectric constant $\varepsilon_r = 3.02$ and thickness h = 1.6 mm. The antenna is fed by a 4 mm width microstrip line over a small partial

ground plane of 7 mm. The size of the reduced-size structure is 54 mm x 44 mm with a width of 2 mm and a gap of 2 mm between the spirals as shown in Fig. 3.1.
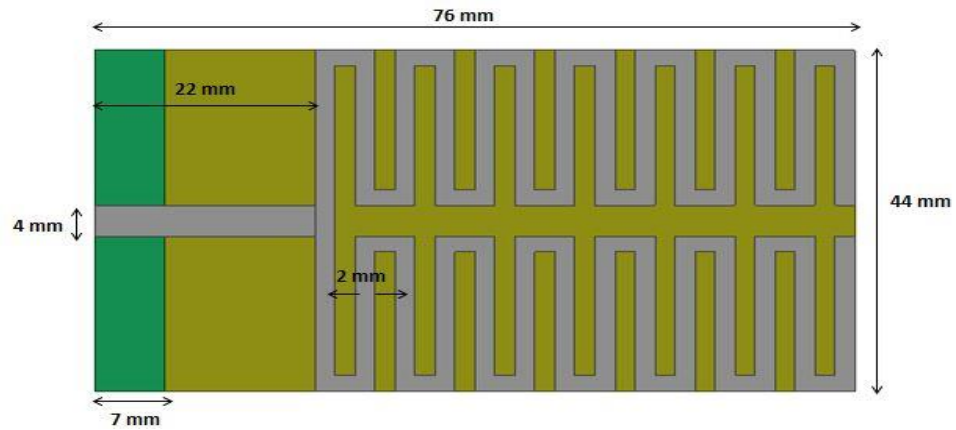
(a)
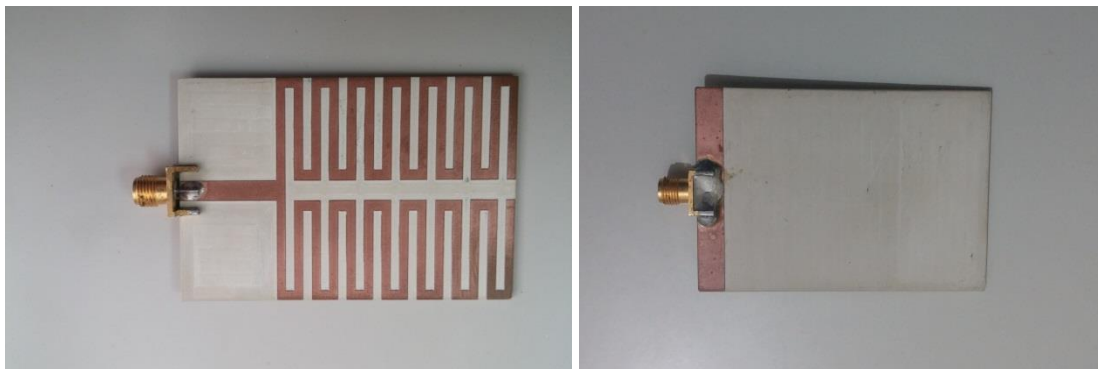
(b)

Fig. 3.1: (a): Configuration and dimensions of the reduced-size monopole antenna, (b): Photo of the fabricated prototype

The size of this antenna is very small compared to antennas operating in the UHF band. This small size allows this antenna to be utilized in portable devices such as mobile phones, tablets, and notebooks.

In this antenna, the meander wire is used as a radiating element, and this is done to reduce the size of the antenna. Globally, the meander line is widely employed as a small radiating element. However, the radiation power and the transmission gain are reduced since the direction of the current on the meander line is usually opposite for neighboring wire, therefore the antenna gain will be low. Yet, the gain can be acceptable given the small size of the antenna. The antenna is designed and simulated using Ansoft HFSS [67].

The fabricated prototype has undergone the needed measurements. The simulated and the measured reflection coefficient plots of the proposed reduced-size printed monopole antenna are given in Fig. 3.2. It is observed that the simulation results and the measurements results are similar with little difference due to some fabrication issues. As stated in [68], antennas used for DVB transmission in the TV band can operate on frequencies having the reflection coefficients below -6 dB. This antenna can operate in the band 785-875 MHz, thus it can be suitable for transmission in cognitive radio applications in the TV band.

Fig. 3.2: Simulated and measured reflection coefficient plots of the reduced-size
monopole antenna

Fig. 3.3 shows the simulated and the measured radiation patterns of the reduced-size
printed monopole antenna. It is observed that the radiation patterns are omni-directional
over its band of operation, with almost equal radiation in the H-plane, and radiation with
the shape of digit 8 in the E-plane.

Fig. 3.3: Simulated and measured radiation patterns of the reduced-size monopole

antenna

Fig. 3.4 shows the simulated and the measured gains for the reduced-size printed monopole antenna in the operating frequency range. It is observed that the peak gain is about 2.25 dBi, and it is located at the resonance frequency of the antenna. The simulation results and the measurements results are similar with little difference. This gain can be considered a good gain given the small size of this antenna.
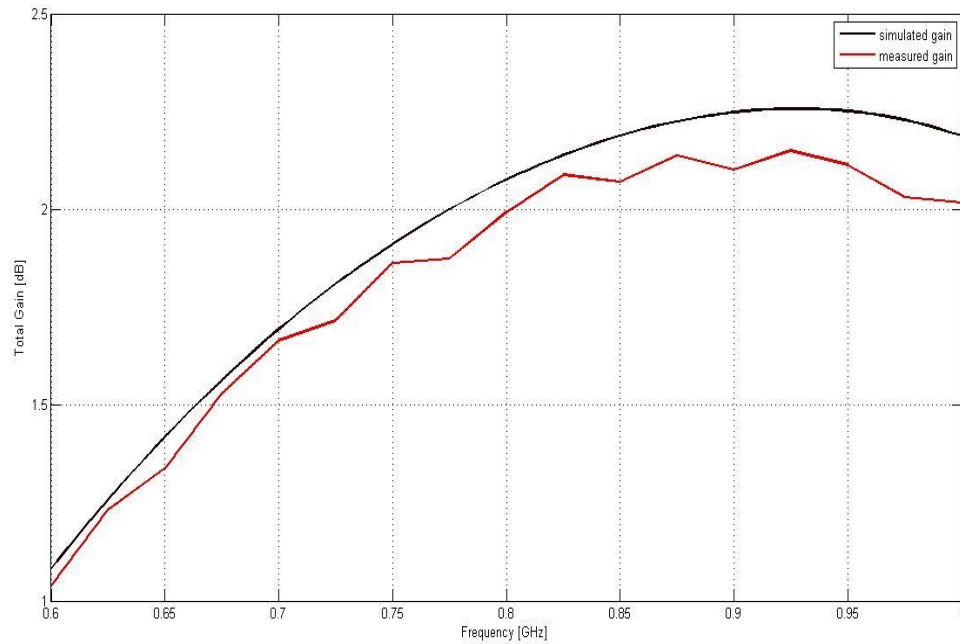
Fig. 3.4 Simulated and measured gain plots of the reduced-size monopole antenna

3.2.2 *Meander Loop Monopole Antenna*

A meander loop monopole antenna, shown in Figure 3.5, is designed on a 150 mm x 40 mm Rogers RO3203 substrate with dielectric constant of 3.02 and thickness h = 1.6 mm. The antenna is fed by microstrip line which starts with a width of 6mm at the port of the antenna and ends with a width of 2 mm at the patch as shown in Fig. 3.5. This shape of the feed line is designed in order to maintain perfect matching of the antenna. The antenna is designed over a partial ground plane with a slot in it. The antenna consists of a meander structure with two straight strip lines with a width of 3 mm.
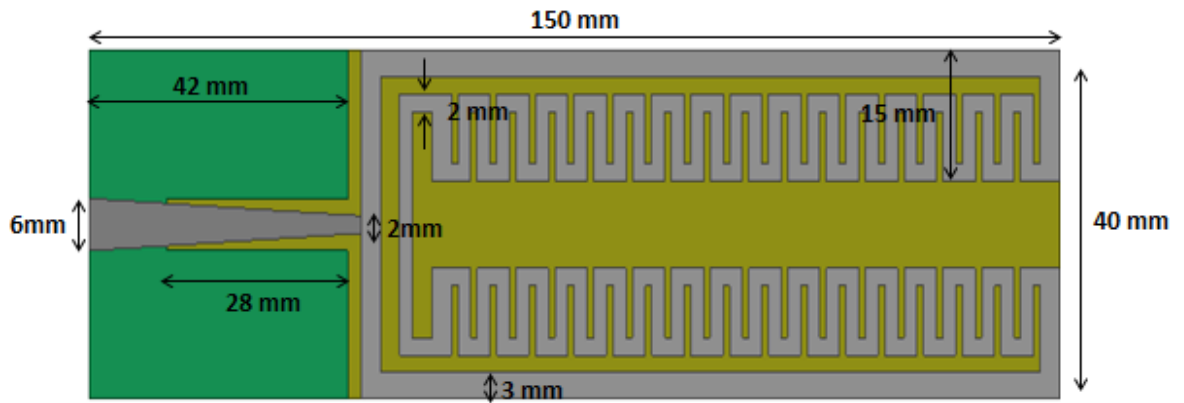
(a)
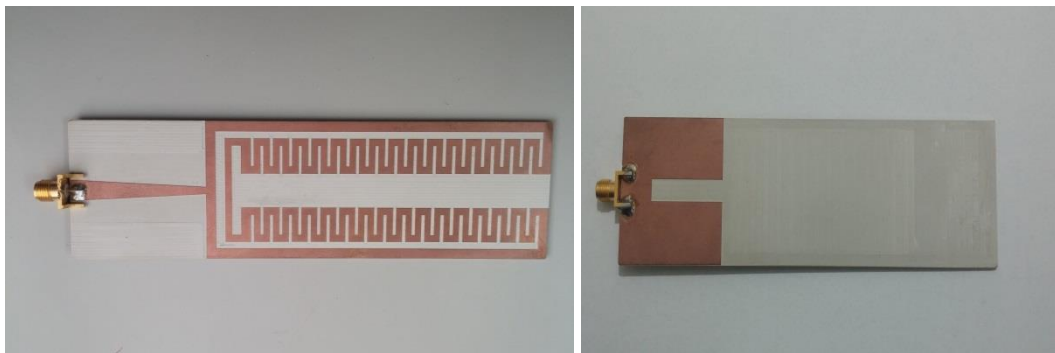
(b)

Fig. 3.5: (a): Configuration and dimensions of the meander loop monopole antenna, (b): Photo of the fabricated prototype

The size of this antenna makes it appropriated for applications in tablets and notebooks. The meander structure is used as a radiating element. The notch in the ground plane serves as an effective way for the gap between the radiating element and the ground plane, and consequently is responsible for the wide operation. The antenna is designed and simulated using Ansoft HFSS [67].

The fabricated prototype of the meander loop monopole antenna has undergone the needed measurements. The simulated and the measured reflection coefficient plots

of the proposed antenna are given in Fig. 3.6. It is observed that the simulation results and the measurements results follow the same pattern with little difference due to some fabrication issues. This antenna can operate in the band 700-900 MHz, thus it can be suitable for transmission in cognitive radio applications in the TV band.
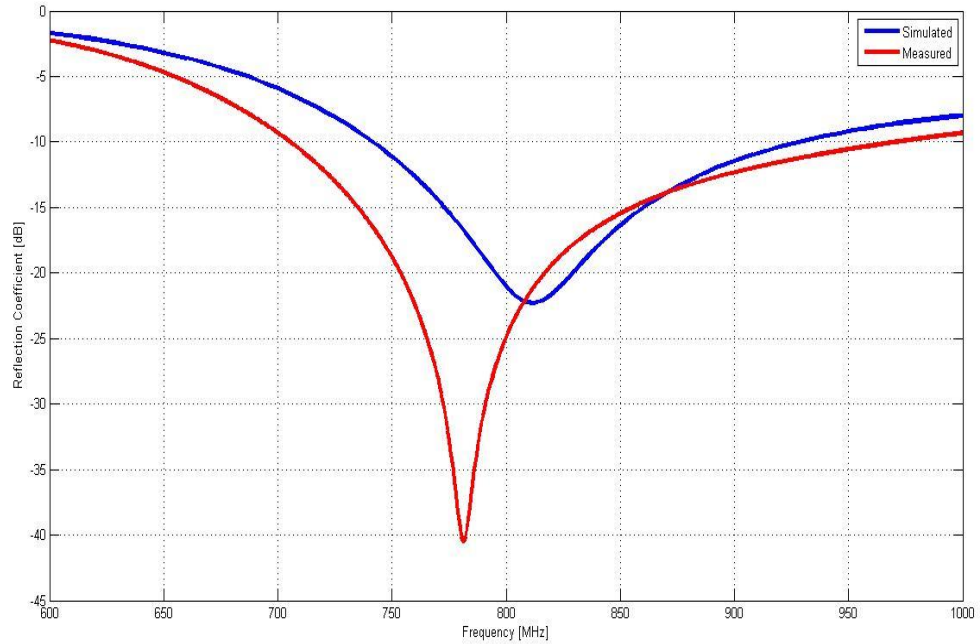
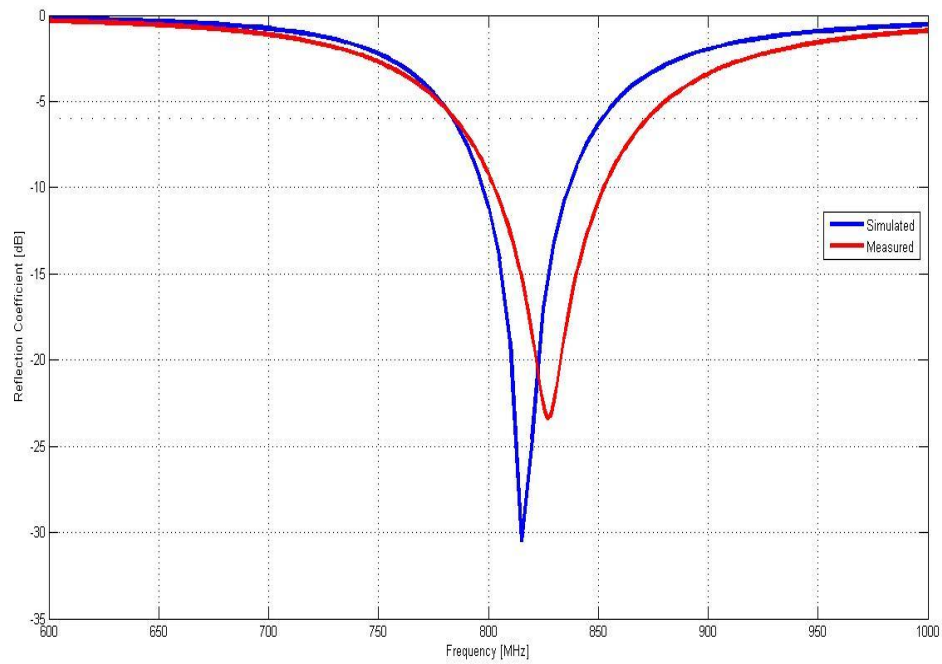Fig. 3.6: Simulated and measured reflection coefficient plots of the meander loop monopole antenna

Fig. 3.7 shows the simulated and the measured radiation patterns of the meander loop monopole antenna. It is observed that the radiation patterns are omni-directional over its band of operation, with almost equal radiation in the H-plane, and radiation with the shape of digit 8 in the E-plane.
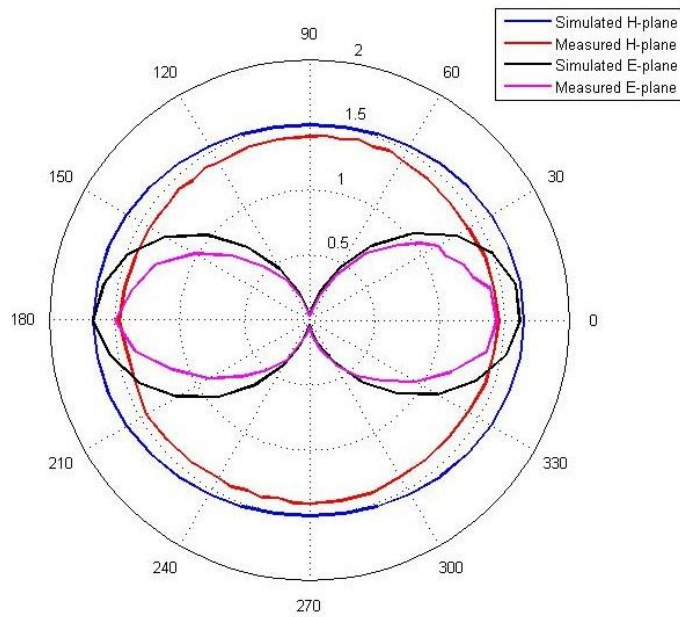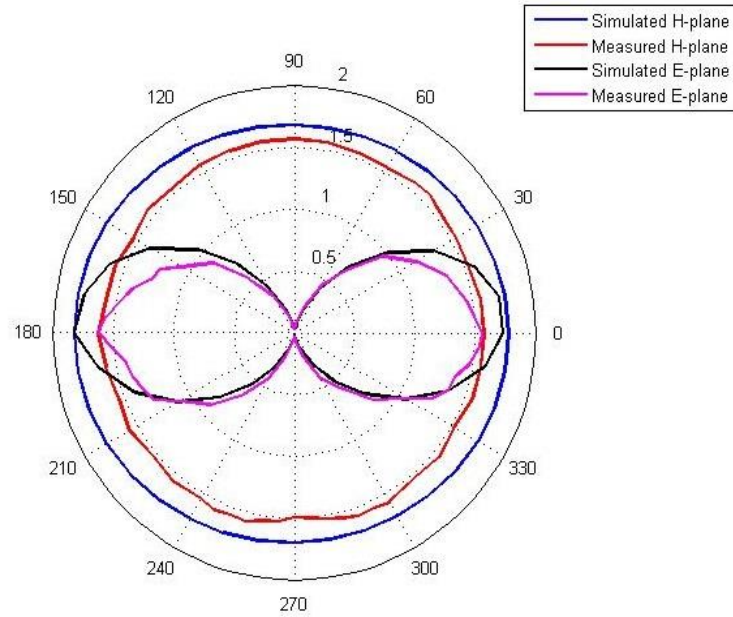
Fig. 3.7: Simulated and measured radiation patterns of the meander loop monopole

antenna

Fig. 3.8 shows the simulated and the measured gains for the meander loop monopole antenna in the operating frequency range. It is observed that the peak gain is about 2.5 dBi, and the gain pattern is approximately flat in the operating frequency band of the antenna. The simulation results and the measurements results are similar with little difference due to some fabrication and measurements issues, with an acceptable gain value.
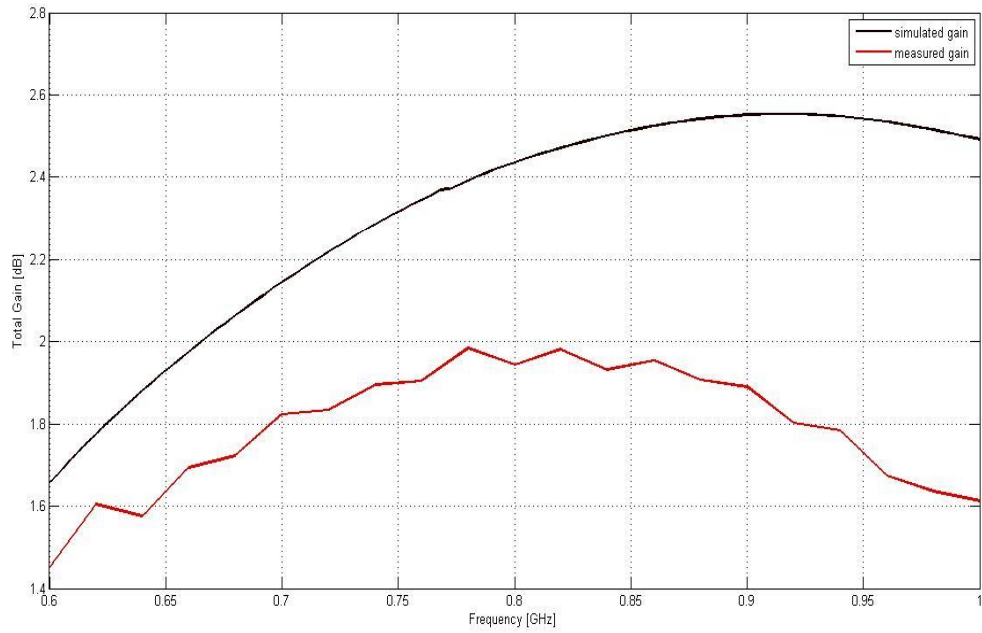
Fig. 3.8: Simulated and measured gain plots of the meander loop monopole antenna

This meander loop monopole antenna has a greater size than the previous mentioned reduced-size printed monopole antenna. However, its resonance bandwidth which is about 200 MHz is much larger than the resonance bandwidth of the first antenna which is about 90 MHz. Therefore, there is a trade-off between the size and the bandwidth, and one can use one of these two antennas according to the type of applications and the number of channels used in the cognitive radio design.

3.2.3 PIFA Antenna

A PIFA antenna is also proposed in this thesis, and its configuration is shown in Fig. 3.9. It is a simple 50 mm x 35 mm patch designed over a full ground plane of dimensions 120 mm x 50 mm. The patch and the ground are connected through a feeding strip and a grounding strip. In order to attain optimum results, the dimensions

are optimized. The width of the feeding strip is 1 mm and that of the grounding strip is 2 mm, and the distance between them is 5 mm.
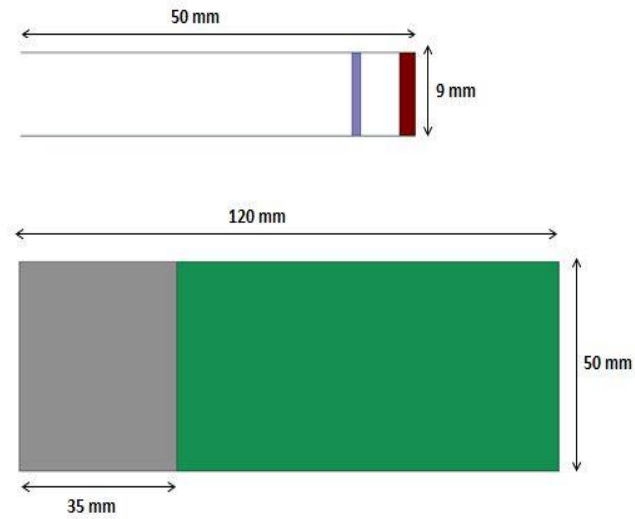
(a)
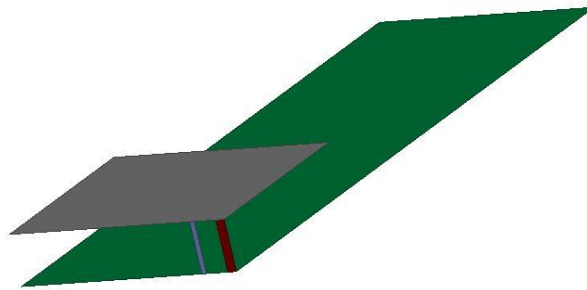
(b)

Fig. 3.9: Configuration and dimensions of the proposed PIFA antenna – (a): Side view and front view, (b): Panoramic view

PIFA antennas are popular for portable wireless devices because of their low profile, small size, built-in structure, and omnidirectional patterns. In mobile phones, there is a single large ground plane that can be placed at the bottom layer of the phone,

and the patch which is of much reduced dimensions can be placed on the opposite layer of the phone. Since the radiation is from the patch away from the ground plane, the energy is directed away from the head giving low values of absorption rates.

The simulated reflection coefficient plots of the proposed PIFA antenna are given in Fig. 3.10. The antenna is simulated via HFSS and CST microwave studio. It is observed that the simulation results of the two software tools follow the same pattern with little difference as the software tools follow two different methodologies (frequency versus time). This antenna can operate in the band 730-900 MHz, and also can be suitable for transmission in cognitive radio applications in the TV band.
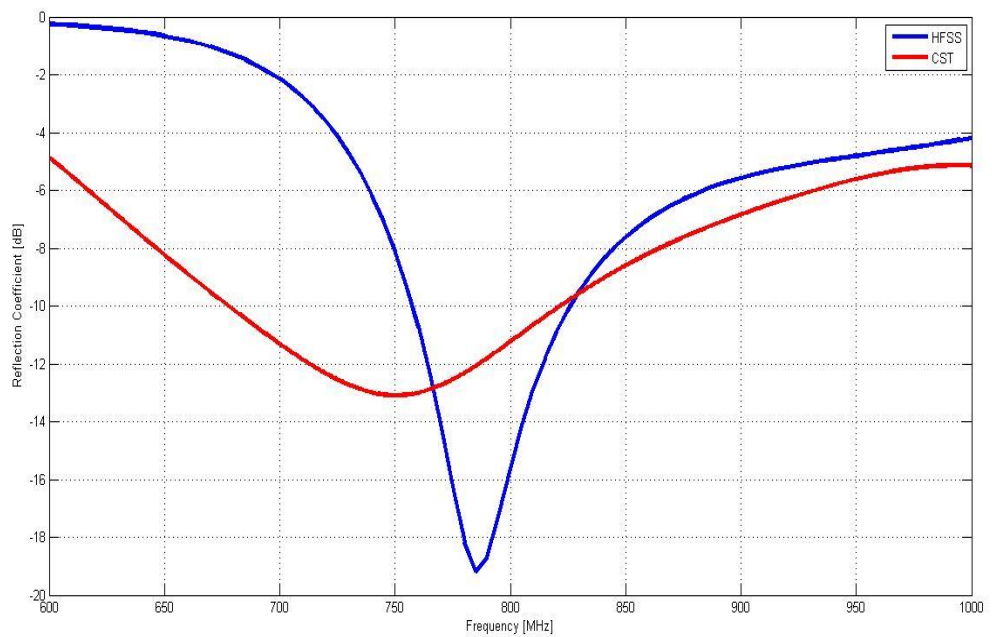

Fig. 3.10: Simulated (HFSS and CST) reflection coefficient plots of the PIFA antenna

Fig. 3.11 shows the HFSS and the CST simulated radiation patterns of the PIFA antenna. It is observed that the radiation patterns are omni-directional over its band of

operation, with almost equal radiation in the H-plane, and radiation with the shape of digit 8 in the E-plane.
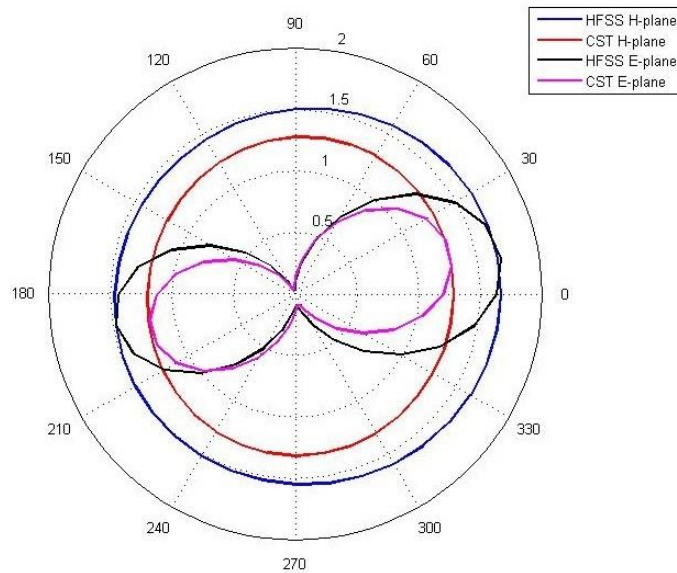
Fig. 3.11: Simulated (HFSS and CST) radiation patterns of the PIFA antenna

Fig. 3.12 shows the HFSS and the CST simulated gains for the PIFA antenna in the operating frequency range. It is observed that the peak gain is about 2.5 dBi, and the gain pattern is approximately flat in the operating frequency band of the antenna. The simulation results of the two software tools are also similar with an acceptable gain given the antenna's dimensions.
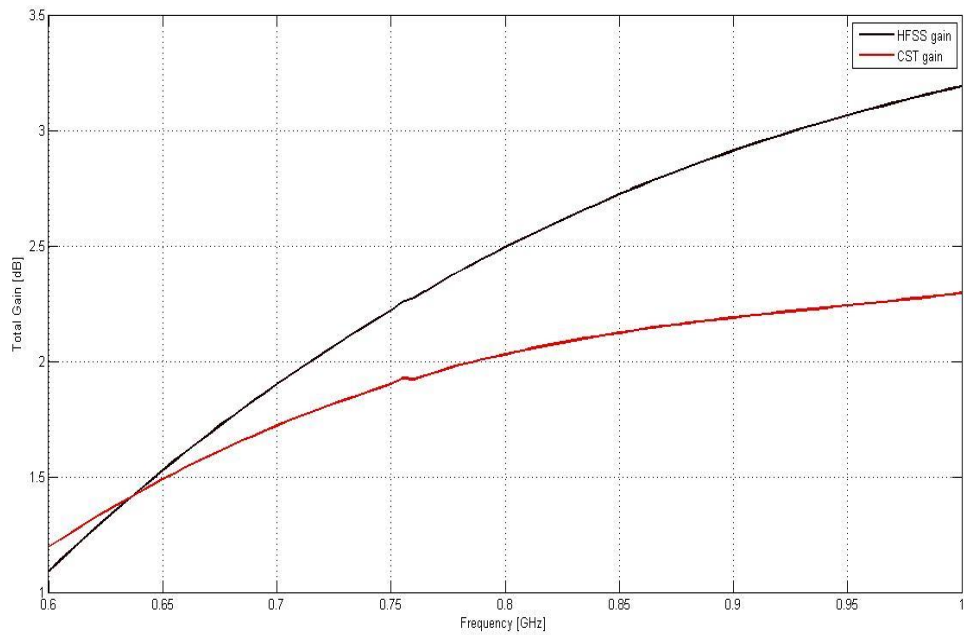
Fig. 3.12: Simulated (HFSS and CST) gain plots of the PIFA antenna

The main advantages of this PIFA antenna in comparison with the two mentioned microstrip antennas are the simple structure and the small size of the patch. These properties allow the PIFA antenna to be fabricated inside handsets and portable devices with low manufacturing cost. However, the PIFA antenna is not printed, as this demands a very high accuracy in fabrication. In addition, this PIFA's bandwidth is higher than the bandwidth of the microstrip antennas since a thick air substrate is used.

3.3   Reconfigurable Antenna

3.3.1   *Reconfigurable Compact Spiral Monopole Antenna*

A square spiral monopole antenna, shown in Fig. 3.13, is designed on a 105 mm x 40 mm FR4 epoxy substrate of thickness h = 0.8 mm and fed by a 2 mm width

microstrip line over a partial ground plane. The size of the spiral structure is 50 mm x 30 mm with a width of 1 mm and a gap of 5 mm between the spirals as shown in Fig. 3.13.
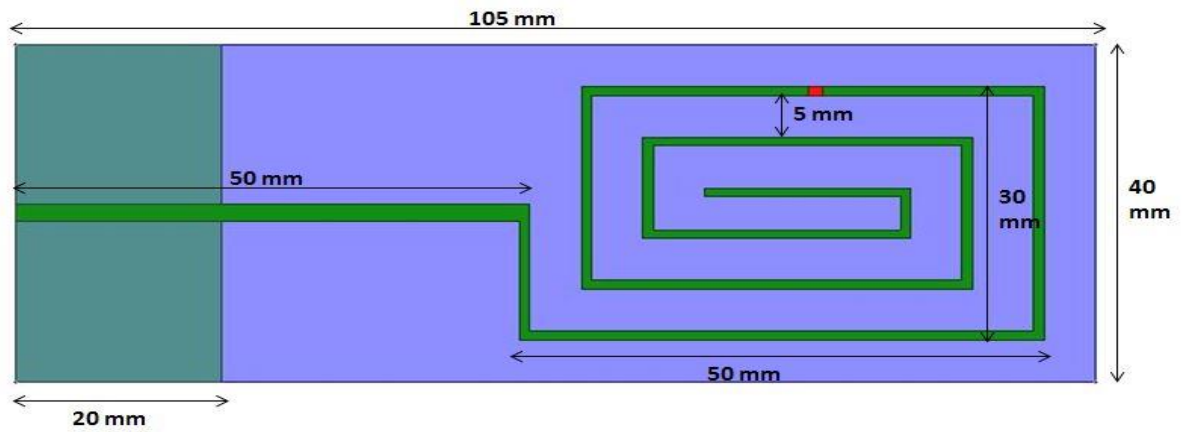
(a)
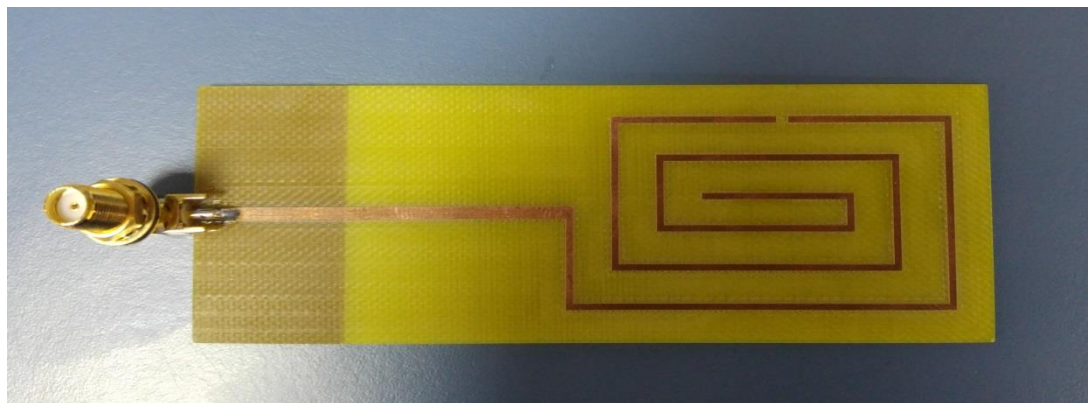
(b)

Fig. 3.13: (a): Configuration and dimensions of the reconfigurable spiral monopole antenna, (b): Photo of the fabricated prototype

The spiral wire is used as a radiating element of the monopole antenna to minimize the size of antenna. As a small radiating element, the meander line is widely employed. However, the radiation power is reduced since the direction of the current on the meander line is opposite for neighboring wire, therefore the antenna gain will be

very low. In our design, the current in the spiral structure is in the same direction for neighboring wire, thus the radiation efficiency is enhanced and the gain is improved.

Frequency reconfigurability is obtained by inserting a tunable inductor (Chip Inductor – 0603CT) on the spiral monopole as shown in Fig. 3.13 (red color) and modifying its inductance. This idea of reconfigurability was used in [69]. The size of the tunable inductor is compatible with the size of the spiral and its inductance ranges between 1 and 56 nH. The antenna is designed and simulated using Ansoft HFSS [67].

The simulated reflection coefficient plots of the reconfigurable antenna are given in Fig. 3.14 for the indicated inductance values. It is clear that frequency reconfigurability has been achieved. Considering four different values for the inductor, i.e. L= 1, 5, 10.5 and, 27 nH, frequency reconfigurability is attained in the higher part of the UHF band (600 - 800 MHz) and the antenna can operate at different bands in this 600 – 800 MHz range. These bands range between 15 to 20 MHz which is suitable for TVWS applications especially for mobile communications, TV broadcasts, and WhiteFi applications.
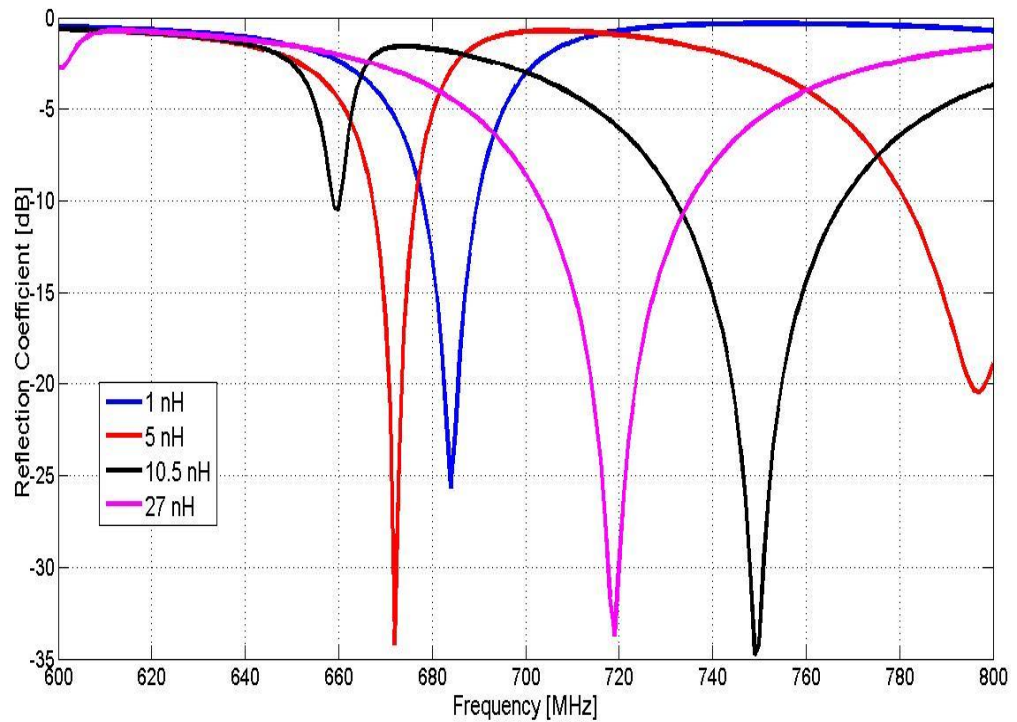
Fig. 3.14: Simulated reflection coefficient plots of the reconfigurable spiral monopole antenna for different inductance values

The fabricated prototype has undergone the needed measurements. The inductor is added and welded in its place on the spiral monopole as shown in Fig. 3.15. Three inductors from the SMD 0603 CT kit are welded and they have undergone S-parameters measurements. The inductor values are: 1 nH, 10.5 nH, and 27 nH.
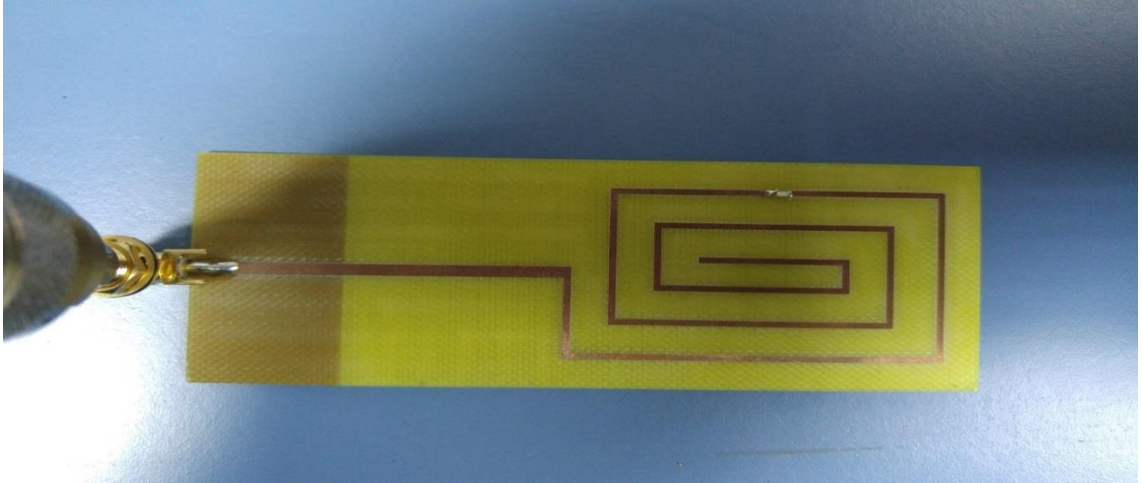
Fig. 3.15: Photo of the fabricated prototype with the inductor welded in its place

Fig. 3.16 shows the reflection coefficients of the simulated and the measured results for the inductance values: 1 nH, 10.5 nH, and 27 nH. It is observed that the simulation and the measurements results are similar following the same shape with a little shift due to some fabrication and measurements errors. Considering these three values of inductance, we can notice that reconfigurability of this antenna is also revealed in measurements.

(a)

60
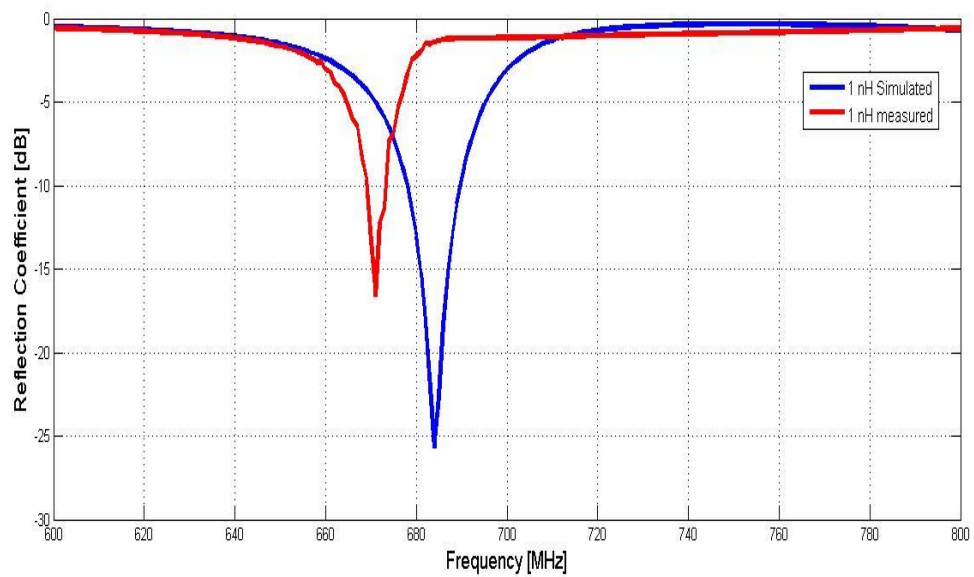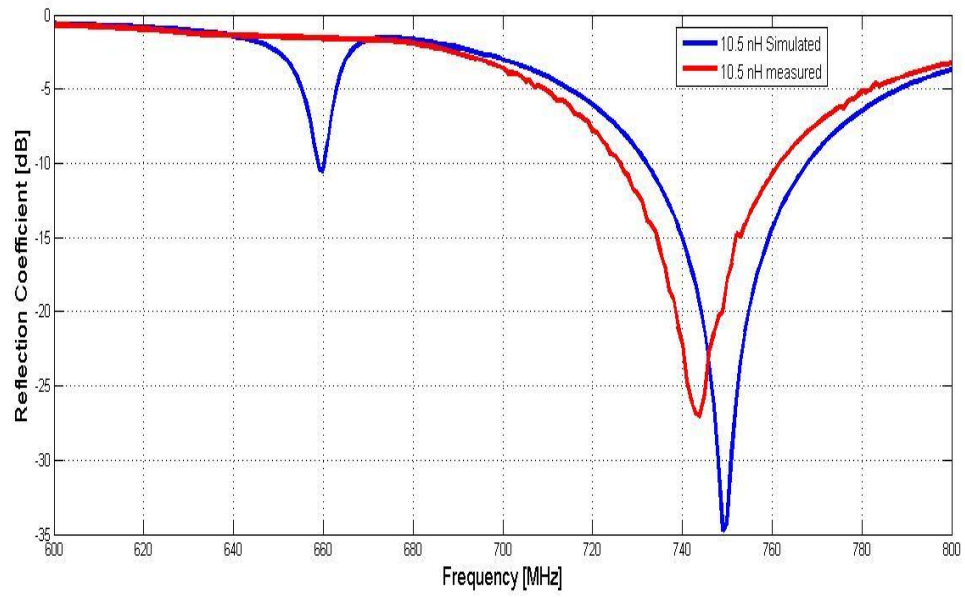
(b)
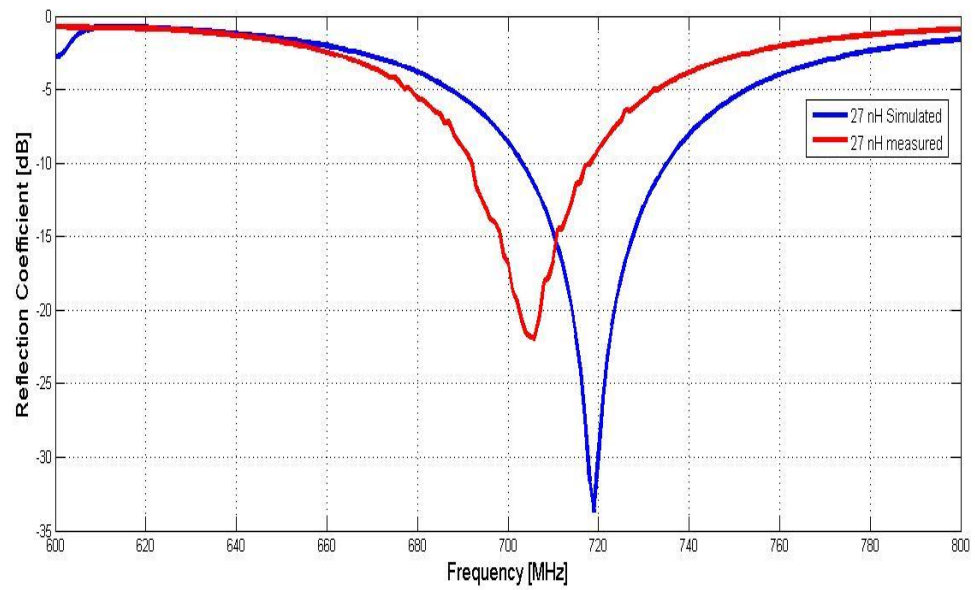
(c)

Fig. 3.16: Simulated and measured reflection coefficient plots of the reconfigurable

spiral monopole antenna for the inductance values: (a): 1 nH, (b): 10.5 nH, (c): 27 nH

The gain of the proposed antenna is given in Fig. 3.17. It is about 1 dB: a good gain given the small size of this antenna. The radiation patterns of this antenna are omni-directional over its bands of operation, as shown in Fig. 3.18, with almost equal radiation in the H-plane, and radiation with the shape of digit 8 in the E-plane.
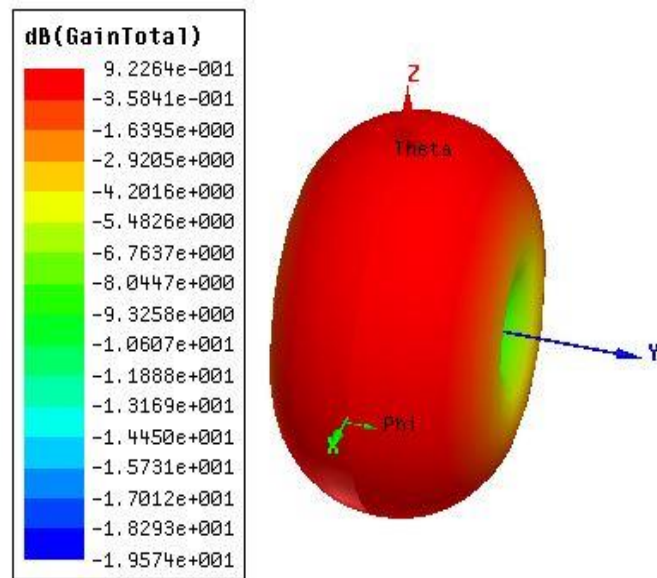
Fig. 3.17: Simulated gain of the reconfigurable spiral monopole antenna
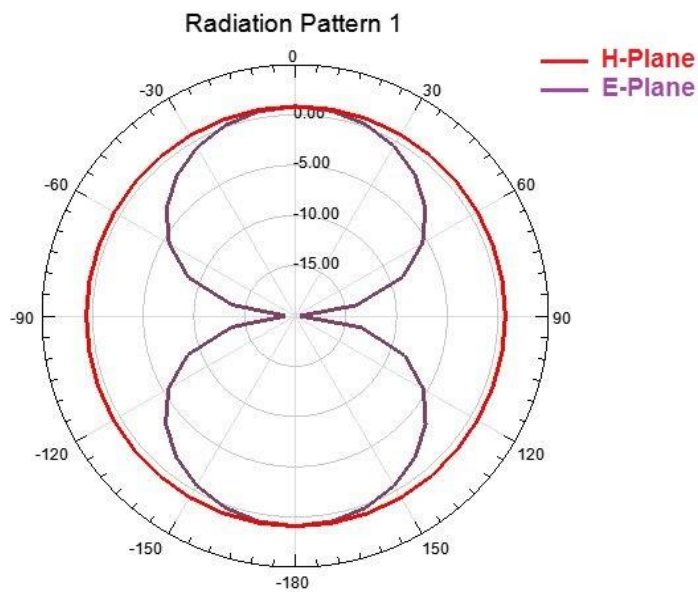
Fig. 3.18: Simulated radiation patterns of the reconfigurable spiral monopole antenna

In comparison with the antennas surveyed in this thesis, it is clearly demonstrated that our designed antennas have simpler structure and reduced dimensions. This is shown in Table 3.1.

Work	Dimensions
[14]	128 mm x 51 mm
[15]	170 mm x 15 mm
[17]	247 mm x 35 mm
[18]	247 mm x 35 mm
[19] (IFA)	90 mm x 50 mm
[20]	60 mm x 49 mm for patch 107.5 mm x 73 mm for ground
Reduced-size Printed Monopole Antenna	76 mm x 44 mm
Meander Loop Monopole Antenna	150 mm x 40 mm
PIFA	35 mm x 50 mm for patch 120 mm x 50 mm for ground
Reconfigurable Spiral Monopole Antenna	105 mm x 40 mm

Table 3.1: Comparison between the proposed antennas in this thesis and previous surveyed antennas

3.4 Summary

In this chapter, a reduced-size printed monopole antenna, a meander loop monopole antenna and a planar inverted F antenna suitable for cognitive radio applications in the TV band have been presented. Moreover, a reconfigurable compact planar spiral monopole antenna suitable for TVWS applications has been also proposed. These antennas have compact size and reduced dimensions, and operate in the TV frequency band, with omni-directional patterns and acceptable gains. These characteristics make them convenient for portable devices such as laptops, notebooks, tablets and mobile phones. In addition, these antennas can be implemented in the CR transmitter system.

CHAPTER 4

PROPOSED POWER AMPLIFIER DESIGNS

4.1 Introduction

This chapter deals with the design of power amplifiers suitable for TV band applications. In this chapter, an AB power Amplifier and a Doherty power amplifier utilizing the previous amplifier and a designed class C power amplifier are designed. A class AB power amplifier is firstly implemented using a commercial GaN HEMT from Cree incorporation, achieving a high power-added-efficiency of 77.78% and a 40.593 dBm output power with an associated gain of 21.65 dB. The Doherty amplifier has then been designed following the previous class AB scheme for the main amplifier and a class C scheme for the peak one. This amplifier attained a high power-added-efficiency of 81.94%, a 42.77 dBm output power, an associated gain of 21.32 dB, and an operating frequency bandwidth between 550 and 1000 MHz (58.06 % fractional bandwidth) which make it suitable for TV band applications. The characteristics of these proposed power amplifiers make them good candidates to be mounted in the cognitive radio transmitter system.

4.2 AB Power Amplifier

The schematic of this proposed class AB amplifier is shown in Fig. 4.1. The amplifier is simulated in both software, ADS and National Instruments AWR Design

Environment [70]. The active device employed in the AB amplifier is the CGH40010 from Cree inc., a GaN HEMT with a typical output power of 10 W at the suggested drain bias voltage of 28 V. The detailed datasheet of the Cree model CGH40010 is given in Appendix A. This transistor offers high efficiency, high gain, and wideband capabilities. The amplifier circuit was simulated with a constant drain supply voltage Vsup = 28 V and the gate bias voltage Vg = -2.1 V which represents a bias condition of a conventional class AB amplifier. The substrate parameters were set according to FR4 epoxy substrate with dielectric constant ε_r = 4.4 and thickness h = 1.6 mm, on which the amplifier is designed.
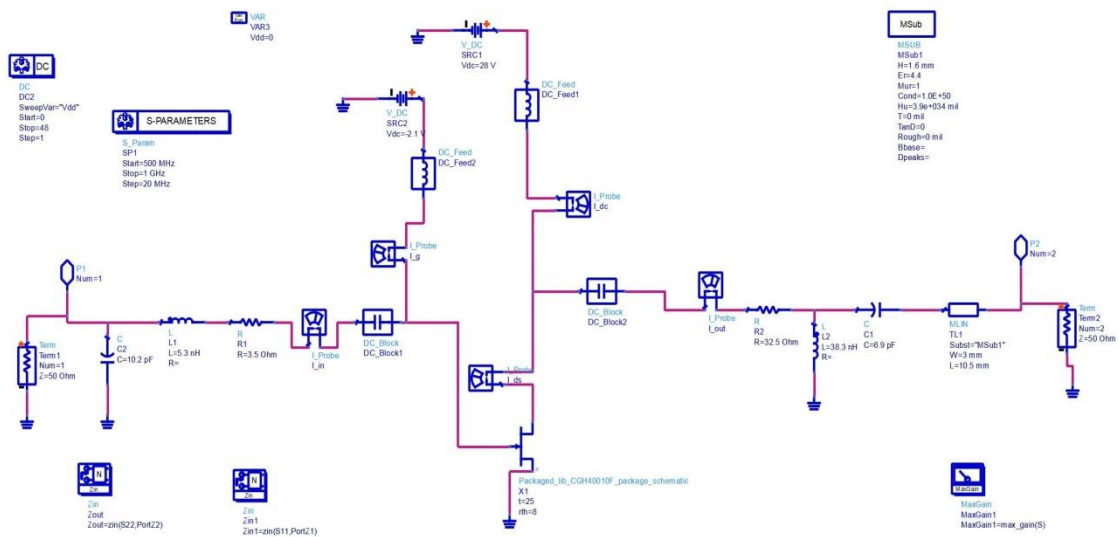
(a)
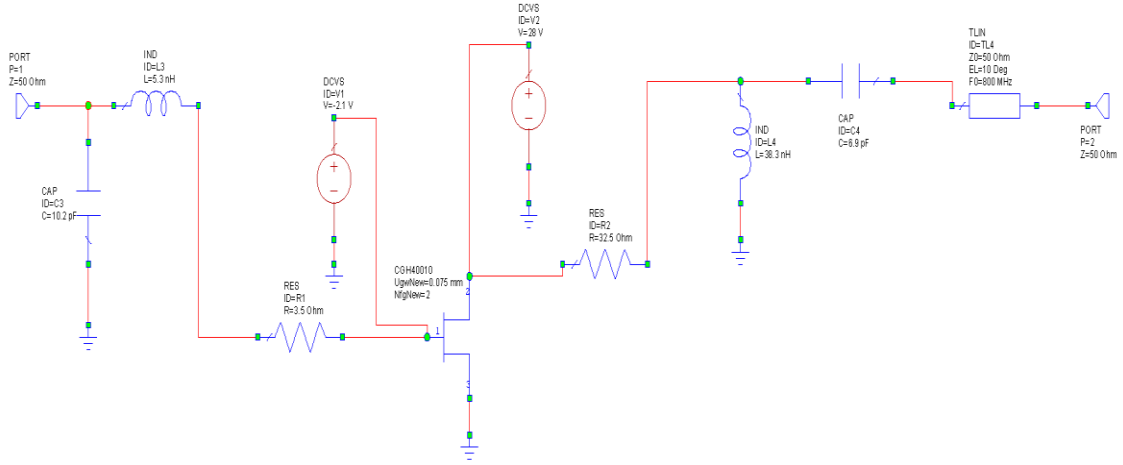
(b)

Fig. 4.1: Schematic of the class AB power amplifier with input and output stability

resistors and matching circuits − (a): in ADS, (b): in AWR

To verify the accurate representation of the Cree CGH40010 model, the signal
scattering parameters generated from ADS for the frequency 800 MHz were compared
to the ones given in the datasheet. Close agreement, as presented in Table 4.1, is
obtained.

	S11	**S12**	**S21**	**S22**
Simulation	$0.911 \llcorner -154^0$	$0.023 \llcorner 3.54^0$	$11.933 \llcorner 89.38^0$	$0.298 \llcorner -132.5^0$
Datasheet	$0.894 \llcorner -146.96^0$	$0.029 \llcorner 6.84^0$	$11.58 \llcorner 91.78^0$	$0.317 \llcorner -109.84^0$

Table 4.1: S-parameters of the GaN transistor at 800 MHz

After carrying out the stability test of this amplifier, it is found that the device is potentially unstable in the frequency range of interest. Indeed, the stability parameters, Δ, and the rollet factor k are calculated and found to be:

$\Delta = 0.092 \angle -8.6^0$

$k = 0.163$

This means that the device is potentially unstable. Stabilization methods were performed and series resistances were added to the input and the output of the transistor as shown in Fig. 4.1. The input resistance is 3.5 Ohms and the output resistance is 32.5 Ohms. After adding these resistances, the stability parameters were recalculated and found to be:

$\Delta = 0.162 \angle -146.4^0$

$k = 1.57$

After adding the stability resistances, the signal scattering parameters at 800 MHz had changed. The scattering parameters were simulated and found to be (at 800 MHz):

$S11 = 0.772 \angle -157.51^0$

$S12 = 0.016 \angle -0.034^0$

$S21 = 8.057 \angle 85.81^0$

$S22 = 0.17 \angle -39.773^0$

In order to maintain maximum power transfer, we need to match the impedance of the load to that of the source, so matching circuits are designed at the input and the output of the transistor. These circuits are accomplished by using passive networks and microstrip transmission lines as shown in Fig. 4.2.

(a)   (b)
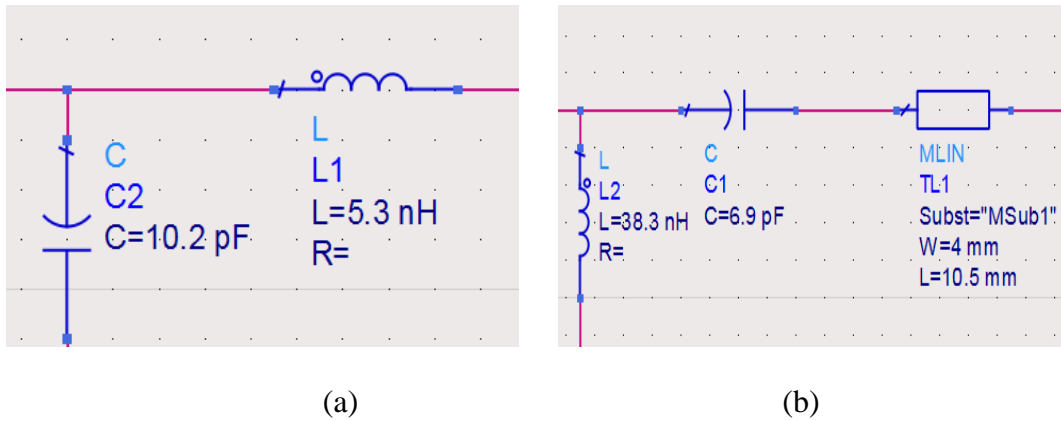
Fig. 4.2: (a) Input matching network, (b) Output matching network of the class AB

power amplifier

After completing the stability and the matching of the amplifier, the final signal

scattering parameters at 800 MHz were simulated and found to be:

$S11 = 0.056 \angle -119.8^0$

$S12 = 0.024 \angle -72.2^0$

$S21 = 12.073 \angle 13.6^0$

$S22 = 0.438 \angle -89.4^0$

By feeding the amplifier with an optimum 800 MHz, 18.943 dBm input power,

the output power of the amplifier circuit was found to be 40.593 dBm and the gain is

21.65 dB. The DC power is simulated and found to be:

Pdc = 28 x 0.522 = 14.62 W

Thus, the power added efficiency (PAE) is computed to be around 77.78 %. All the

results are summarized in Table 4.2.

Input Power (dBm)	DC power (W)	Output Power (dBm)	Gain (dB)	PAE (%)	Drain efficiency (%)
18.943	14.62	40.593	21.65	77.78	78.4

Table 4.2: Final results of the class AB power amplifier

The amplifier efficiency depends on the DC supply voltage and respectively on the input power. Fig. 4.3 shows the output power sweep curve as well as the corresponding PAE. As the DC voltage increases, the output power increases fairly linearly indicating that the amplifier has a constant gain. The efficiency also increases approximately linearly until it reaches the maximum at the optimum 28 volt DC supply voltage. In addition, while varying the DC voltage, the output varies and thus, the transmit power can be varied, and this is a need of a cognitive radio transmitter.
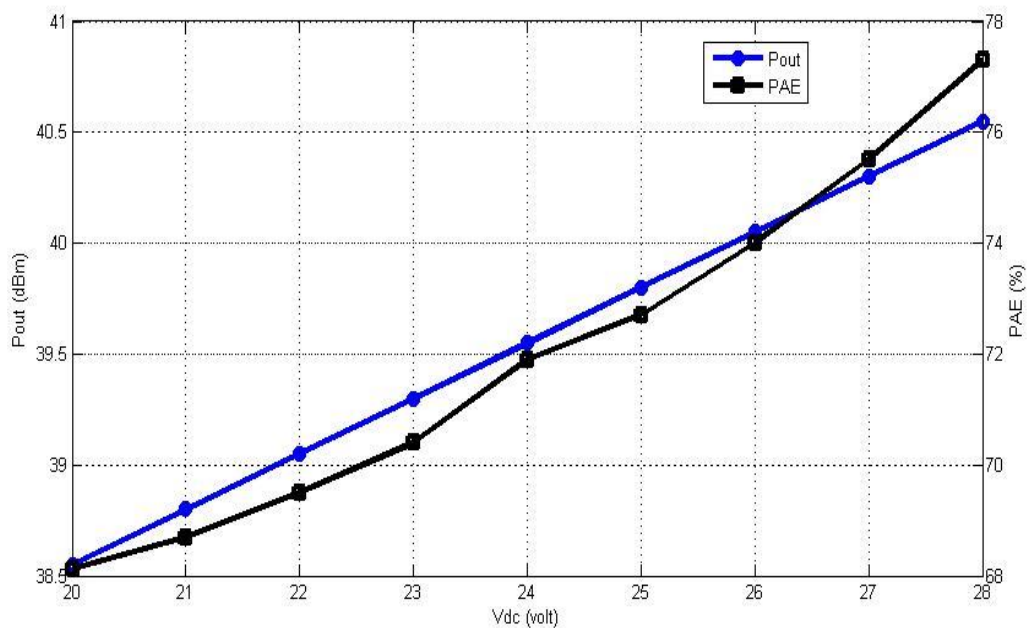
Fig. 4.3: Output power and PAE versus DC voltage in the class AB power amplifier

70

The voltage standing wave ratio (VSWR), which is a measure of how efficiently RF power is transmitted from the power source through the AB amplifier to the antenna, is found to be as follows:

VSWR$_{in}$ = 1.12:1

VSWR$_{out}$ = 1.56:1

The VSWR of the AB amplifier is approximately equal to 1 which means most of the power is transferred in the amplifier.

The simulated reflection coefficient plots of the class AB amplifier are given in Fig. 4.4. The amplifier is simulated via ADS and AWR software. It is clearly shown that this amplifier can operate from 650 MHz to 910 MHz, thus it is suitable for applications in the TV band. It is observed that the simulation results of the two software tools follow the same pattern with little difference.

The percentage bandwidth or the fractional bandwidth, which is a measure of how wideband the amplifier is, is given by this equation:

$\%BW = (f2 - f1)/((f1 + f2)/2)$

The percentage bandwidth of this amplifier is 33.33 %.
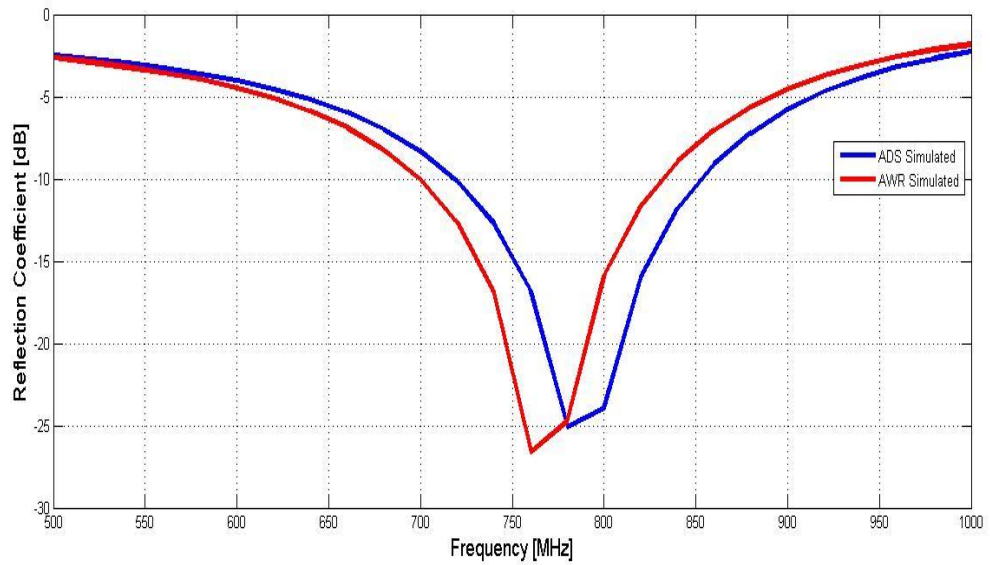
Fig. 4.4: Simulated (ADS and AWR) reflection coefficient plots of the class AB power amplifier

The power gain plot of the class AB amplifier is given in Fig. 4.5. It is clearly shown that this amplifier has a good power gain above 19 dB for the operation frequency bandwidth. However, it suffers from little non-linearity above 830 MHz.
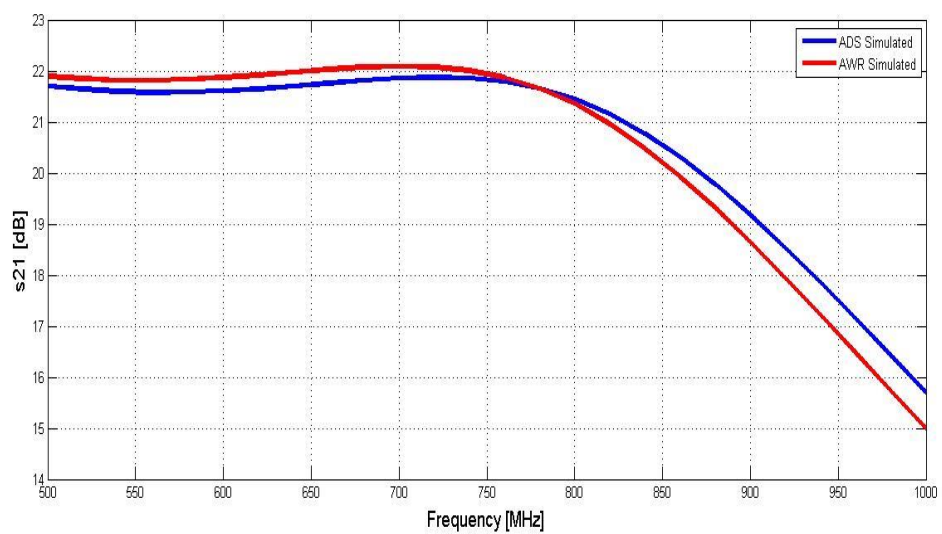
Fig. 4.5: Simulated (ADS and AWR) power gain plots of the class AB power amplifier

4.3   C Power Amplifier

In this chapter, a C class amplifier using an InGaP HBT device is firstly proposed. It is designed to operate in the high part of the UHF band with a center frequency of 800 MHz. The amplifier is successfully simulated with matching circuits at the input and the output achieving a high power added efficiency of 77.51%, 38.32 dBm output power, and an associated gain of 20.46 dB.

This class C amplifier is performed using ADS. For this particular design, a packaged InGaP HBT (ADL 5602) was chosen. To verify that the model provided an accurate representation of our device samples, small signal scattering parameters generated from ADS were compared to the ones given in the datasheet and it shows close agreement. The detailed datasheet of the ADL 5602 device is given in Appendix B.

$s11 = 0.007 \angle -130.764^0$

$s12 = 0.072 \angle 2.303^0$

$s21 = 10.541 \angle 166.476^0$

$s22 = 0.048 \angle 136.68^0$

A schematic of this amplifier is shown in Fig. 4.6. L-type input and output matching circuits using inductors and capacitors are added to the amplifier in order to have a 50 ohm impedance matching.
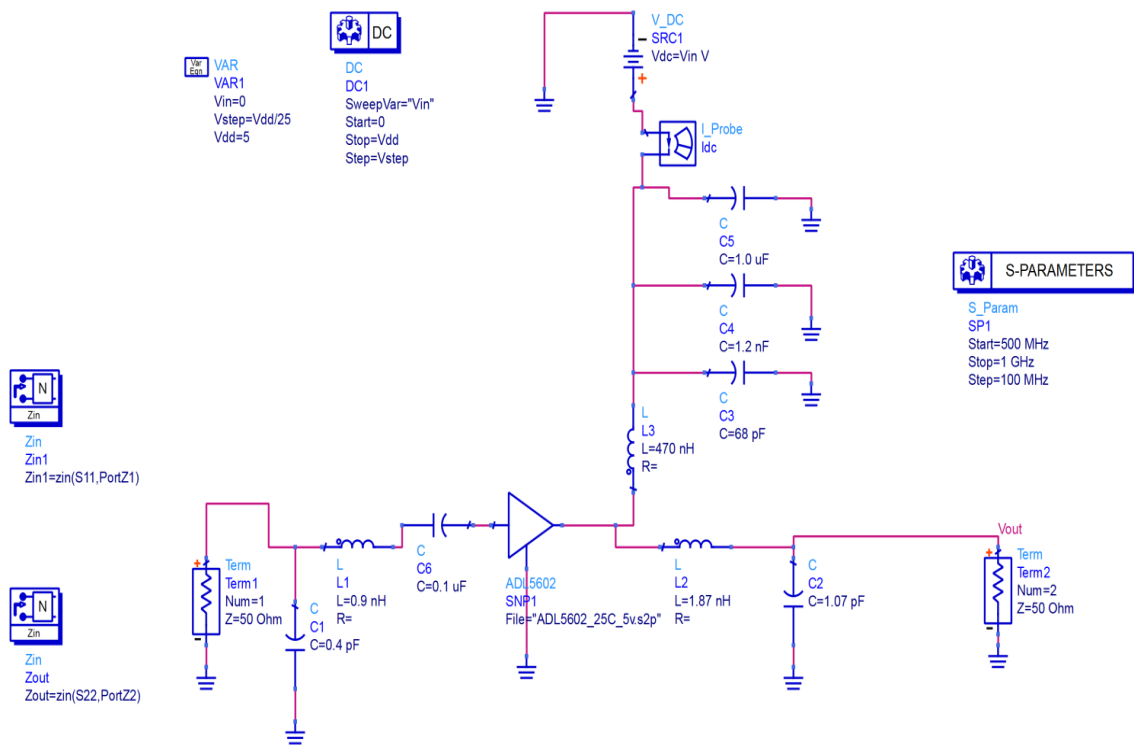
Fig. 4.6: ADS schematic of the class C power amplifier

The simulation results focus on the dc supply voltage, the current waveforms and the s-parameters. At a supply voltage Vdd = 5 volts, the dc power if found to be 8.7 W. The gain is calculated and found to be equal to 20.45 dB. With an input power of 17.87 dBm and a dc supply power of 8.7 W, the output power is 6.805 W (38.32 dBm). This gives a power added efficiency PAE = 77.51%.

4.4 Doherty Power Amplifier

One of the key elements of any power amplifier design is the efficiency level. This affects many issues including overall power consumption, battery life, and output device capability, etc. As shown in the two previous designed power amplifiers, the

efficiency is not as good as what power amplifiers need. The efficiency of the C class power amplifier is better than that of the AB power amplifier; however its output power is less than that of the AB one. In order to increase the efficiency and have a respectable output power and a linear amplifier operating mode, a Doherty power amplifier is designed. This amplifier is designed from the two previous amplifiers; where the AB amplifier is used as a carrier amplifier and the C class one is used as peak amplifier. Respective input matching network and output matching network are designed and the two power amplifiers are connected at the output through a quarter-wave transmission line.

The DPA configuration used in this thesis is the well-known conventional AB-C scheme as shown in Fig. 4.7.
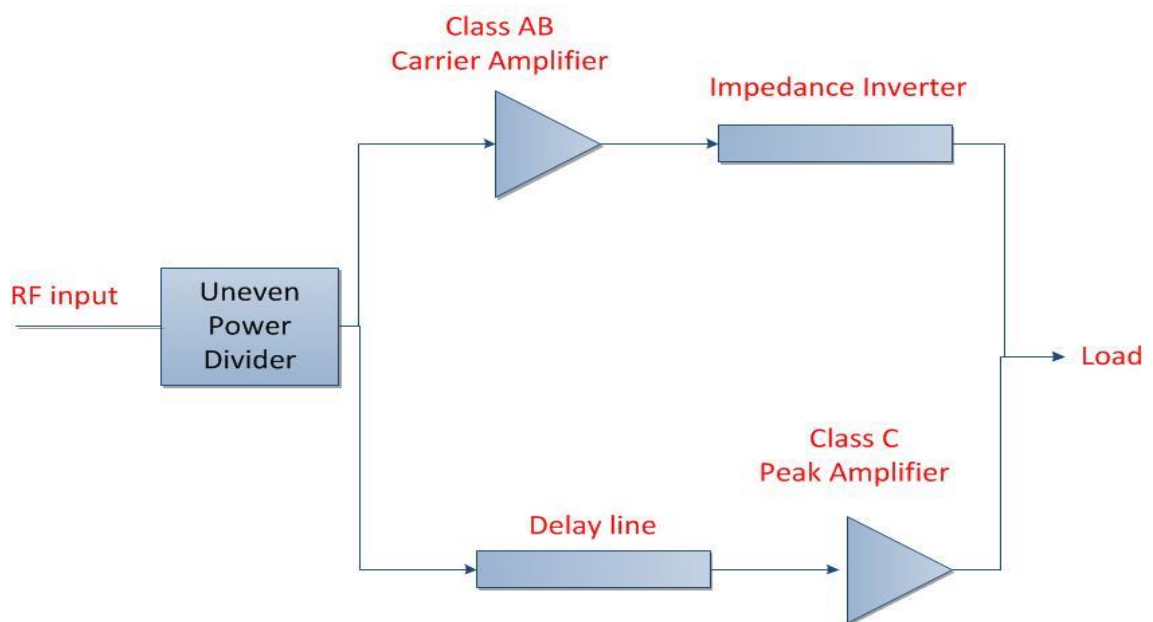
Fig. 4.7: Block scheme of the designed AB-C DPA

Before looking at the Doherty amplifier design, it is necessary to look at the basic operation of the amplifier. The DPA operating principle is based on the idea to

modulate the load of the carrier device by using a peak device. The signal enters the overall amplifier through a power divider. This creates two signals that are phase shifted by 90° with respect to each other. As previously mentioned, the 90° split is needed because the peaking amplifier output requires a 90° delay with respect to the carrier amplifier in order to be in step with the carrier amplifier output. This is materialized through the delay transmission line. One output is presented to the carrier amplifier which is used to accommodate the lower power levels encountered around the average power level. In this case, the amplifier operates near its compression point and provides optimum efficiency for these power levels. The signal is also presented to the peaking amplifier. When the carrier amplifier goes into compression and large peaks appear, in which it is not able to accommodate on its own, the peaking amplifier starts operating and boosts the output power in order to meet the higher power level conditions. Being a high power amplifier, the carrier amplifier can not provide high levels of efficiency itself, and therefore the peaking amplifier operates when higher power levels are present. In this way optimum efficiency is obtained over all the power ranges. Once the signal passes through the two amplifier circuits themselves, the outputs are combined. The output of the carrier amplifier is presented to an impedance inverter which also has a 90° phase shift. This is used to counteract the phase shift at the input. As a result, the signals from the two amplifier sections remain in phase.

Moving to the design of the DPA, some interesting issues are introduced. The main design challenges include:

- Impedance matching: Ensuring that the impedance of both amplifiers is sufficiently maintained over the operating range.

76

- Bandwidth: Ensuring that the amplifier can operate on the required band.

- Linearity maintenance: Maintaining linearity operation over the whole operating range because some disturbances in the linearity of the amplifier can occur as the peaking amplifier starts to operate.

Hereby is a detailed procedure of designing a Doherty power amplifier.

1. The active devices (transistors) employed in the DPA are specified. They must operate on a wide range of frequencies and have an adequate output power.

2. These active devices are fully matched to ensure maximum power transfer, so input and output matching networks are implemented in the main and the peak amplifiers.

3. Stability of the main and the peak amplifiers are investigated to make sure the two amplifiers are unconditionally stable.

4. The two amplifiers are connected to each other following the well-known Doherty circuit with two transmission lines serving as impedance transformers in order to achieve the main load modulation.

5. An input power divider is inserted before the two amplifiers in order to split the power between the main and the peak amplifiers.

6. The DPA is then matched to attain maximum power transfer, so input and output matching circuits are designed for this purpose.

7. The stability of the DPA is examined and updated so that the DPA is unconditionally stable.

8. Finally, the circuit is fabricated on a primarily specified substrate.

A flow chart which briefly describes steps of designing a Doherty Amplifier is given in Fig. 4.8
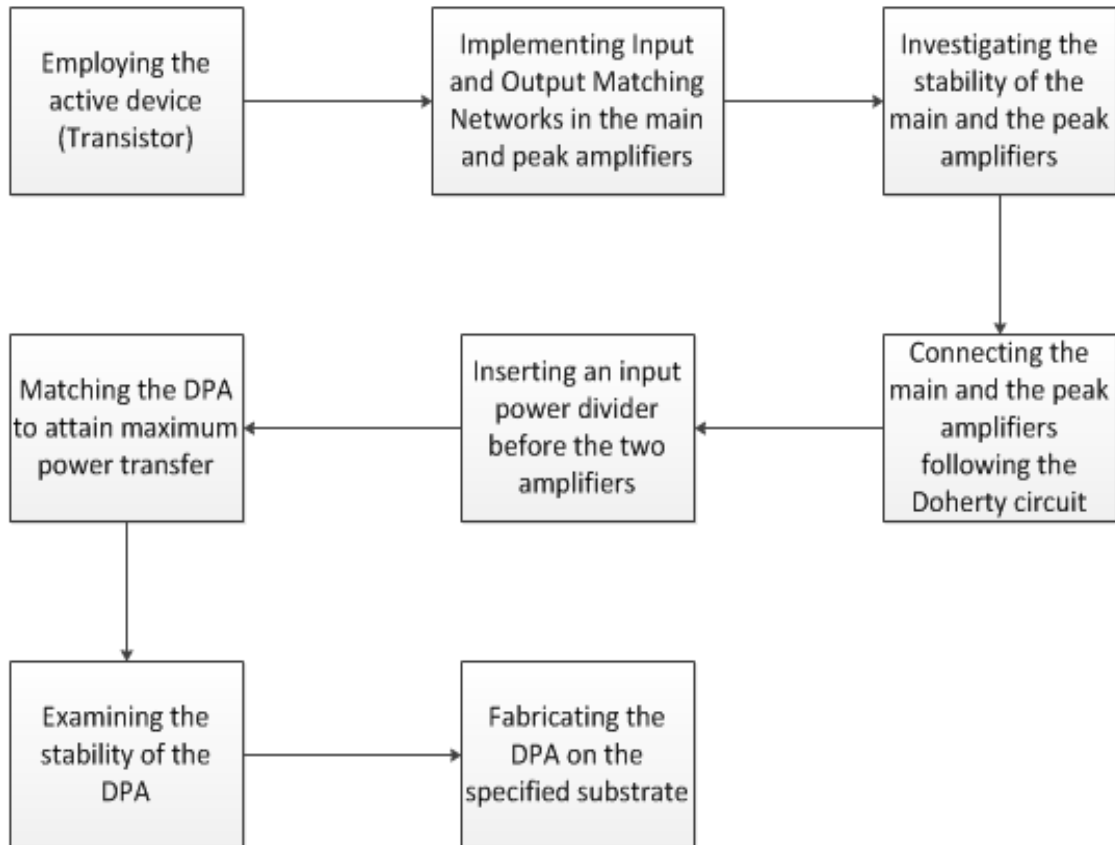
Fig. 4.8: A flow chart of the steps of designing a Doherty power amplifier

Fig. 4.9 shows the simulated circuit schematic of the proposed AB-C DPA, where the main and the peak amplifiers are as mentioned before. The amplifier is simulated in both software, ADS and AWR. A broadband 90^0 hybrid coupler was used at the input in order to split the signals between the carrier and the peak amplifying paths. The electrical lengths of the delay and the impedance inverter microstrip lines were optimized to ensure maximum power transfer, maximum efficiency, and adequate output power.
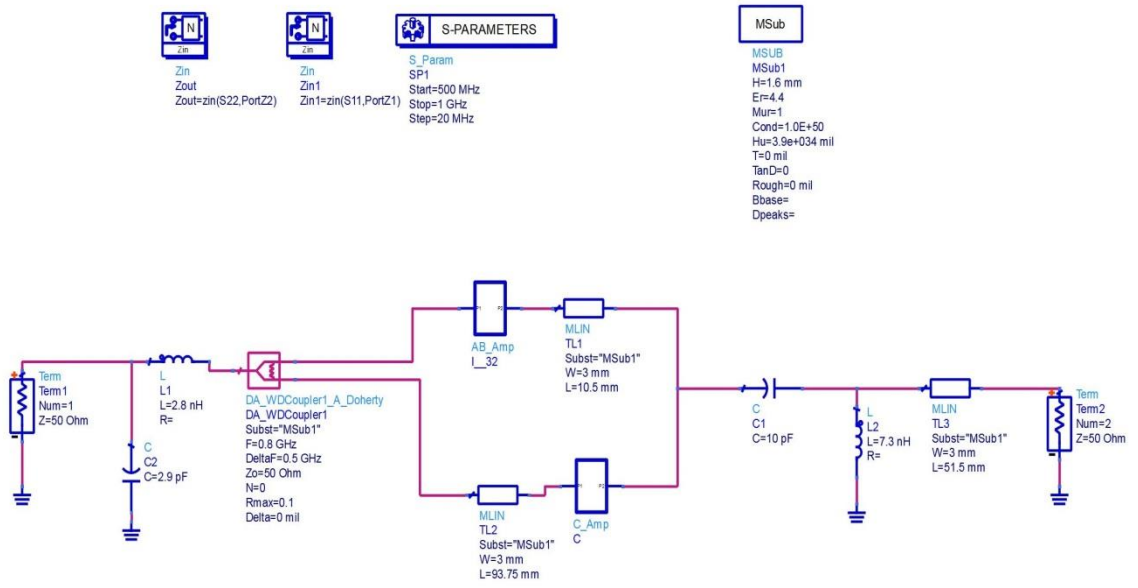
(a)
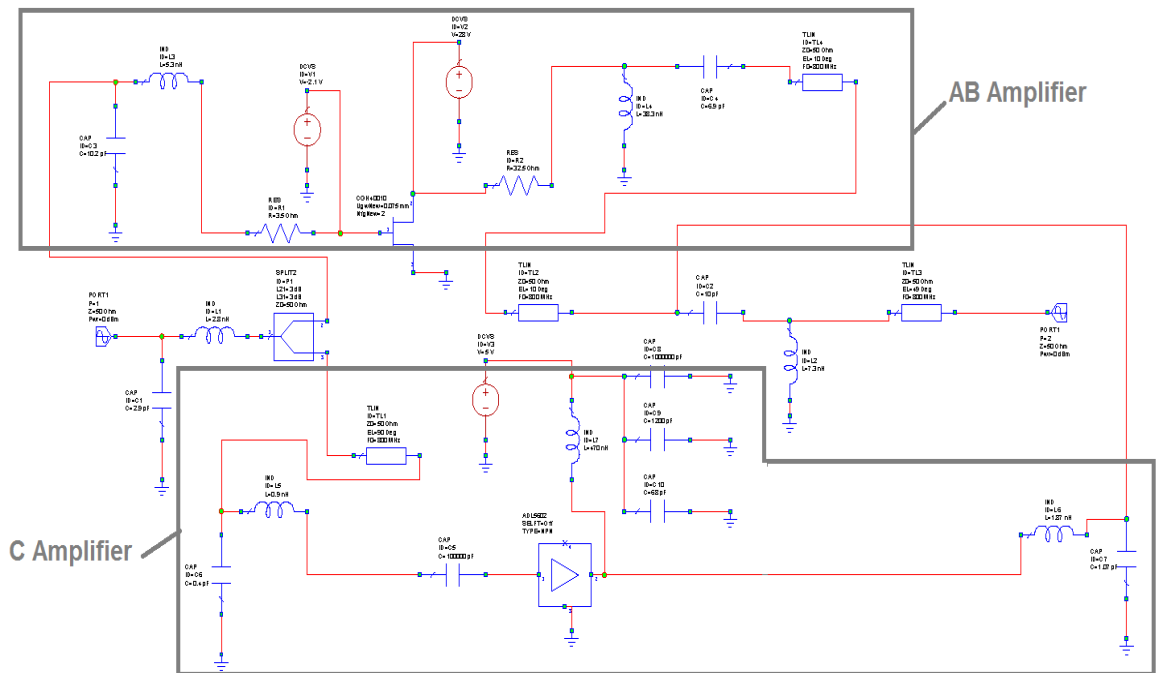
(b)

Fig. 4.9: Schematic of the Doherty power amplifier with matching circuits – (a): in

ADS, (b): in AWR

After carrying out the stability test of the Doherty amplifier, it is found that the device is unconditionally stable in the frequency range of interest. The stability parameters, Δ, and the rollet factor k are calculated and found to be:

$\Delta = 0.43 \angle -61.48^0$

$k = 1.4$

In order to maintain maximum power transfer, matching circuits are designed at the input and the output of the transistor. These circuits are accomplished by using passive networks and microstrip transmission lines as shown in Fig. 4.10.

(a)   (b)
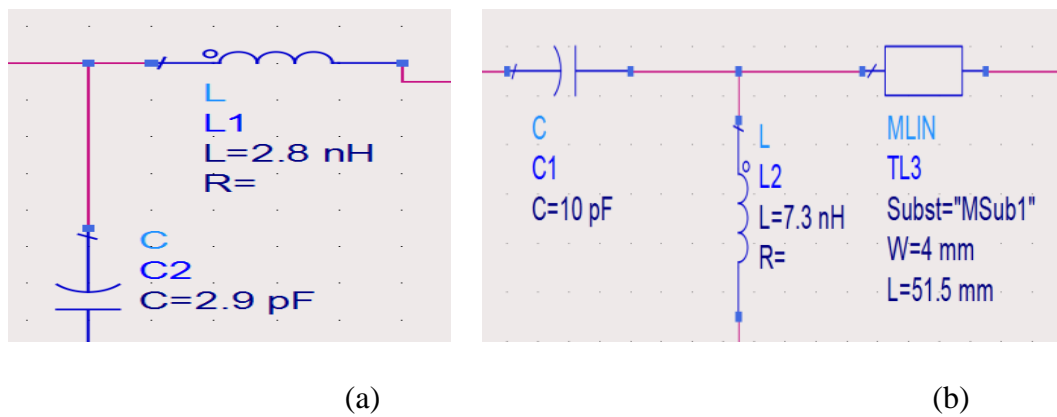
Fig. 4.10: (a) Input matching network, (b) Output matching network of the DPA

Once the amplifier matching is complete, the final signal scattering parameters at 800 MHz were simulated and found to be:

$S11 = 0.198 \angle -99.259^0$

$S12 = 0.035 \angle -55.086^0$

$S21 = 11.407 \angle 94.509^0$

$S22 = 0.175 \angle -90.038^0$

By feeding the Doherty amplifier at an optimum 800 MHz, 21.45 dBm input power, the output power of the Doherty amplifier circuit was found to be 42.77 dBm and the gain is 21.32 dB. The DC power is simulated and found to be: Pdc = 22.92 W. Thus, the power added efficiency (PAE) is around 81.94 %. All the results are summarized in Table 4.3. It is clearly shown that the efficiency of the DPA is higher than that of the class AB power amplifier. This is due to the Doherty principle implemented in this design and to the electrical lengths of the delay and impedance inverter transmission line previously mentioned.

Input Power (dBm)	DC power (W)	Output Power (dBm)	Gain (dB)	PAE (%)	Drain efficiency (%)
21.45	22.92	42.77	21.32	81.94	82.548

Table 4.3: Final results of the Doherty power amplifier

Fig. 4.11 shows the output power sweep curve as well as the corresponding PAE. As the DC voltage increases, the output power increases fairly linearly indicating that the amplifier has a constant gain. The efficiency also increases approximately linearly until it reaches the maximum at the optimum 28 volt DC supply voltage. Moreover, while varying the DC voltage, the output varies and thus, the transmit power can be varied, and this is a need of a cognitive radio transmitter.
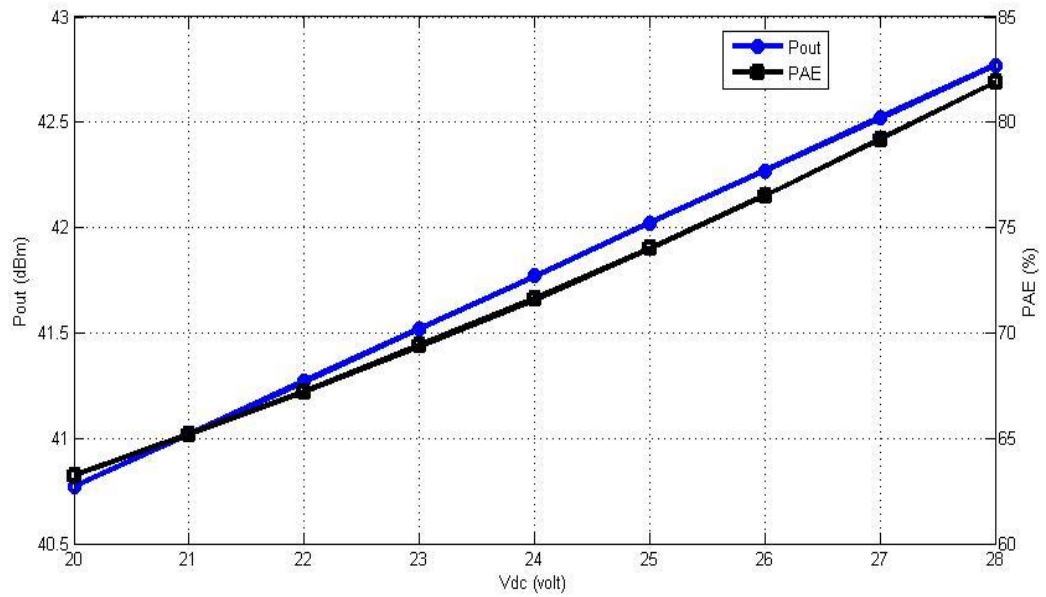
Fig. 4.11: Output power and PAE versus DC voltage in the DPA

The voltage standing wave ratio (VSWR) of the Doherty power amplifier is found to be as follows:

$VSWR_{in} = 1.49:1$

$VSWR_{out} = 1.42:1$

The VSWR of the AB amplifier is approximately equal to 1 which means most of the power is transferred in the amplifier.

A prototype of the DPA using the Cree CGH40010 and the ADL5602 transistors is shown in Fig. 4.12. The DPA is fabricated on an FR4 epoxy substrate of thickness h = 1.6 mm. The input and the output of the circuit are clearly shown.
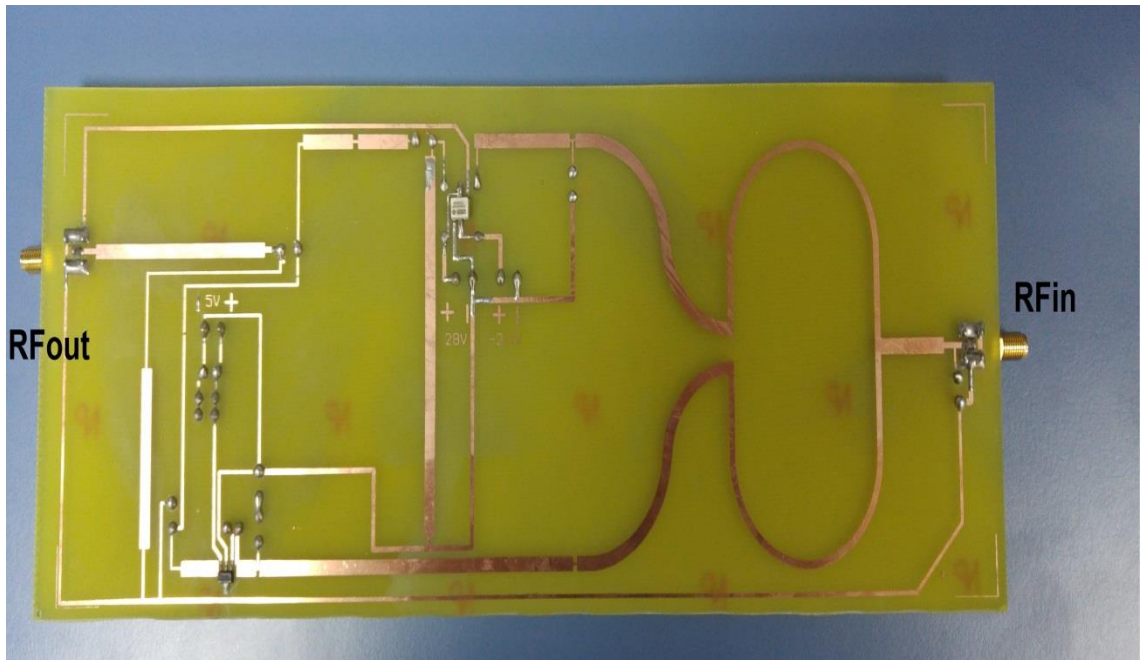
(a)
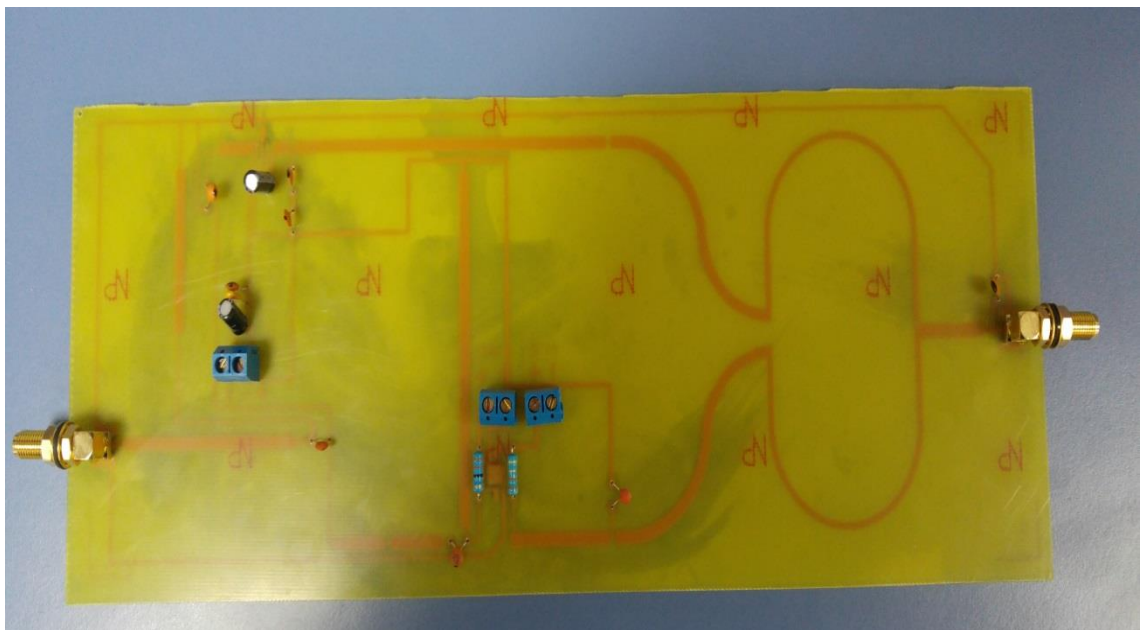
(b)

Fig. 4.12: A photo of the DPA fabricated prototype – (a): top layer, (b): bottom layer

The fabricated prototype has undergone the scattering parameters measurements. The simulated and the measured reflection coefficients of the DPA are given in Fig. 4.13. It is clearly shown that this amplifier can operate from 550 MHz to 1000 MHz, thus it is suitable for all applications in the TV band. Little difference is found between the simulated and the measured plots due to some measurements and fabrication issues.

Another advantage of the proposed Doherty amplifier rather than the efficiency increment is that the bandwidth has increased, and the proposed DPA can be suitable for more applications in the TV band. The percentage bandwidth of this DPA is 58.06 % which is higher than that of the class AB power amplifier and higher than Doherty power amplifiers previously designed such as in [13], [15], and [17].
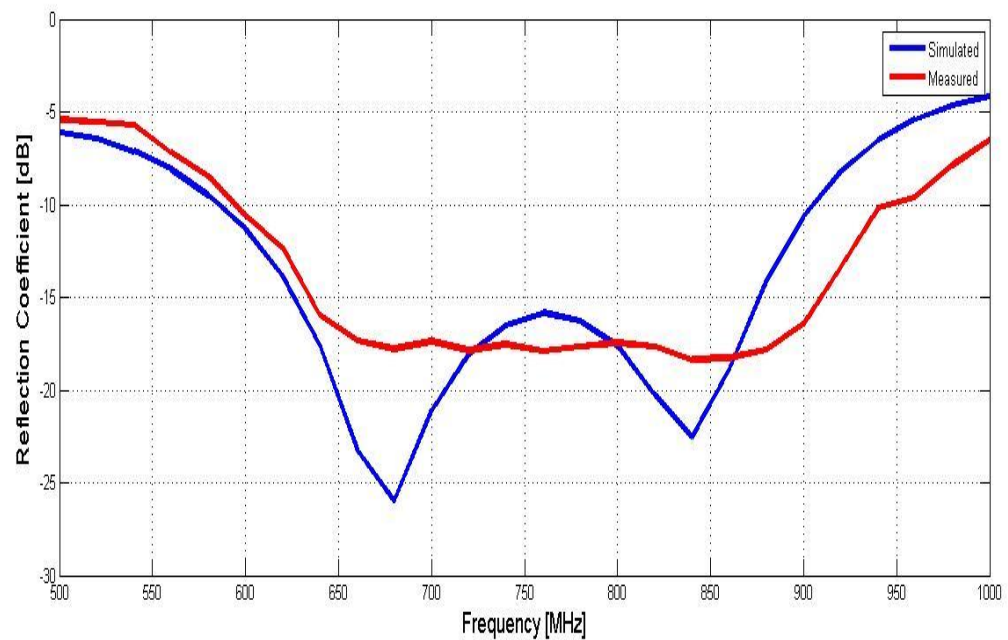
Fig. 4.13: Simulated and measured reflection coefficient plots of the DPA

The simulated and measured power gain plots of the Doherty power amplifier are given in Fig. 4.14. It is clearly shown that this amplifier has a good power gain above 19 dB for the operation bandwidth. However, it suffers from a small non-linearity.
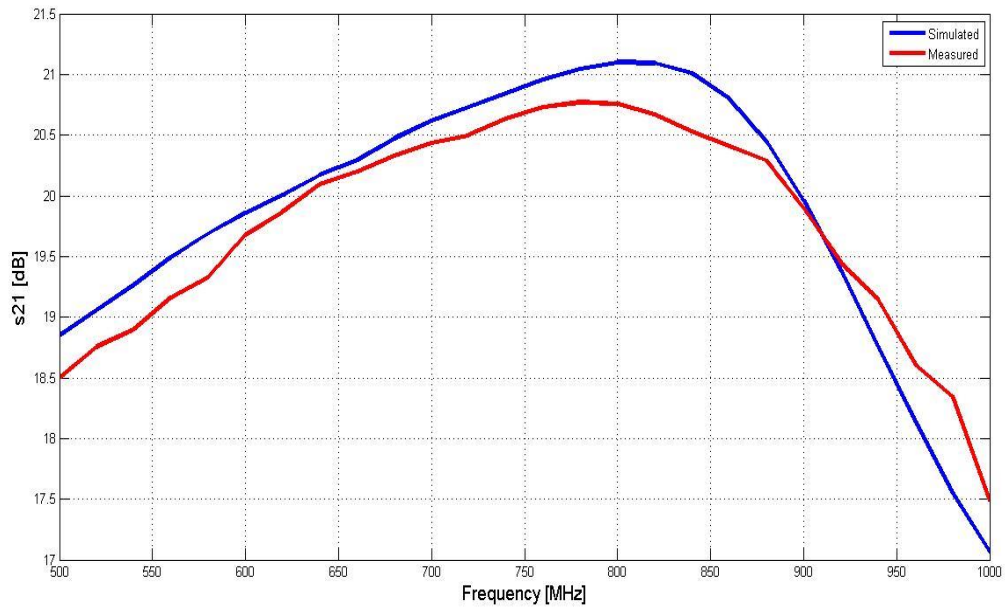
Fig. 4.14: Simulated and measured power gain plots of the DPA

In comparison with the previous surveyed designs on power amplifiers, it is obviously demonstrated that the designed power amplifiers in this thesis have higher efficiency. The Doherty power amplifier, which is the main achievement, has the highest efficiency and a better relation between the efficiency and the fractional bandwidth. This is shown in Table 4.4.

Work	Efficiency	Fractional Bandwidth
[39]	20 %	85.7 %
[41]	60 %	67%
[42]	75 %	10.3 %
[44]	69.2 %	-
[46]	70 % 60 %	41% 54 %
[47]	-	3.6%
[48]	69 %	35 %
[49]	65 %	4.85 %
[50]	45 %	-
[51]	66 %	18.18 %
AB Power Amplifier	77.78 %	33.33 %
Doherty Power Amplifier	81.94 %	58.06 %

Table 4.4: Comparison between the proposed power amplifiers in this thesis and previous surveyed power amplifiers

4.5 Summary

A class AB power amplifier and a high efficiency Doherty one were designed for the TV band applications and have been presented in this chapter. A class AB power

amplifier was first proposed using a commercial GaN HEMT from Cree incorporation. A Doherty power amplifier has been then designed in order to increase the efficiency and have a respectable output power and a linear amplifier operating mode. This DPA has been applied using the previous class AB amplifier as the main carrier amplifier and a proposed class C amplifier as the peak one. The proposed DPA has attained a high power-added-efficiency with a sufficient output power, a good associated gain and, an operating frequency bandwidth between 550 and 1000 MHz. Hence, this DPA can be a convenient power amplifier that can be used in TV band applications and implemented in the CR transmitter system.

CHAPTER 5

CONCLUSION

This chapter summarizes the contributions of the work done in this thesis and shed light on the future additions and investigation.

5.1 Contributions

Cognitive radio is an innovative spectrum allocation technology. It allows unlicensed users to access spectrum bands licensed to primary users. This technology needs a transmitter and a receiver like any communication system, however, cognitive radios does not only perform signal transmission and reception, but also sense the occupancy of any channel in the whole system and tune to transmit on the free channel. These constraints require special and strict issues in the design of antennas, power amplifiers, and frequency synthesizers. Cognitive radio in the TV band is of special interest. The vacant channels in the cognitive radio TV transmission are called the TV white spaces. These TVWSs have higher propagation characteristics and greater coverage, and require relatively cheap infrastructure. Therefore the ability to design adequate and developed components in the radio frequency transmitter is an essential technological issue in cognitive radio architectures and applications.

In the first part of the thesis work, a reduced-size printed monopole antenna, a meander loop monopole antenna and a planar inverted F antenna suitable for cognitive

radio applications in the TV band are proposed. These antennas are printed with small dimensions and can operate in the frequency band 700 – 900 MHz, with omni-directional patterns and an acceptable gain of about 2.5 dB. The bandwidth and the size of these antennas make them suitable for portable devices such as laptops, notebooks, tablets and mobile phones. These antennas are broadband antennas that can be implemented in the CR transmitter system.

A reconfigurable compact planar spiral monopole antenna suitable for TVWS applications is also proposed in this thesis. Frequency reconfigurability is attained through inserting a tunable inductor on the spiral monopole and changing its inductance. This antenna can operate at different bands which range between 15 to 20 MHz, in the 600 – 800 MHz band, with omni-directional patterns and an acceptable gain of 1 dB given the small size of the antenna. This bandwidth, the small and the compact size of this antenna, and the frequency reconfigurability make this antenna a practical one that can be used for cognitive radio communicating applications in the TV band and employed in the CR transmitter system.

In the second part of the thesis work, a class AB power amplifier and a high efficiency Doherty one were implemented for the TV band applications. A class AB power amplifier was first designed using a commercial GaN HEMT from Cree incorporation. The Doherty amplifier has been implemented, using the previous class AB amplifier as the main amplifier and a proposed class C amplifier as the peak one. This proposed DPA attained a high power-added-efficiency of 81.94%, a 42.77 dBm output power, an associated gain of 21.32 dB, and an operating frequency bandwidth

between 550 and 1000 MHz which make it a convenient power amplifier that can be used in TV band applications and mounted in the cognitive radio transmitter system.

5.2 Future Work

After developing broadband and reconfigurable antennas and implementing and designing broadband power amplifiers that can be used in the cognitive radio transmitter system, extra work will be performed on the other blocks in order to develop an adequate front-end transmitter system for cognitive radio applications in the TV band. This work is summarized as follows:

1. Optimizing a tunable band pass filter previously designed in order to operate in the TV band and can tune to any unoccupied channel within this band.

2. Investigating and designing a tunable oscillator in which it can tune and deliver the desired frequencies of the system after mixing it with the baseband signal. It is intended to attain a tunable oscillator that can materialize the challengeable characteristics: wide tuning range and low phase noise. Moreover fast settling behavior, high dissipation and high power are also targeted.

5.3 Thesis Related Publications

Journal Papers

- **M. Y. Abou-Shahine**, M. Al-Husseini, A. H. Ramadan, K. Y. Kabalan, and Y. Nasser, "Antenna Designs for Cognitive Radio Application in the TV Band", *International Journal of Scientific and Engineering Research*, Vol. 6, Issue 2, pp. 975-980, February 2015.

- **M. Y. Abou-Shahine**, Y. Nasser, and K. Y. Kabalan, "A High Efficiency Doherty Power Amplifier for TV Band Applications", *Journal of Electromagnetic Analysis and Applications*, Vol. 7, No. 12, pp. 291-301, December 2015.

Conference Papers

- **M. Y. Abou Shahine**, M. Al-Husseini, Y. Nasser, K. Y. Kabalan, and A. El-Hajj, "A Reconfigurable Miniaturized Spiral Monopole Antenna for TV White Spaces", *in Proceedings of Progress In Electromagnetics Research Symposium (PIERS), Stockholm,* pp. 1026-1029, August 12-15, 2013.

- **M. Y. Abou Shahine**, A.H. Ramadan, K.Y. Kabalan, Y. Nassr, "Different Antenna Designs for Cognitive Radio Applications in the TV Band", *Irbid First International Engineering Conference (IIEC-2014)*, Irbid, Jordan, October 14-16, 2014.

- **M. Y. Abou-Shahine**, M. Al-Husseini, Y. Nasser, and K.Y. Kabalan, "A Varactor-Based Tunable Microstrip Band Pass Filter", *Progress in Electromagnetics Research Symposium (PIERS 2015)*, Prague, Czech Republic, July 6-9, 2015.

APPENDIX A

CGH40010 DATASHEET

CGH40010
10 W, RF Power GaN HEMT

Cree's CGH40010 is an unmatched, gallium nitride (GaN) high electron mobility transistor (HEMT). The CGH40010, operating from a 28 volt rail, offers a general purpose, broadband solution to a variety of RF and microwave applications. GaN HEMTs offer high efficiency, high gain and wide bandwidth capabilities making the CGH40010 ideal for linear and compressed amplifier circuits. The transistor is available in both screw-down, flange and solder-down, pill packages.
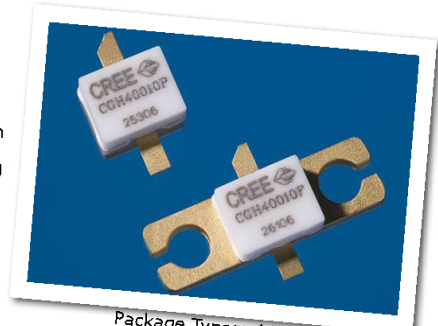
Package Types: 440166, & 440196
PN's: CGH40010F & CGH40010P

FEATURES

- Up to 6 GHz Operation
- 16 dB Small Signal Gain at 2.0 GHz
- 14 dB Small Signal Gain at 4.0 GHz
- 13 W typical P_{SAT}
- 65 % Efficiency at P_{SAT}
- 28 V Operation

APPLICATIONS

- 2-Way Private Radio
- Broadband Amplifiers
- Cellular Infrastructure
- Test Instrumentation
- Class A, AB, Linear amplifiers suitable for OFDM, W-CDMA, EDGE, CDMA waveforms

RoHS COMPLIANT

Large Signal Models Available for SiC & GaN

92

Absolute Maximum Ratings (not simultaneous) at 25˚C Case Temperature

Parameter	Symbol	Rating	Units	Conditions
Drain-Source Voltage	V_{DSS}	84	Volts	25˚C
Gate-to-Source Voltage	V_{GS}	-10, +2	Volts	25˚C
Storage Temperature	T_{STG}	-65, +150	˚C	
Operating Junction Temperature	T_J	225	˚C	
Maximum Forward Gate Current	I_{GMAX}	4.0	mA	25˚C
Maximum Drain Current[1]	I_{DMAX}	1.5	A	25˚C
Soldering Temperature[2]	T_S	245	˚C	
Screw Torque	τ	60	in-oz	
Thermal Resistance, Junction to Case[3]	$R_{\theta JC}$	8.0	˚C/W	85˚C
Case Operating Temperature[3,4]	T_C	-40, +150	˚C	

Note:
[1] Current limit for long term, reliable operation
[2] Refer to the Application Note on soldering at www.cree.com/products/wireless_appnotes.asp
[3] Measured for the CGH40010F at P_{DISS} = 14 W.
[4] See also, the Power Dissipation De-rating Curve on Page 6.

Electrical Characteristics (T_C = 25˚C)

Characteristics	Symbol	Min.	Typ.	Max.	Units	Conditions
DC Characteristics[1]						
Gate Threshold Voltage	$V_{GS(th)}$	-3.8	-3.0	-2.3	V_{DC}	V_{DS} = 10 V, I_D = 3.6 mA
Gate Quiescent Voltage	$V_{GS(Q)}$	–	-2.7	–	V_{DC}	V_{DS} = 28 V, I_D = 200 mA
Saturated Drain Current	I_{DS}	2.9	3.5	–	A	V_{DS} = 6.0 V, V_{GS} = 2.0 V
Drain-Source Breakdown Voltage	V_{BR}	120	–	–	V_{DC}	V_{GS} = -8 V, I_D = 3.6 mA
RF Characteristics[2] (T_C = 25˚C, F_0 = 3.7 GHz unless otherwise noted)						
Small Signal Gain	G_{SS}	12.5	14.5	–	dB	V_{DD} = 28 V, I_{DQ} = 200 mA
Power Output[3]	P_{SAT}	10	12.5	–	W	V_{DD} = 28 V, I_{DQ} = 200 mA
Drain Efficiency[4]	η	55	65	–	%	V_{DD} = 28 V, I_{DQ} = 200 mA, P_{SAT}
Output Mismatch Stress	VSWR	–	–	10 : 1	Ψ	No damage at all phase angles, V_{DD} = 28 V, I_{DQ} = 200 mA, P_{OUT} = 10 W CW
Dynamic Characteristics						
Input Capacitance	C_{GS}	–	4.5	–	pF	V_{DS} = 28 V, V_{gs} = -8 V, f = 1 MHz
Output Capacitance	C_{DS}	–	1.3	–	pF	V_{DS} = 28 V, V_{gs} = -8 V, f = 1 MHz
Feedback Capacitance	C_{GD}	–	0.2	–	pF	V_{DS} = 28 V, V_{gs} = -8 V, f = 1 MHz

Notes:
[1] Measured on wafer prior to packaging.
[2] Measured in CGH40010-TB.
[3] P_{SAT} is defined as I_G = 0.36 mA.
[4] Drain Efficiency = P_{OUT} / P_{DC}

**Small Signal Gain and Return Loss vs Frequency
of the CGH40010 in the CGH40010-TB**

Chart annotations:
- 3.4 GHz 14.9 dB
- 3.8 GHz 14.31 dB
- 3.6 GHz 14.89 dB
- 3.7 GHz 14.7 dB
- 3.7 GHz -7.49 dB
- 3.4 GHz -10.65 dB
- 3.6 GHz -7.497 dB
- 3.8 GHz -8.549 dB

Legend:
- DB(|S(2,1)|)
- DB(|S(1,1)|)

Axes: Gain (dB), Return Loss (dB) vs Frequency (GHz)
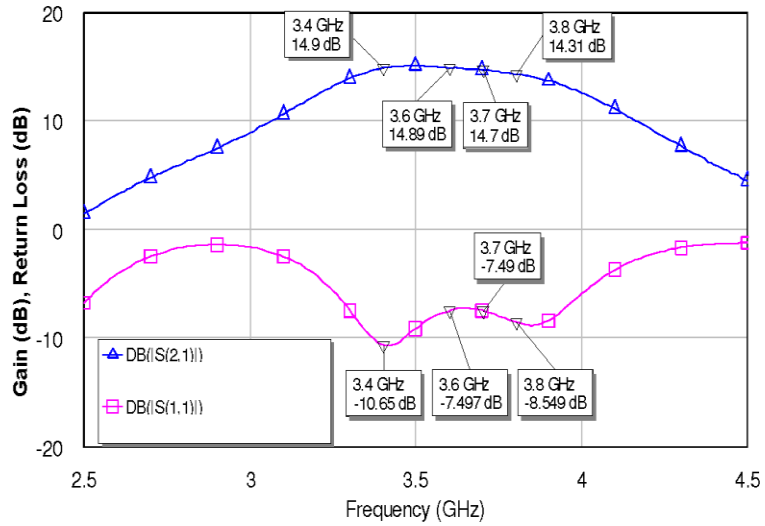
P_{SAT}**, Gain, and Drain Efficiency vs Frequency of the
CGH40010F in the CGH40010-TB
V_{DD} = 28 V, I_{DQ} = 200 mA**

Legend:
- Psat
- Gain
- Drain Eff

Axes: P_{SAT} (W), Gain (dB) and Drain Efficiency (%) vs Frequency (GHz)

Labels: Efficiency, Gain, P_{SAT}
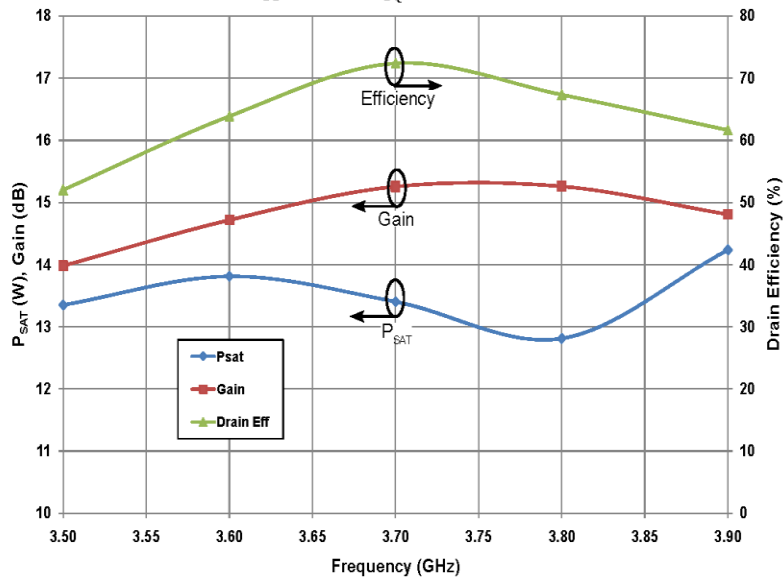
Typical Performance

Swept CW Data of CGH40010F vs. Output Power with Source and Load Impedances Optimized for Drain Efficiency at 2.0 GHz
V_{DD} = 28 V, I_{DQ} = 200 mA

Swept CW Data of CGH40010F vs. Output Power with Source and Load Impedances Optimized for Drain Efficiency at 3.6 GHz
V_{DD} = 28 V, I_{DQ} = 200 mA

95

Swept CW Data of CGH40010F vs. Output Power with Source and Load Impedances Optimized for P1 Power at 3.6 GHz
V_{DD} = 28 V, I_{DQ} = 200 mA
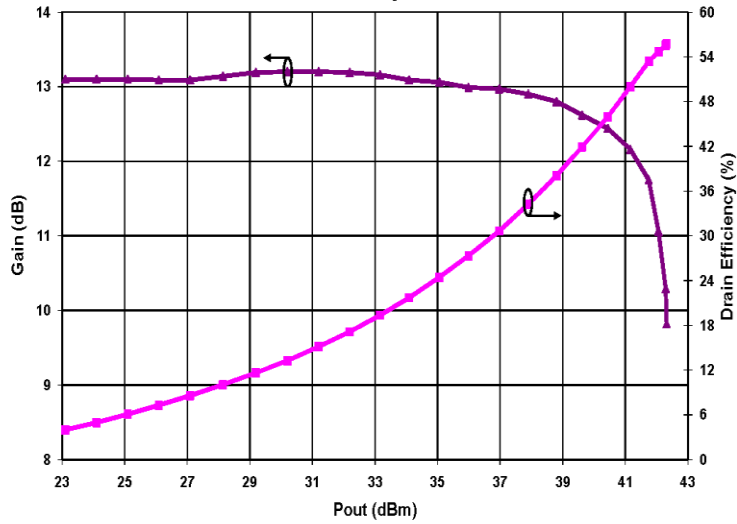
Simulated Maximum Available Gain and K Factor of the CGH40010F
V_{DD} = 28 V, I_{DQ} = 200 mA
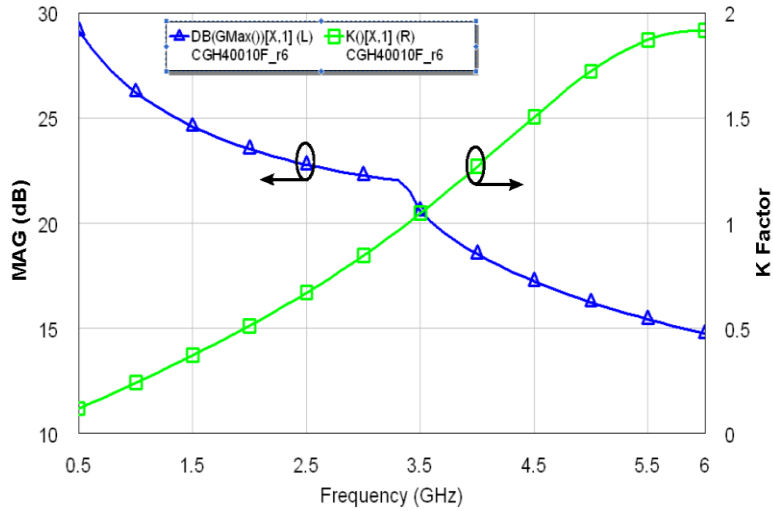
Typical Noise Performance

Simulated Minimum Noise Figure and Noise Resistance vs Frequency of the CGH40010F
V_{DD} = 28 V, I_{DQ} = 100 mA
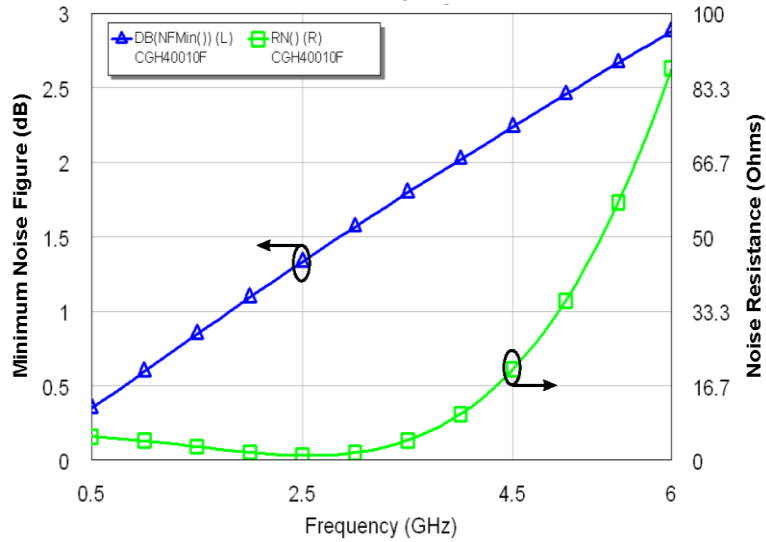
Electrostatic Discharge (ESD) Classifications

Parameter	Symbol	Class	Test Methodology
Human Body Model	HBM	1A > 250 V	JEDEC JESD22 A114-D
Charge Device Model	CDM	1 < 200 V	JEDEC JESD22 C101-C

Source and Load Impedances
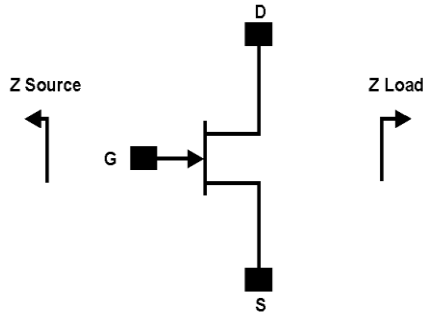
Frequency (MHz)	Z Source	Z Load
500	20.2 + j16.18	51.7 + j15.2
1000	8.38 + j9.46	41.4 + j28.5
1500	7.37 + j0	28.15 + j29
2500	3.19 - j4.76	19 + j9.2
3500	3.18 - j13.3	14.6 + j7.46

Note 1. V_{DD} = 28V, I_{DQ} = 200mA in the 440166 package.
Note 2. Optimized for power, gain, P_{SAT} and PAE.
Note 3. When using this device at low frequency, series resistors should be used to maintain amplifier stability.

CGH40010 Power Dissipation De-rating Curve
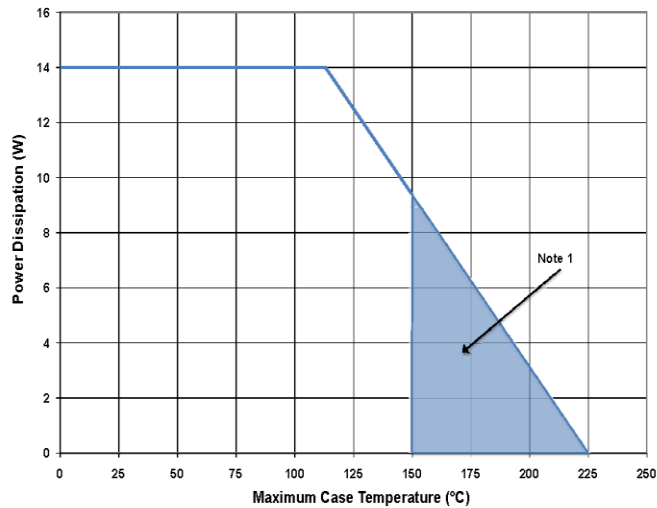
Note 1. Area exceeds Maximum Case Operating Temperature (See Page 2).

CGH40010-TB Demonstration Amplifier Circuit Bill of Materials

Designator	Description	Qty
R1,R2	RES,1/16W,0603,1%,0 OHMS	1
R3	RES,1/16W,0603,1%,47 OHMS	1
R4	RES,1/16W,0603,1%,100 OHMS	1
C6	CAP, 470PF, 5%,100V, 0603	1
C17	CAP, 33 UF, 20%, G CASE	1
C16	CAP, 1.0UF, 100V, 10%, X7R, 1210	1
C8	CAP 10UF 16V TANTALUM	1
C14	CAP, 100.0pF, +/-5%, 0603	1
C1	CAP, 0.5pF, +/-0.05pF, 0603	1
C2	CAP, 0.7pF, +/-0.1pF, 0603	1
C10,C11	CAP, 1.0pF, +/-0.1pF, 0603	2
C4,C12	CAP, 10.0pF,+/-5%, 0603	2
C5,C13	CAP, 39pF, +/-5%, 0603	2
C7,C15	CAP,33000PF, 0805,100V, X7R	2
J3,J4	CONN SMA STR PANEL JACK RECP	1
J2	HEADER RT>PLZ.1CEN LK 2 POS	1
J1	HEADER RT>PLZ .1CEN LK 5POS	1
-	PCB, RO4350B, Er = 3.48, h = 20 mil	1
Q1	CGH40010F or CGH40010P	1

CGH40010-TB Demonstration Amplifier Circuit

CGH40010-TB Demonstration Amplifier Circuit Schematic
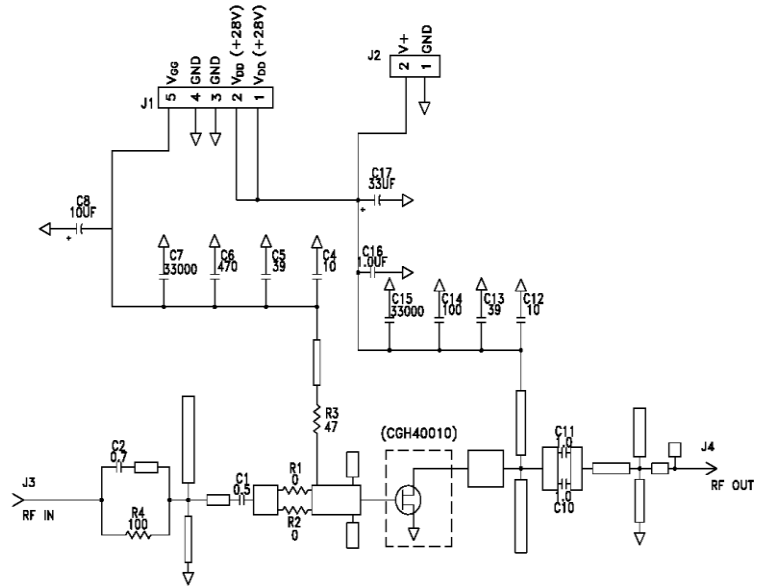
CGH40010-TB Demonstration Amplifier Circuit Outline

100
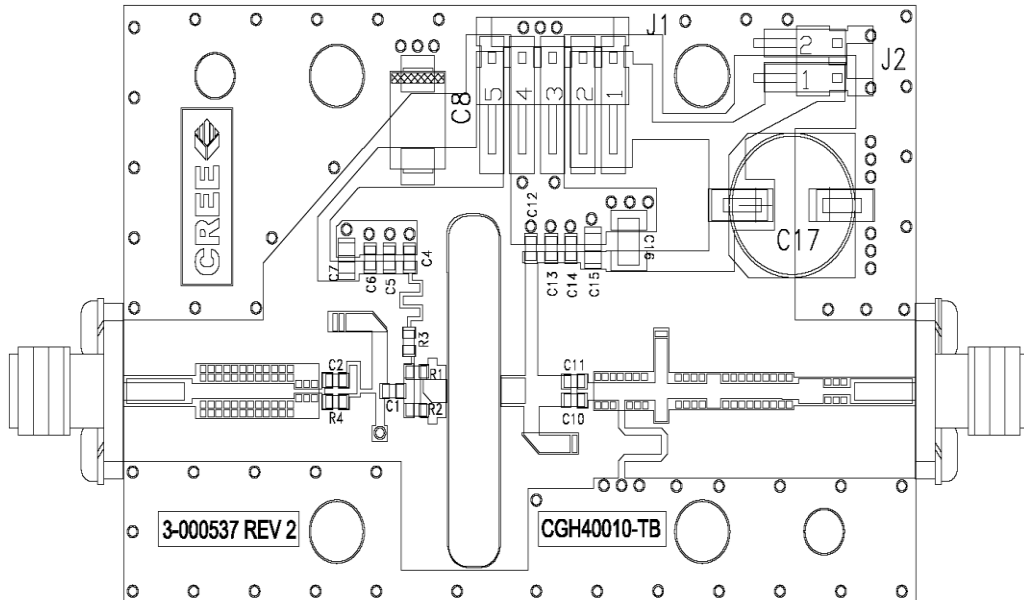
Typical Package S-Parameters for CGH40010
(Small Signal, V_{DS} = 28 V, I_{DQ} = 100 mA, angle in degrees)

Frequency	Mag S11	Ang S11	Mag S21	Ang S21	Mag S12	Ang S12	Mag S22	Ang S22
500 MHz	0.909	-123.34	17.19	108.22	0.027	21.36	0.343	-90.81
600 MHz	0.902	-133.06	14.86	101.82	0.028	15.60	0.329	-98.65
700 MHz	0.897	-140.73	13.04	96.45	0.028	10.87	0.321	-104.84
800 MHz	0.894	-146.96	11.58	91.78	0.029	6.84	0.317	-109.84
900 MHz	0.891	-152.16	10.41	87.61	0.029	3.33	0.316	-113.95
1.0 GHz	0.890	-156.60	9.43	83.82	0.029	0.19	0.318	-117.42
1.1 GHz	0.889	-160.47	8.62	80.31	0.029	-2.66	0.321	-120.40
1.2 GHz	0.888	-163.90	7.93	77.02	0.029	-5.28	0.326	-123.02
1.3 GHz	0.887	-166.99	7.34	73.90	0.029	-7.72	0.332	-125.36
1.4 GHz	0.887	-169.80	6.82	70.92	0.029	-10.01	0.338	-127.51
1.5 GHz	0.887	-172.39	6.38	68.05	0.029	-12.18	0.345	-129.50
1.6 GHz	0.887	-174.80	5.98	65.28	0.028	-14.24	0.353	-131.37
1.7 GHz	0.887	-177.07	5.63	62.59	0.028	-16.21	0.360	-133.15
1.8 GHz	0.887	-179.22	5.32	59.97	0.028	-18.09	0.369	-134.87
1.9 GHz	0.887	178.73	5.04	57.41	0.028	-19.91	0.377	-136.54
2.0 GHz	0.888	176.76	4.78	54.89	0.027	-21.66	0.385	-138.17
2.1 GHz	0.888	174.86	4.55	52.42	0.027	-23.35	0.393	-139.77
2.2 GHz	0.888	173.02	4.34	49.99	0.027	-24.98	0.402	-141.34
2.3 GHz	0.888	171.23	4.15	47.60	0.026	-26.56	0.410	-142.90
2.4 GHz	0.889	169.48	3.97	45.24	0.026	-28.08	0.418	-144.45
2.5 GHz	0.889	167.76	3.81	42.90	0.026	-29.55	0.426	-145.99
2.6 GHz	0.890	166.07	3.66	40.59	0.025	-30.98	0.434	-147.53
2.7 GHz	0.890	164.39	3.53	38.30	0.025	-32.36	0.442	-149.06
2.8 GHz	0.890	162.74	3.40	36.03	0.025	-33.69	0.450	-150.59
2.9 GHz	0.891	161.10	3.28	33.78	0.024	-34.97	0.458	-152.12
3.0 GHz	0.891	159.46	3.17	31.55	0.024	-36.20	0.465	-153.65
3.2 GHz	0.892	156.21	2.97	27.12	0.023	-38.51	0.479	-156.72
3.4 GHz	0.893	152.96	2.79	22.73	0.022	-40.63	0.493	-159.80
3.6 GHz	0.893	149.69	2.64	18.38	0.022	-42.52	0.505	-162.90
3.8 GHz	0.894	146.38	2.50	14.05	0.021	-44.17	0.517	-166.03
4.0 GHz	0.894	143.03	2.38	9.72	0.020	-45.56	0.527	-169.19
4.2 GHz	0.894	139.61	2.28	5.40	0.019	-46.67	0.537	-172.39
4.4 GHz	0.895	136.11	2.18	1.07	0.019	-47.46	0.546	-175.64
4.6 GHz	0.895	132.53	2.09	-3.29	0.018	-47.90	0.554	-178.95
4.8 GHz	0.895	128.85	2.01	-7.68	0.017	-47.96	0.561	177.69
5.0 GHz	0.895	125.06	1.94	-12.10	0.017	-47.61	0.568	174.25
5.2 GHz	0.895	121.15	1.88	-16.58	0.016	-46.84	0.573	170.72
5.4 GHz	0.895	117.11	1.82	-21.12	0.016	-45.67	0.578	167.10
5.6 GHz	0.895	112.94	1.77	-25.73	0.015	-44.12	0.582	163.38
5.8 GHz	0.895	108.62	1.72	-30.42	0.015	-42.30	0.586	159.54
6.0 GHz	0.895	104.15	1.68	-35.20	0.015	-40.33	0.589	155.56

Download this s-parameter file in ".s2p" format at http://www.cree.com/products/wireless_s-parameters.asp

Typical Package S-Parameters for CGH40010
(Small Signal, V_{DS} = 28 V, I_{DQ} = 200 mA, angle in degrees)

Frequency	Mag S11	Ang S11	Mag S21	Ang S21	Mag S12	Ang S12	Mag S22	Ang S22
500 MHz	0.911	-130.62	18.41	105.41	0.022	19.44	0.303	-112.24
600 MHz	0.906	-139.65	15.80	99.47	0.023	14.31	0.299	-119.83
700 MHz	0.902	-146.70	13.80	94.50	0.023	10.17	0.298	-125.50
800 MHz	0.899	-152.41	12.22	90.19	0.023	6.68	0.299	-129.85
900 MHz	0.898	-157.17	10.96	86.34	0.024	3.67	0.302	-133.28
1.0 GHz	0.896	-161.24	9.92	82.82	0.024	0.99	0.305	-136.05
1.1 GHz	0.896	-164.79	9.06	79.56	0.024	-1.41	0.309	-138.34
1.2 GHz	0.895	-167.95	8.33	76.49	0.024	-3.62	0.314	-140.30
1.3 GHz	0.895	-170.80	7.70	73.57	0.023	-5.66	0.320	-142.01
1.4 GHz	0.894	-173.41	7.17	70.78	0.023	-7.56	0.326	-143.54
1.5 GHz	0.894	-175.82	6.70	68.08	0.023	-9.35	0.332	-144.94
1.6 GHz	0.894	-178.09	6.28	65.47	0.023	-11.05	0.338	-146.24
1.7 GHz	0.894	179.78	5.92	62.92	0.023	-12.66	0.345	-147.48
1.8 GHz	0.894	177.75	5.59	60.43	0.023	-14.19	0.352	-148.68
1.9 GHz	0.894	175.81	5.30	57.99	0.023	-15.65	0.358	-149.84
2.0 GHz	0.894	173.94	5.04	55.59	0.022	-17.05	0.365	-150.99
2.1 GHz	0.894	172.13	4.80	53.23	0.022	-18.39	0.372	-152.12
2.2 GHz	0.894	170.37	4.58	50.91	0.022	-19.67	0.379	-153.26
2.3 GHz	0.895	168.65	4.38	48.61	0.022	-20.90	0.386	-154.39
2.4 GHz	0.895	166.96	4.20	46.33	0.021	-22.08	0.393	-155.54
2.5 GHz	0.895	165.30	4.03	44.08	0.021	-23.20	0.400	-156.69
2.6 GHz	0.895	163.66	3.88	41.84	0.021	-24.27	0.407	-157.85
2.7 GHz	0.895	162.04	3.74	39.63	0.021	-25.28	0.414	-159.03
2.8 GHz	0.895	160.43	3.60	37.43	0.020	-26.25	0.420	-160.22
2.9 GHz	0.896	158.83	3.48	35.24	0.020	-27.16	0.427	-161.42
3.0 GHz	0.896	157.24	3.37	33.06	0.020	-28.02	0.433	-162.64
3.2 GHz	0.896	154.06	3.16	28.74	0.019	-29.57	0.446	-165.13
3.4 GHz	0.896	150.87	2.98	24.44	0.019	-30.88	0.457	-167.69
3.6 GHz	0.896	147.66	2.82	20.16	0.018	-31.95	0.468	-170.31
3.8 GHz	0.897	144.41	2.68	15.89	0.018	-32.76	0.478	-173.00
4.0 GHz	0.897	141.10	2.56	11.61	0.017	-33.30	0.488	-175.77
4.2 GHz	0.897	137.72	2.45	7.33	0.017	-33.55	0.497	-178.61
4.4 GHz	0.897	134.26	2.35	3.03	0.017	-33.50	0.505	178.47
4.6 GHz	0.897	130.71	2.26	-1.31	0.016	-33.18	0.512	175.46
4.8 GHz	0.896	127.06	2.17	-5.68	0.016	-32.58	0.518	172.36
5.0 GHz	0.896	123.30	2.10	-10.09	0.016	-31.74	0.524	169.16
5.2 GHz	0.896	119.42	2.04	-14.57	0.016	-30.72	0.529	165.86
5.4 GHz	0.896	115.41	1.98	-19.10	0.016	-29.60	0.534	162.44
5.6 GHz	0.896	111.26	1.92	-23.71	0.016	-28.46	0.537	158.89
5.8 GHz	0.895	106.97	1.87	-28.40	0.017	-27.41	0.540	155.20
6.0 GHz	0.895	102.53	1.82	-33.19	0.017	-26.54	0.543	151.36

Download this s-parameter file in ".s2p" format at http://www.cree.com/products/wireless_s-parameters.asp

Typical Package S-Parameters for CGH40010
(Small Signal, V_{DS} = 28 V, I_{DQ} = 500 mA, angle in degrees)

Frequency	Mag S11	Ang S11	Mag S21	Ang S21	Mag S12	Ang S12	Mag S22	Ang S22
500 MHz	0.914	-135.02	18.58	103.70	0.020	18.36	0.300	-126.80
600 MHz	0.909	-143.57	15.88	98.05	0.020	13.67	0.302	-133.51
700 MHz	0.906	-150.23	13.83	93.33	0.021	9.90	0.304	-138.40
800 MHz	0.904	-155.61	12.23	89.23	0.021	6.77	0.307	-142.08
900 MHz	0.903	-160.09	10.95	85.56	0.021	4.08	0.311	-144.94
1.0 GHz	0.902	-163.93	9.91	82.21	0.021	1.71	0.314	-147.23
1.1 GHz	0.901	-167.29	9.04	79.09	0.021	-0.41	0.319	-149.10
1.2 GHz	0.901	-170.29	8.31	76.15	0.021	-2.35	0.323	-150.69
1.3 GHz	0.900	-173.00	7.69	73.35	0.021	-4.12	0.328	-152.07
1.4 GHz	0.900	-175.50	7.15	70.66	0.021	-5.78	0.333	-153.29
1.5 GHz	0.900	-177.81	6.69	68.07	0.021	-7.32	0.338	-154.41
1.6 GHz	0.900	-179.98	6.27	65.54	0.021	-8.77	0.344	-155.44
1.7 GHz	0.900	177.96	5.91	63.08	0.020	-10.15	0.349	-156.43
1.8 GHz	0.899	176.00	5.59	60.67	0.020	-11.45	0.355	-157.38
1.9 GHz	0.899	174.12	5.30	58.30	0.020	-12.68	0.361	-158.30
2.0 GHz	0.899	172.31	5.04	55.97	0.020	-13.85	0.366	-159.22
2.1 GHz	0.899	170.54	4.80	53.67	0.020	-14.96	0.372	-160.14
2.2 GHz	0.900	168.83	4.58	51.40	0.020	-16.01	0.378	-161.06
2.3 GHz	0.900	167.15	4.39	49.16	0.019	-17.01	0.384	-161.99
2.4 GHz	0.900	165.49	4.21	46.94	0.019	-17.95	0.390	-162.93
2.5 GHz	0.900	163.87	4.04	44.73	0.019	-18.85	0.396	-163.88
2.6 GHz	0.900	162.26	3.89	42.54	0.019	-19.69	0.402	-164.86
2.7 GHz	0.900	160.66	3.75	40.37	0.019	-20.48	0.407	-165.85
2.8 GHz	0.900	159.08	3.62	38.21	0.019	-21.21	0.413	-166.86
2.9 GHz	0.900	157.51	3.50	36.05	0.018	-21.89	0.418	-167.89
3.0 GHz	0.900	155.93	3.39	33.91	0.018	-22.52	0.424	-168.95
3.2 GHz	0.900	152.79	3.18	29.65	0.018	-23.61	0.435	-171.12
3.4 GHz	0.900	149.64	3.00	25.40	0.017	-24.48	0.445	-173.38
3.6 GHz	0.900	146.45	2.85	21.17	0.017	-25.11	0.454	-175.73
3.8 GHz	0.900	143.23	2.71	16.93	0.017	-25.51	0.463	-178.17
4.0 GHz	0.900	139.94	2.58	12.69	0.017	-25.67	0.471	179.30
4.2 GHz	0.900	136.58	2.47	8.43	0.016	-25.60	0.479	176.67
4.4 GHz	0.899	133.14	2.38	4.15	0.016	-25.32	0.486	173.94
4.6 GHz	0.899	129.61	2.29	-0.17	0.016	-24.85	0.492	171.12
4.8 GHz	0.899	125.97	2.21	-4.53	0.016	-24.24	0.498	168.18
5.0 GHz	0.898	122.23	2.13	-8.94	0.016	-23.54	0.503	165.13
5.2 GHz	0.898	118.36	2.07	-13.41	0.016	-22.80	0.507	161.96
5.4 GHz	0.898	114.36	2.01	-17.95	0.017	-22.11	0.511	158.66
5.6 GHz	0.897	110.22	1.95	-22.56	0.017	-21.54	0.514	155.22
5.8 GHz	0.897	105.94	1.90	-27.26	0.018	-21.16	0.517	151.63
6.0 GHz	0.897	101.51	1.86	-32.04	0.019	-21.04	0.519	147.87

Download this s-parameter file in ".s2p" format at http://www.cree.com/products/wireless_s-parameters.asp

Product Dimensions CGH40010F (Package Type — 440166)
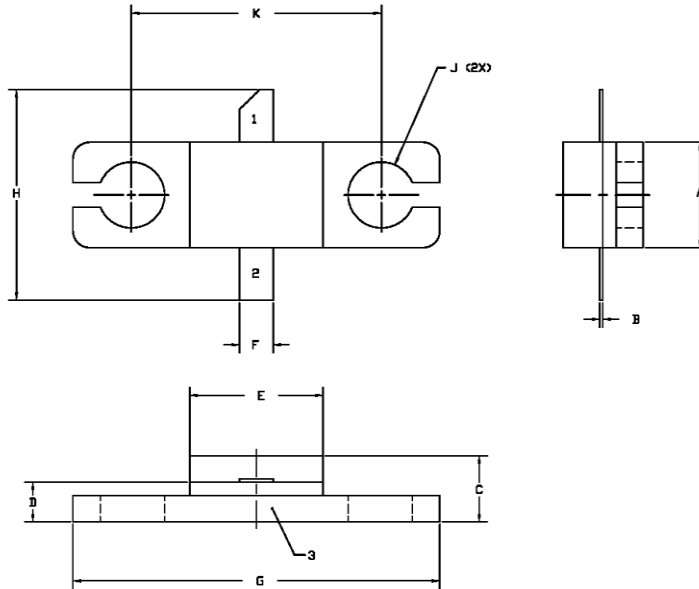
DIM	INCHES		MILLIMETERS	
	MIN	MAX	MIN	MAX
A	0.155	0.165	3.94	4.19
B	0.004	0.006	0.10	0.15
C	0.115	0.135	2.92	3.43
D	0.057	0.067	1.45	1.70
E	0.195	0.205	4.95	5.21
F	0.045	0.055	1.14	1.40
G	0.545	0.555	13.84	14.09
H	0.280	0.360	7.11	9.14
J	⌀ .100		2.54	
K	0.375		9.53	

PIN 1. GATE
PIN 2. DRAIN
PIN 3. SOURCE

Product Dimensions CGH40010P (Package Type — 440196)
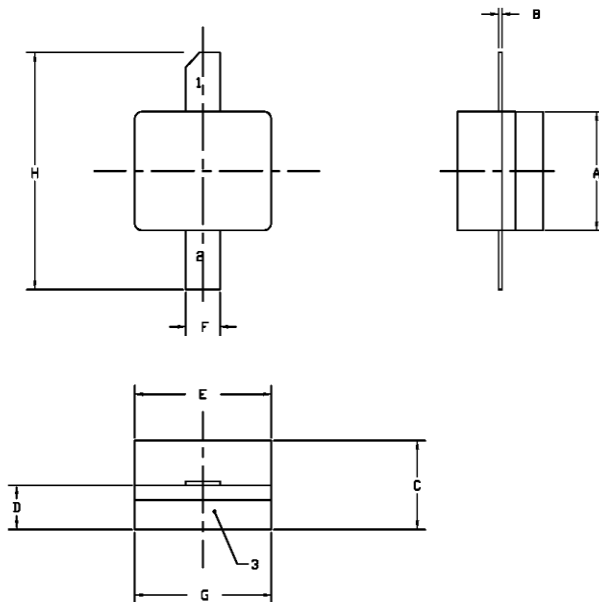
DIM	INCHES		MILLIMETERS	
	MIN	MAX	MIN	MAX
A	0.155	0.165	3.94	4.19
B	0.003	0.006	0.10	0.15
C	0.115	0.135	2.92	3.17
D	0.057	0.067	1.45	1.70
E	0.195	0.205	4.95	5.21
F	0.045	0.055	1.14	1.40
G	0.195	0.205	4.95	5.21
H	0.280	0.360	7.11	9.14

PIN 1. GATE
PIN 2. DRAIN
PIN 3. SOURCE

CREE

Disclaimer

Specifications are subject to change without notice. Cree, Inc. believes the information contained within this data sheet to be accurate and reliable. However, no responsibility is assumed by Cree for any infringement of patents or other rights of third parties which may result from its use. No license is granted by implication or otherwise under any patent or patent rights of Cree. Cree makes no warranty, representation or guarantee regarding the suitability of its products for any particular purpose. "Typical" parameters are the average values expected by Cree in large quantities and are provided for information purposes only. These values can and do vary in different applications and actual performance can vary over time. All operating parameters should be validated by customer's technical experts for each application. Cree products are not designed, intended or authorized for use as components in applications intended for surgical implant into the body or to support or sustain life, in applications in which the failure of the Cree product could result in personal injury or death or in applications for planning, construction, maintenance or direct operation of a nuclear facility.

For more information, please contact:

Cree, Inc.
4600 Silicon Drive
Durham, North Carolina, USA 27703
www.cree.com/wireless

Sarah Miller
Marketing & Export
Cree, RF Components
1.919.407.5302

Ryan Baker
Marketing
Cree, RF Components
1.919.407.7816

Tom Dekker
Sales Director
Cree, RF Components
1.919.407.5639

Cree, Inc.
4600 Silicon Drive
Durham, North Carolina, USA 27703
USA Tel: +1.919.313.5300
Fax: +1.919.869.2733
www.cree.com/wireless

APPENDIX B

ADL5602 DATASHEET

ANALOG DEVICES

50 MHz to 4.0 GHz RF/IF Gain Block

Data Sheet

ADL5602

FEATURES

Fixed gain of 20 dB
Operation from 50 MHz to 4.0 GHz
Highest dynamic range gain block
Input/output internally matched to 50 Ω
Integrated bias control circuit
OIP3 of 42.0 dBm at 2.0 GHz
P1dB of 19.3 dBm at 2.0 GHz
Noise figure of 3.3 dB at 2.0 GHz
Single 5 V power supply
Low quiescent current of 89 mA
Thermally efficient SOT-89 package
ESD rating of ±1.5 kV (Class 1C)

FUNCTIONAL BLOCK DIAGRAM

Figure 1.

GENERAL DESCRIPTION

The ADL5602 is a broadband 20 dB linear amplifier that operates at frequencies up to 4 GHz. The device can be used in a wide variety of cellular, CATV, military, and instrumentation equipment.

The ADL5602 provides the highest dynamic range available from an internally matched gain block. This is accomplished by providing extremely low noise figures and very high OIP3 specifications simultaneously, across the entire 4 GHz frequency range.

The ADL5602 provides a gain of 20 dB, which is stable over frequency, temperature, power supply, and from device to device. The device is internally matched to 50 Ω at the input and output, making the ADL5602 very easy to implement in a wide variety of applications. Only input/output ac coupling capacitors, power supply decoupling capacitors, and an external inductor are required for operation.

The ADL5602 is fabricated on an InGaP HBT process and has an ESD rating of ±1.5 kV (Class 1C). The device is available in a thermally efficient SOT-89 package.

The ADL5602 consumes 89 mA on a single 5 V supply and is fully specified for operation from –40°C to +85°C.

A fully populated RoHS-compliant evaluation board is available.

106

TABLE OF CONTENTS

REVISION HISTORY

11/13—Rev. 0 to Rev. A

6/09—Revision 0: Initial Version

SPECIFICATIONS

$V_{CC} = 5$ V and $T_A = 25°C$, unless otherwise noted.

Table 1.

Parameter	Conditions	Min	Typ	Max	Unit
OVERALL FUNCTION					
Frequency Range		50		4000	MHz
FREQUENCY = 50 MHz					
Gain			18.3		dB
Output 1 dB Compression Point (P1dB)			18.0		dBm
Output Third-Order Intercept (OIP3)	Δf = 1 MHz, output power (P_OUT) = 0 dBm per tone		27.5		dBm
Second Harmonic	P_OUT = 0 dBm		−40.5		dBc
Third Harmonic	P_OUT = 0 dBm		−46.1		dBc
Noise Figure			2.9		dB
FREQUENCY = 140 MHz					
Gain			17.0		dB
vs. Frequency	±50 MHz		±1.2		dB
vs. Temperature	−40°C ≤ T_A ≤ +85°C		±0.03		dB
vs. Supply Voltage	4.75 V to 5.25 V		±0.04		dB
Output 1 dB Compression Point (P1dB)			18.3		dBm
Output Third-Order Intercept (OIP3)	Δf = 1 MHz, output power (P_OUT) = 0 dBm per tone		25.0		dBm
Second Harmonic	P_OUT = 0 dBm		−45.1		dBc
Third Harmonic	P_OUT = 0 dBm		−55.1		dBc
Noise Figure			2.9		dB
FREQUENCY = 350 MHz					
Gain			19.7		dB
vs. Frequency	±50 MHz		±0.20		dB
vs. Temperature	−40°C ≤ T_A ≤ +85°C		±0.31		dB
vs. Supply Voltage	4.75 V to 5.25 V		±0.01		dB
Output 1 dB Compression Point (P1dB)			20.0		dBm
Output Third-Order Intercept (OIP3)	Δf = 1 MHz, output power (P_OUT) = 0 dBm per tone		36.5		dBm
Second Harmonic	P_OUT = 0 dBm		−49.9		dBc
Third Harmonic	P_OUT = 0 dBm		−83.7		dBc
Noise Figure			3.0		dB
FREQUENCY = 700 MHz					
Gain		19.0	20.2	21.0	dB
vs. Frequency	±50 MHz		±0.01		dB
vs. Temperature	−40°C ≤ T_A ≤ +85°C		±0.28		dB
vs. Supply Voltage	4.75 V to 5.25 V		±0.01		dB
Output 1 dB Compression Point (P1dB)		19.0	20.1		dBm
Output Third-Order Intercept (OIP3)	Δf = 1 MHz, output power (P_OUT) = 0 dBm per tone		38.5		dBm
Second Harmonic	P_OUT = 0 dBm		−50.3		dBc
Third Harmonic	P_OUT = 0 dBm		−78.4		dBc
Noise Figure			3.0		dB

Parameter	Conditions	Min	Typ	Max	Unit
FREQUENCY = 900 MHz					
Gain		19.0	20.2	21.0	dB
vs. Frequency	±50 MHz		±0.01		dB
vs. Temperature	−40°C ≤ T_A ≤ +85°C		±0.28		dB
vs. Supply Voltage	4.75 V to 5.25 V		±0.01		dB
Output 1 dB Compression Point (P1dB)		19.0	20.1		dBm
Output Third-Order Intercept (OIP3)	Δf = 1 MHz, output power (P_{OUT}) = 0 dBm per tone		40.0		dBm
Second Harmonic	P_{OUT} = 0 dBm		−59.4		dBc
Third Harmonic	P_{OUT} = 0 dBm		−77.3		dBc
Noise Figure			2.9		dB
FREQUENCY = 2000 MHz					
Gain			19.5		dB
vs. Frequency	±50 MHz		±0.04		dB
vs. Temperature	−40°C ≤ T_A ≤ +85°C		±0.35		dB
vs. Supply Voltage	4.75 V to 5.25 V		±0.04		dB
Output 1 dB Compression Point (P1dB)			19.3		dBm
Output Third-Order Intercept (OIP3)	Δf = 1 MHz, output power (P_{OUT}) = 0 dBm per tone		42.0		dBm
Second Harmonic	P_{OUT} = 0 dBm		−53.1		dBc
Third Harmonic	P_{OUT} = 0 dBm		−60.7		dBc
Noise Figure			3.3		dB
FREQUENCY = 2600 MHz					
Gain			19.2		dB
vs. Frequency	±50 MHz		±0.01		dB
vs. Temperature	−40°C ≤ T_A ≤ +85°C		±0.28		dB
vs. Supply Voltage	4.75 V to 5.25 V		±0.05		dB
Output 1 dB Compression Point (P1dB)			18.7		dBm
Output Third-Order Intercept (OIP3)	Δf = 1 MHz, output power (P_{OUT}) = 0 dBm per tone		36.5		dBm
Second Harmonic	P_{OUT} = 0 dBm		−52.8		dBc
Third Harmonic	P_{OUT} = 0 dBm		−67.4		dBc
Noise Figure			3.4		dB
FREQUENCY = 3500 MHz					
Gain			19.3		dB
vs. Frequency	±50 MHz		±0.03		dB
vs. Temperature	−40°C ≤ T_A ≤ +85°C		±0.37		dB
vs. Supply Voltage	4.75 V to 5.25 V		±0.07		dB
Output 1 dB Compression Point (P1dB)			17.4		dBm
Output Third-Order Intercept (OIP3)	Δf = 1 MHz, output power (P_{OUT}) = 0 dBm per tone		31.5		dBm
Second Harmonic	P_{OUT} = 0 dBm		−42.9		dBc
Third Harmonic	P_{OUT} = 0 dBm		−66.4		dBc
Noise Figure			3.8		dB
FREQUENCY = 4000 MHz					
Gain			18.5		dB
vs. Frequency	±50 MHz		±0.19		dB
vs. Temperature	−40°C ≤ T_A ≤ +85°C		±0.73		dB
vs. Supply Voltage	4.75 V to 5.25 V		±0.08		dB
Output 1 dB Compression Point (P1dB)			15.2		dBm
Output Third-Order Intercept (OIP3)	Δf = 1 MHz, output power (P_{OUT}) = 0 dBm per tone		28.0		dBm
Second Harmonic	P_{OUT} = 0 dBm		−44.1		dBc
Third Harmonic	P_{OUT} = 0 dBm		−64.0		dBc
Noise Figure			4.2		dB

Parameter	Conditions	Min	Typ	Max	Unit
POWER INTERFACE	VCC				
Supply Voltage (V$_{CC}$)		4.5	5	5.5	V
Supply Current			89	106	mA
vs. Temperature	−40°C ≤ T$_A$ ≤ +85°C		±3		mA
Power Dissipation	V$_{CC}$ = 5 V		0.45		W

TYPICAL SCATTERING PARAMETERS (S PARAMETERS)

V$_{CC}$ = 5 V and T$_A$ = 25°C, the effects of the test fixture have been de-embedded up to the pins of the device.

Table 2.

Frequency (MHz)	S11		S21		S12		S22	
	Magnitude (dB)	Angle (°)	Magnitude (dB)	Angle (°)	Magnitude (dB)	Angle (°)	Magnitude (dB)	Angle (°)
50	−12.75	+32.81	18.14	+163.00	−25.27	−9.54	−8.96	−145.86
100	−8.98	−7.00	15.77	−179.92	−27.59	+4.56	−7.07	−178.96
150	−10.11	−34.04	17.27	−169.01	−26.11	+16.05	−7.89	+159.89
200	−11.97	−50.46	18.50	−168.73	−24.84	+16.55	−9.33	+147.22
250	−13.85	−62.42	19.21	−171.01	−24.14	+14.79	−10.87	+140.02
300	−15.69	−72.90	19.64	−173.77	−23.70	+12.89	−12.23	+136.16
350	−17.40	−81.30	19.90	−176.45	−23.43	+11.02	−13.56	+134.03
400	−19.17	−88.48	20.07	−178.86	−23.26	+9.65	−14.79	+132.79
450	−20.86	−97.45	20.18	+178.79	−23.14	+8.07	−15.99	+132.72
500	−22.52	−107.32	20.25	+176.86	−23.08	+7.11	−17.02	+133.33
550	−24.32	−112.89	20.32	+174.84	−23.00	+6.15	−18.21	+133.04
600	−26.07	−120.03	20.35	+173.09	−22.97	+5.24	−19.45	+135.06
650	−27.89	−128.79	20.39	+171.35	−22.93	+4.35	−20.73	+136.29
700	−30.79	−133.19	20.42	+169.67	−22.91	+3.72	−22.22	+136.96
750	−34.53	−136.03	20.42	+167.93	−22.91	+2.93	−23.91	+135.39
800	−42.59	−130.76	20.46	+166.48	−22.88	+2.30	−26.35	+136.07
850	−46.49	−2.93	20.47	+164.85	−22.88	+1.67	−29.40	+132.08
900	−34.26	+15.99	20.47	+163.17	−22.86	+0.98	−34.27	+116.48
950	−29.55	+9.83	20.48	+161.77	−22.86	+0.39	−40.86	+41.72
1000	−25.87	+5.52	20.48	+160.25	−22.86	−0.21	−31.44	−10.36
1050	−23.03	+1.85	20.47	+158.65	−22.89	−0.84	−26.19	−18.99
1100	−21.25	+0.10	20.45	+157.18	−22.90	−1.43	−23.27	−22.34
1150	−19.31	−1.89	20.45	+155.50	−22.92	−2.06	−20.70	−22.26
1200	−17.72	−4.09	20.40	+153.93	−22.96	−2.72	−18.67	−24.44
1250	−16.13	−6.53	20.35	+152.44	−23.04	−3.38	−16.92	−24.75
1300	−14.81	−8.71	20.31	+150.88	−23.07	−4.04	−15.44	−25.79
1350	−13.65	−10.01	20.24	+149.35	−23.16	−4.60	−14.14	−25.36
1400	−12.68	−11.33	20.18	+147.91	−23.22	−5.06	−13.12	−25.73
1450	−11.72	−12.65	20.11	+146.40	−23.32	−5.76	−12.04	−25.59
1500	−10.92	−13.56	20.04	+145.13	−23.39	−6.16	−11.20	−25.40
1550	−10.21	−14.37	19.97	+143.86	−23.49	−6.54	−10.49	−25.60
1600	−9.58	−15.37	19.88	+142.58	−23.57	−6.93	−9.77	−25.59
1650	−9.05	−15.74	19.80	+141.40	−23.69	−7.16	−9.21	−25.31
1700	−8.52	−16.73	19.72	+140.23	−23.76	−7.45	−8.66	−25.42
1750	−8.13	−17.13	19.64	+139.13	−23.87	−7.60	−8.26	−25.32
1800	−7.76	−17.59	19.57	+138.12	−23.94	−7.80	−7.91	−24.96
1850	−7.46	−17.76	19.50	+137.16	−24.05	−7.88	−7.56	−24.77
1900	−7.19	−17.92	19.43	+136.25	−24.13	−7.91	−7.35	−24.46
1950	−6.98	−17.84	19.39	+135.31	−24.18	−7.94	−7.13	−23.92

Frequency (MHz)	S11		S21		S12		S22	
	Magnitude (dB)	Angle (°)	Magnitude (dB)	Angle (°)	Magnitude (dB)	Angle (°)	Magnitude (dB)	Angle (°)
2000	−6.85	−18.00	19.35	+134.44	−24.26	−7.99	−6.96	−23.55
2050	−6.74	−17.93	19.31	+133.61	−24.29	−7.91	−6.86	−22.70
2100	−6.63	−17.57	19.29	+132.74	−24.37	−7.81	−6.75	−22.45
2150	−6.66	−17.34	19.25	+132.06	−24.42	−7.58	−6.76	−22.01
2200	−6.65	−17.26	19.29	+131.19	−24.40	−7.63	−6.78	−21.42
2250	−6.69	−17.10	19.30	+130.47	−24.41	−7.59	−6.82	−20.82
2300	−6.77	−16.90	19.33	+129.54	−24.42	−7.40	−6.87	−20.25
2350	−6.87	−16.65	19.36	+128.72	−24.40	−7.46	−7.04	−19.57
2400	−7.05	−16.25	19.42	+127.81	−24.38	−7.50	−7.20	−18.85
2450	−7.22	−16.11	19.49	+126.89	−24.35	−7.46	−7.42	−18.17
2500	−7.45	−16.00	19.53	+125.82	−24.31	−7.75	−7.66	−17.76
2550	−7.64	−15.84	19.58	+124.74	−24.31	−7.86	−7.91	−17.18
2600	−7.95	−15.66	19.66	+123.61	−24.25	−8.20	−8.29	−16.64
2650	−8.29	−15.64	19.74	+122.46	−24.19	−8.54	−8.66	−16.15
2700	−8.62	−15.95	19.81	+121.20	−24.17	−8.90	−8.97	−15.97
2750	−8.95	−15.92	19.89	+119.91	−24.13	−9.35	−9.41	−15.67
2800	−9.31	−16.23	19.94	+118.47	−24.08	−9.95	−9.87	−15.96
2850	−9.67	−16.74	20.03	+117.02	−24.05	−10.55	−10.34	−16.17
2900	−9.99	−17.33	20.07	+115.47	−24.07	−11.17	−10.83	−16.68
2950	−10.28	−18.00	20.14	+113.95	−24.02	−11.71	−11.28	−17.66
3000	−10.53	−19.16	20.18	+112.28	−24.03	−12.51	−11.69	−19.15
3050	−10.69	−20.29	20.21	+110.53	−24.10	−13.72	−12.17	−21.42
3100	−10.86	−21.94	20.25	+108.77	−24.04	−14.66	−12.54	−24.24
3150	−10.91	−23.61	20.27	+107.15	−24.09	−15.23	−12.83	−27.07
3200	−10.70	−25.42	20.28	+105.16	−24.18	−16.23	−12.92	−32.00
3250	−10.57	−27.33	20.28	+103.09	−24.17	−17.39	−13.04	−36.71
3300	−10.38	−29.60	20.26	+101.20	−24.22	−18.24	−12.99	−42.66
3350	−9.92	−31.76	20.21	+99.05	−24.39	−20.06	−12.57	−48.16
3400	−9.48	−34.25	20.15	+96.98	−24.49	−20.74	−12.19	−54.36
3450	−8.98	−36.47	20.08	+94.93	−24.61	−21.69	−11.64	−59.44
3500	−8.44	−38.18	20.00	+92.80	−24.72	−23.44	−11.00	−64.07
3550	−7.92	−40.32	19.90	+90.88	−24.88	−24.35	−10.34	−68.43
3600	−7.34	−42.20	19.74	+88.69	−25.15	−25.31	−9.59	−72.77
3650	−6.79	−43.72	19.57	+86.66	−25.35	−26.95	−8.90	−76.09
3700	−6.29	−45.15	19.41	+84.80	−25.56	−27.76	−8.29	−79.17
3750	−5.82	−46.51	19.23	+82.83	−25.90	−28.90	−7.69	−81.76
3800	−5.37	−47.51	19.00	+81.05	−26.16	−29.05	−7.12	−84.30
3850	−4.93	−48.36	18.78	+79.53	−26.46	−30.35	−6.65	−86.42
3900	−4.56	−48.94	18.55	+78.02	−26.81	−29.93	−6.20	−88.14
3950	−4.23	−49.33	18.32	+76.71	−27.08	−31.04	−5.83	−89.69
4000	−3.97	−49.71	18.08	+75.39	−27.50	−30.65	−5.50	−91.14

ABSOLUTE MAXIMUM RATINGS

Table 3.

Parameter	Rating
Supply Voltage, V_{CC}	6.5 V
Input Power (re: 50 Ω)	16 dBm
Internal Power Dissipation (Paddle Soldered)	600 mW
θ_{JA} (Junction to Air)	30.7°C/W
θ_{JC} (Junction to Paddle)	5.0°C/W
Maximum Junction Temperature	150°C
Lead Temperature (Soldering, 60 sec)	240°C
Operating Temperature Range	−40°C to +85°C
Storage Temperature Range	−65°C to +150°C

Stresses above those listed under Absolute Maximum Ratings may cause permanent damage to the device. This is a stress rating only; functional operation of the device at these or any other conditions above those indicated in the operational section of this specification is not implied. Exposure to absolute maximum rating conditions for extended periods may affect device reliability.

ESD CAUTION

ESD (electrostatic discharge) sensitive device. Charged devices and circuit boards can discharge without detection. Although this product features patented or proprietary protection circuitry, damage may occur on devices subjected to high energy ESD. Therefore, proper ESD precautions should be taken to avoid performance degradation or loss of functionality.
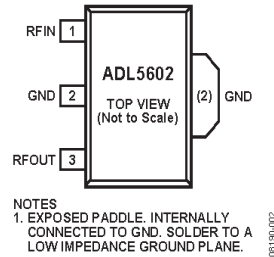
PIN CONFIGURATION AND FUNCTION DESCRIPTIONS

Figure 2. Pin Configuration

Table 4. Pin Function Descriptions

Pin No.	Mnemonic	Description
1	RFIN	RF Input. This pin requires a dc blocking capacitor.
2	GND	Ground. Connect this pin to a low impedance ground plane.
3	RFOUT	RF Output and Supply Voltage. DC bias is provided to this pin through an inductor that is connected to the external power supply. The RF path requires a dc blocking capacitor.
(2)	Exposed Paddle	Exposed Paddle. Internally connected to GND. Solder to a low impedance ground plane.

113

TYPICAL PERFORMANCE CHARACTERISTICS
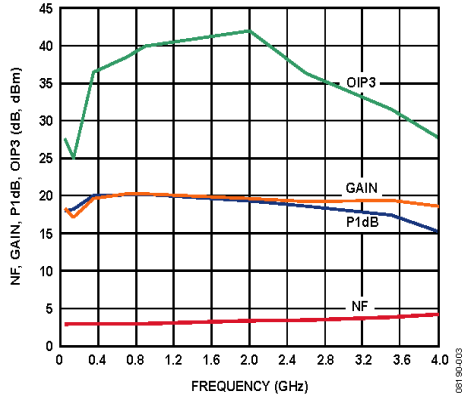
Figure 3. Noise Figure, Gain, P1dB, and OIP3 vs. Frequency
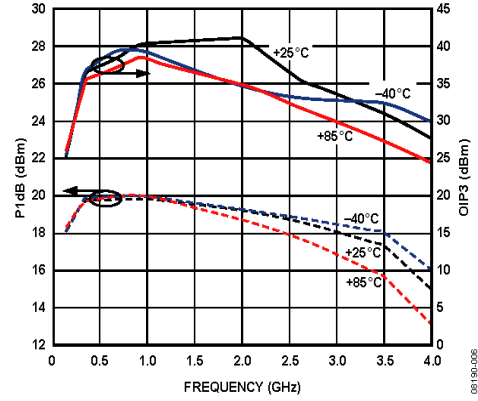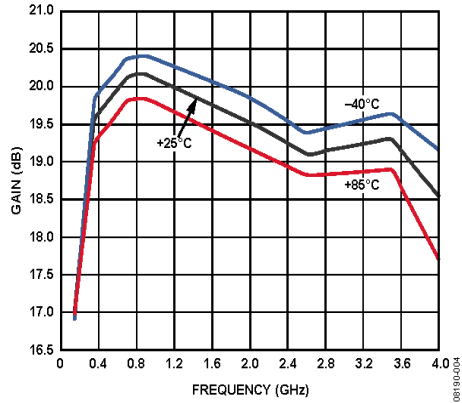

Figure 6. P1dB and OIP3 vs. Frequency and Temperature
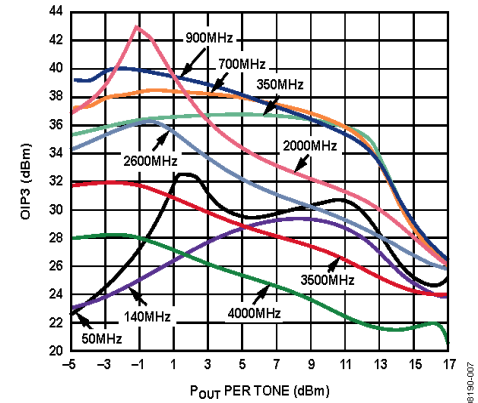

Figure 4. Gain vs. Frequency and Temperature

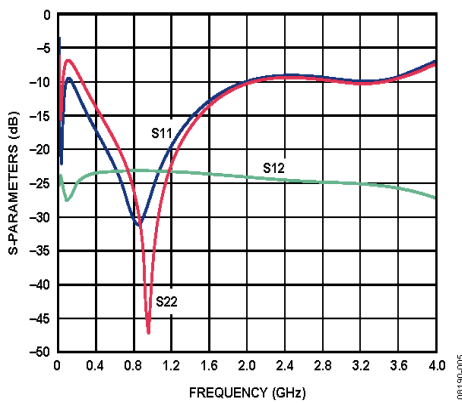*Figure 7. OIP3 vs. Output Power (P_{OUT}) and Frequency*

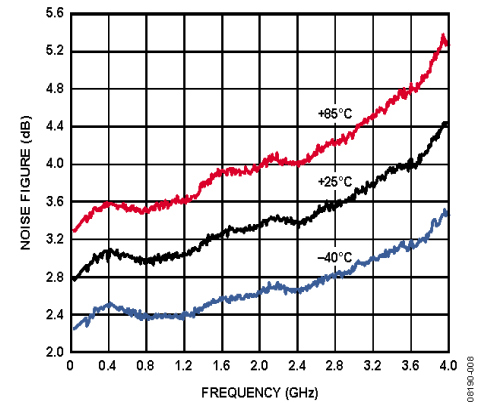*Figure 5. Input Return Loss (S11), Output Return Loss (S22), and Reverse Isolation (S12) vs. Frequency*
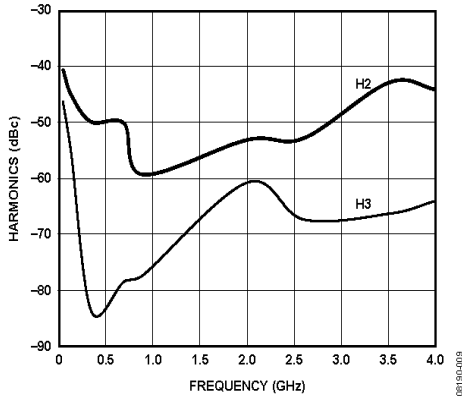

Figure 8. Noise Figure vs. Frequency and Temperature

114

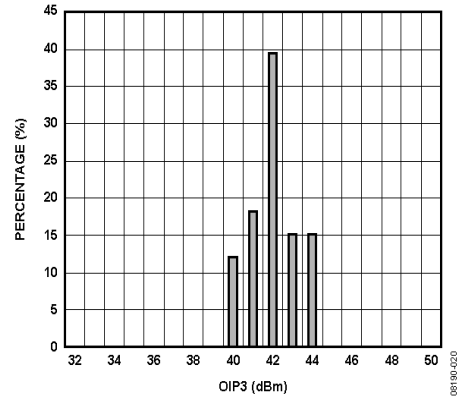Figure 9. Single Tone Harmonics vs. Frequency, $P_{OUT} = 0$ dBm

Figure 12. OIP3 Distribution at 2000 MHz, $P_{OUT} = 0$ dBm
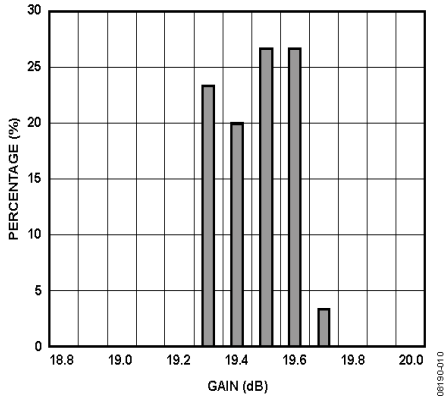

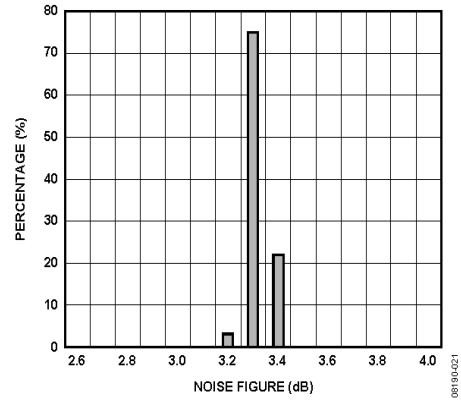Figure 10. Gain Distribution at 2000 MHz
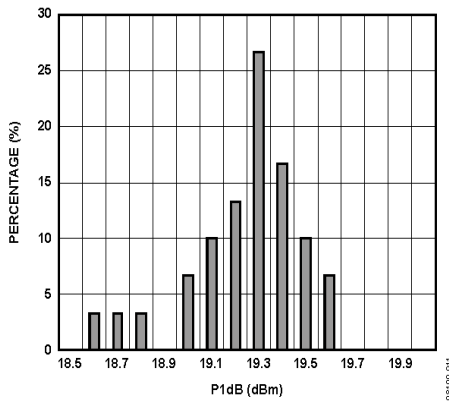

Figure 13. Noise Figure Distribution at 2000 MHz
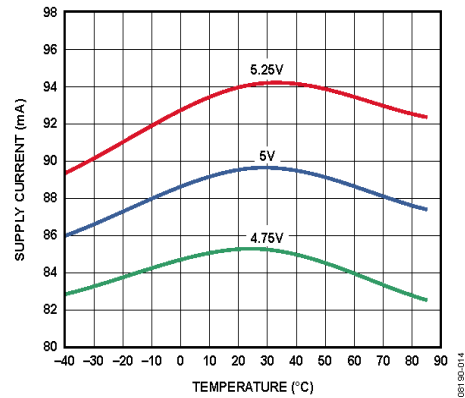

Figure 11. P1dB Distribution at 2000 MHz

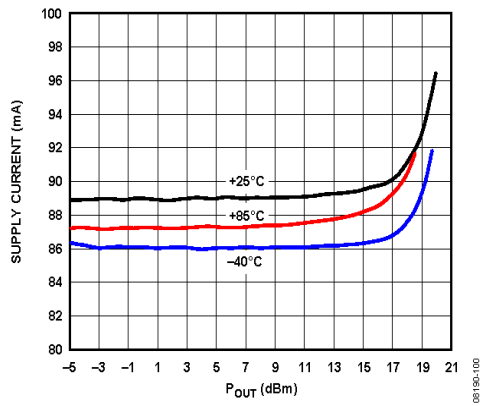Figure 14. Supply Current vs. Temperature

115

Figure 15. Supply Current vs. P_OUT and Temperature V_CC = 5 V

BASIC CONNECTIONS

The basic connections for operating the ADL5602 are shown in Figure 16. Recommended components are listed in Table 5. The input and output should be ac-coupled with appropriately sized capacitors (device characterization was performed with 0.1 μF capacitors). A 5 V dc bias is supplied to the amplifier through the bias inductor connected to RFOUT (Pin 3). The bias voltage should be decoupled using a 1 μF capacitor, a 1.2 nF capacitor, and a 68 pF capacitor.
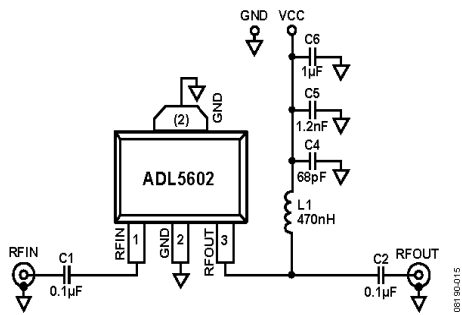
Figure 16. Basic Connections

SOLDERING INFORMATION AND RECOMMENDED PCB LAND PATTERN

Figure 17 shows the recommended land pattern for the ADL5602. To minimize thermal impedance, the exposed paddle on the package underside should be soldered down to a ground plane along with Pin 2. If multiple ground layers exist, they should be stitched together using vias. For more information on land pattern design and layout, refer to the AN-772 Application Note, *A Design and Manufacturing Guide for the Lead Frame Chip Scale Package (LFCSP)*.

Figure 17. Recommended Land Pattern

Table 5. Recommended Components for Basic Connections

Frequency (MHz)	C1	C2	L1	C4	C5	C6
50 to 4000	0.1 μF	0.1 μF	470 nH (Coilcraft 0603LS-NX or equivalent)	68 pF	1.2 nF	1 μF

117

W-CDMA ACPR PERFORMANCE

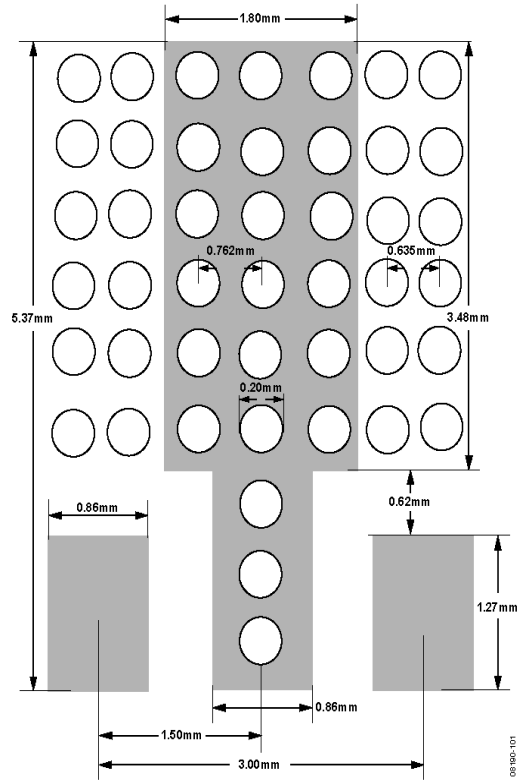Figure 18 shows a plot of adjacent channel power ratio (ACPR) vs. P_OUT for the ADL5602. The signal type being used is a single W-CDMA carrier (Test Model 1-64) at 2140 MHz. This signal is generated by a very low ACPR source. ACPR is measured at the output by a high dynamic range spectrum analyzer, which incorporates an instrument noise correction function.

The ADL5602 achieves an ACPR of −75 dBc at −5 dBm output, at which point device noise and not distortion is beginning to dominate the power in the adjacent channels. At an output power of +5 dBm, ACPR is still very low at −61 dBc, making the device particularly suitable for PA driver applications.
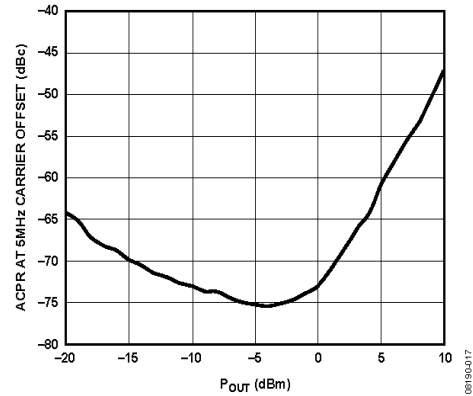
Figure 18. ACPR vs. P_OUT, Single Carrier W-CDMA (Test Model 1-64) at 2140 MHz Evaluation Board

EVALUATION BOARD

Figure 20 shows the schematic for the ADL5602 evaluation board. The board is powered by a single 5 V supply.

The components used on the board are listed in Table 6. Power can be applied to the board through clip-on leads (VCC and GND).
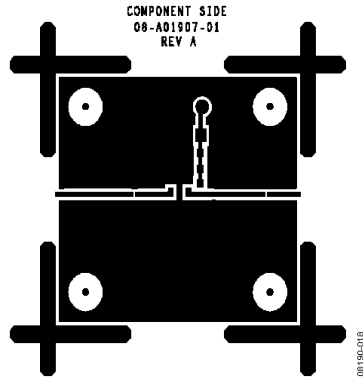
Figure 19. Evaluation Board Layout (Top)
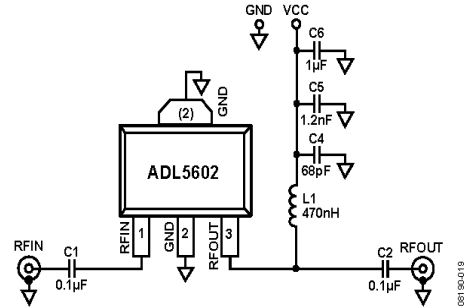
Figure 20. Evaluation Board Schematic

Table 6. Evaluation Board Configuration Options

Component	Description	Default Value
C1, C2	AC-coupling capacitors	0.1 µF, 0402
L1	DC bias inductor	470 nH, 0603 (Coilcraft 0603LS-NX or equivalent)
VCC and GND	Clip-on terminals for power supply	
C4, C5, C6	Power supply decoupling capacitors	C4 = 68 pF, 0603; C5 = 1.2 nF, 0603; C6 = 1 µF, 1206

119

OUTLINE DIMENSIONS
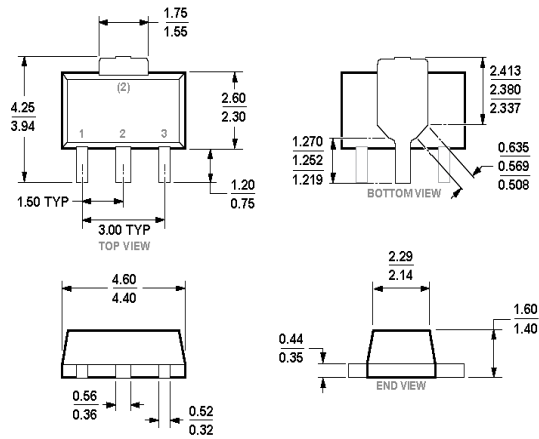
COMPLIANT TO JEDEC STANDARDS TO-243

Figure 21. 3-Lead Small Outline Transistor Package [SOT-89]
(RK-3)
Dimensions shown in millimeters

ORDERING GUIDE

Model[1]	Temperature Range	Package Description	Package Option
ADL5602ARKZ-R7	−40°C to +85°C	3-Lead SOT-89, 7" Tape and Reel	RK-3
ADL5602-EVALZ		Evaluation Board	

[1] Z = RoHS Compliant Part.

120

NOTES

**ANALOG
DEVICES**

www.analog.com

BIBLIOGRAPHY

[1] NTIA, "U.S. Frequency Allocation Chart," tech. rep., http://www.ntia.doc.gov/osmhome/allochrt.pdf, 2003.

[2] J. Mitola, "Cognitive Radio: An Integrated Agent Architecture for Software Defined Radio," *Phd thesis*, Royal Institute of Technology (KTH), Stockholm, Sweden, 2000.

[3] J. Mitola, "The Software Radio Architecture," *IEEE Communications Magazine*, vol. 33, no. 5, pp. 26-38, May 1995.

[4] J. Mitola, "Cognitive Radio: Making Software Radios more Personal," *IEEE Personal Communications*, vol. 6, no. 4, pp. 13-18, August 1999.

[5] I.F. Akyildiz, W.-Y. Lee, M. C. Vuran, and S. Mohanty, "Survey on Spectrum Management in Cognitive Radio Networks," *IEEE Communications Magazine*, 2008.

[6] COGEU D2.1 ICT-248560, "European TV White Spaces Analysis and COGEU Usecases," March 2010.

[7] M. Nekovee, "A Survey of Cognitive Radio Access to TV White Spaces," *International Journal of Digital Multimedia Broadcasting*, Vol. 2010, Article ID 236568, pp. 1-11, April 2010.

[8] P. Bahl, R. Chandra, T. Moscibroda, R. Murty, and M. Welsh, "White Space Networking with Wi-Fi like Connectivity," *Proceedings of the ACM SIGCOMM 2009 Conference on Data Communication*, pp. 27-38, Barcelona, 17-21 August 2009.

[9] N. Zurutuza, "Cognitive Radio and TV White Space Communications," *Norwegian University of Science and Technology*.

[10] "RF Transceiver Architecture for. Cognitive Radio User Equipment," End to End Reconfigurability II (E2R II).

[11] A. Ramadan, "Filter-Antennas and RF Front-End Sensing Receiver for Cognitive Radio Applications," *PhD Dissertation*, American University of Beirut, January 2014.

[12] P.S. Hall, P. Gardner, J. Kelly, E. Ebrahimi, M.R. Hamid, F. Ghanem, F.J. Herraiz-Martínez, and D. Segovia-Vargas, "Reconfigurable Antenna Challenges for Future Radio Systems," *European Conference on Antennas and Propagation (EuCAP)*, pp. 949-955, Berlin, 23-27 March 2009.

[13] K.M.M.W.N.B. Narampanawe, C. Divarathne, J. V. Wijayakulasooriya, J. Kumara, "Ultra Wideband (UWB) Antenna Design for Cognitive Radios in the UHF TV Band," *6th International Conference on Industrial and Information Systems (ICIIS)*, pp. 27-31, Sri Lanka, 16-19 August 2011.

[14] C. –Y. Tsai and O. T.-C. Chen, "Compact Broadband Monopole Slot Antenna for Digital TV Applications," *IEEE Asia-Pacific Conference on Antennas and Propagation (APCAP)*, pp. 61-62, Singapore, 27-29 August 2012.

[15] C.-Y. Pan, J.-H. Duan, and J.-Y. Jan, "Coplanar Printed Monopole Antenna Using Coaxial Feedline for DTV Application," *Progress In Electromagnetics Research Letters,* Vol. 34, pp. 21-29, 2012.

[16] D.-B. Lin, S.-T. Wu, and C.-H. Tseng, "Compact Folded Dipole Antenna for DTV Signal Reception," *Progress In Electromagnetics Research Symposium Proceedings 2008*, pp. 229-232, Cambridge, USA, July 2-6, 2008.

[17] C.-Y. Huang, B.-M. Jeng, and C.-F. Yang, "Wideband Monopole Antenna for DVB-T Applications," *Electronic Letters*, Vol. 44, No. 25, pp. 1448-1450, 2008.

[18] C.-Y. Huang, B.-M. Jeng, and. J.-S Kuo, "Grating Monopole Antenna for DVB-T Applications," *IEEE Transaction on Antennas and Propagation*, Vol. 56, No. 6, pp. 1775-1776, June 2008.

[19] M. Berg, M. Komulainen, V. Palukuru, H. Jantunen, and E. Salonen, "Frequency-Tunable DVB-H Antenna for Mobile Terminals," In *Antennas and Propagation Society International Symposium,* pp. 1072-1075, Honolulu, June 2007.

[20] F. Canneva, J. M. Ribero, , and R, Staraj, "Reconfigurable Meander Antenna for DVB-H Band," In *Antenna Technology (iWAT), 2010 International Workshop,* pp. 1-4. Lisbon, March 2010.

[21] A. Roy, "A Miniature Tunable Antenna for Digital TV Reception," In *IEEE International Symposium on Consumer Electronics (ISCE 2010)*, pp. 1-6, Braunschweig, June 2010.

[22] L. Liu, J. Rigelsford, and R. Langley, "Tunable Multiband Handset Antenna Operating at VHF and UHF Bands," *IEEE Transactions on Antennas and Propagation,* vol. 61, no. 7, pp. 3790-3796, March 2013.

[23] A. Mohammadi and F. M. Ghannouchi, "RF Transceiver Design for MIMO Wireless Communications," *Springer*, 2012.

[24] P.M. Lavradore, T.R. Cunha, P.M. Cabral, and J.C. Pedro, "The Linearity-Efficiency Compromise," *IEEE Microwave Magazine*, vol. 11, no. 5, pp. 44–58, Aug. 2010.

[25] D. Schreurs, M. O'droma, A.A. Goacher, and M. Gadringer, "RF Power Amplifier Behavioral Modeling," *Cambridge University Press*, 2009.

[26] P. Colantonio, F. Giannini, E. Limiti, "High efficiency RF and microwave solid state power amplifier," John Wiley & Sons, Ltd, 2009.

[27] B. Slade, "The Basics of the Doherty Amplifier," *Orban Microwave products*,

[28] W. H. Doherty, "A New High Efficiency Power Amplifier for Modulated Waves," *The Bell System Technical Journal,* vol. 15, no. 3, pp. 469-475, July 1936.

[29] J. J. Xu, W. Yi-Feng, S. Keller, S. Heikman, B. J. Thibeault, U. K. Mishra, and R. A. York, "1-8-GHz GaN-based Power Amplifier Using Flip-chip Bonding," *IEEE Microwave and Wireless Components Letters*, vol. 9, no. 8, pp. 277–279, 1999.

[30] M.J. Schindler, J.P. Wendler, M.P. Zaitlin, M.E. Miller, and J.R. Dormail, "A K/Ka-band Distributed Power Amplifier With Capacitive Drain Coupling," *IEEE Transactions on Microwave Theory and Techniques*, vol. 36, no. 12, pp. 1902–1907, 1988.

[31] M. Hirata, T. Oka, M. Hasegawa, Y. Amano, Y. Ishimaru, H. Kawamura, and K. Sakuno, "Fully-integrated GaAs HBT power amplifier MMIC with high linear output power for 3 GHz-band broadband wireless applications," *Electronic Letters*, vol. 42, no. 22, pp. 1286–1287, 2006.

[32] A. Vasylyev, P. Weger, and W. Simburger, "Ultra-broadband 20.5-31 GHz Monolithically Integrated CMOS Power Amplifier," *Electronic Lett*ers, vol. 41, no. 23, pp. 1281–1282, 2005.

[33] L. Jong-Wook, L.F. Eastman, and K.J. Webb, "A Gallium-Nitride Push Pull Microwave Power Amplifier," *IEEE Transactions on Microwave Theory and Techniques*, vol. 51, no. 11, pp. 2243–2249, 2003.

[34] L. Jong-Wook and K. J. Webb, "Broadband GaN HEMT Push-Pull Microwave Power Amplifier," *IEEE Microwave and Wireless Components Letters*, vol. 11, no. 9, pp. 367–369, 2001.

[35] A. Sayed and G. Boeck, "Two-Stage Ultra wideband 5-W Power Amplifier Using SiC MESFET," *IEEE Transactions on Microwave Theory and Techniques*, vol. 53, no. 7, pp. 2441–2449, 2005.

[36] K. Fujii and H. Morkner, "1 W Power Amplifier MMICs for Mm-Wave Applications," *IEEE MTT-S International Microwave Symposium Digest*, vol. 3, pp. 1665– 1668, 2004.

[37] Z. Haitao, G. Huai, and L. Guann-Pyng, "A Novel Tunable Broadband Power Amplifier Module Operating from 0.8 GHz to 2.0 GHz," *IEEE MTT-S International Microwave Symposium Digest*, pp. 661–664, 2005.

[38]   P.-C. Huang, Z.-M. Tsai, K.-Y. Lin and H. Wang, "A High-Efficiency, Broadband CMOS Power Amplifier for Cognitive Radio Applications," *IEEE Transactions on Microwave Theory and Techniques*, vol. 58, no. 12, pp. 3556–3565, 2010.

[39]   Y.-J.E. Chen, Y. Li-Yuan, and Y. Wei-Chin, "An Integrated Wideband Power Amplifier for Cognitive Radio," *IEEE Transactions on Microwave Theory and Techniques*, vol. 55, no. 10, pp. 2053-2058, October 2007.

[40]   M. Majidi, A. Mohammadi, and A. Abdipour, "Analysis of the Power Amplifier Nonlinearity on the Power Allocation in Cognitive Radio Networks," *IEEE Transactions on Communications*, vol. 62, no. 2, pp. 467-477, January 2014.

[41]   W. Demenitroux, L. Mandica, C. Richardeau, B. Gerfault, N. Berthou, and P. Grandgeorge, "Wideband High Power High Efficiency Linear GaN Power Amplifier for Cognitive Radio Application," In *2014 9th* European Microwave Integrated Circuit Conference (EuMIC), pp. 620-623, Rome, October 2014.

[42]   P. Suebsombut, O. Koch, and S. Chalermwisutkul, "Development of a GaN HEMT Class-AB Power Amplifier for an Envelope Tracking System at 2.45 GHz," In *2010 International Conference on Electrical Engineering/Electronics Computer Telecommunications and Information Technology (ECTI-CON)*, pp. 561-565, Chaing Mai, May 2010.

[43]   Advanced   Design   System   (ADS),   http://www.keysight.com/en/pc-1297113/advanced-design-system-ads?cc=LB&lc=eng

[44] B. Kim, D. Derickson, and C. Sun, "A High Power, High Efficiency Amplifier Using GaN HEMT," In *Asia-Pacific Microwave Conference, 2007 (APMC 2007),* pp. 1-4, 2007.

[45] L. H. Duc, D. B. Gia, "Study, Design, and Fabrication of Power Amplifier Module to be Used for Low-Attitude Radar System Operating at UHF Band (820MHz–900MHz)," In *2012 International Conference on Advanced Technologies for Communications (ATC),* pp. 231-236, Hanoi, October 2012.

[46] J. Zhou, K. Morris, G. Watkins, and K. Yamaguchi, "Wideband Class-E Power Amplifier Covering the Whole UHF Broadcast Band," In *2013 European Microwave Integrated Circuits Conference (EuMIC)*, pp. 336 - 339, Nuremberg, October 2013.

[47] M. Duman, and H. B. Yagci, "UHF Power Amplifier Design for Small Satellites," In *2013 21st Signal Processing and Communications Applications Conference (SIU),* pp. 1-4, Haspolat, April 2013.

[48] K. Bathich, A. Z. Markos, and G. Boeck, "A Wideband GaN Doherty Amplifier with 35% Fractional Bandwidth," In *2010 European Microwave Conference (EuMC),* pp. 1006-1009, Paris, September 2010.

[49] J. M. Rubio, J. Fang, R. Quaglia, V. Camarchia, M. Pirola, S. D. Guerrieri, and G. Ghione, "A 22W 65% Efficiency GaN Doherty Power Amplifier at 3.5 GHz for WiMAX Applications," In *2011 Workshop on Integrated Nonlinear Microwave and Millimetre-Wave Circuits (INMMIC),* pp. 1-4, Vienna, April 2011.

[50] P. Colantonio, F. Giannini, R. Giofrè and L. Piazzon, "Theory and Experimental Results of a Class F AB-C Doherty Power Amplifier," *IEEE Transactions on Microwave Theory and Techniques,* vol. 57, no. 8, pp. 1936-1947, July 2009.

[51] J. M. Rubio, J. Fang, V. Camarchia, R. Quaglia, M. Pirola, and G. Ghione, "3–3.6-GHz Wideband GaN Doherty Power Amplifier Exploiting Output Compensation Stages," *IEEE Transactions on Microwave Theory and Techniques,* vol. 60, no. 8, pp. 2543-2548, June 2012.

[52] S.-J. Park, K.-Y. Lee, and G.M. Rebeiz, "Low-loss 5.15–5.70-GHz RF MEMS switchable filter for wireless LAN applications," *IEEE Transactions on Microwave Theory and Techniques*, vol. 54, no. 11, pp. 3931–3939, November 2006.

[53] K. Entesari and G.M. Rebeiz, "A Differential 4-bit 6.5-10-GHz RF MEMS Tunable Filter," *IEEE Transactions on Microwave Theory and Techniques*, vol. 53, no. 3, pp. 1103–1110, March 2005.

[54] C.-C. Cheng and G.M. Rebeiz, "High-Q 4–6-GHz Suspended Stripline RF MEMS Tunable Filter with Bandwidth Control," *IEEE Transactions on Microwave Theory and Techniques*, vol. 59, no. 10, pp. 2469–2476, October 2011.

[55] G. Rebeiz, K. Entesari, I. Reines, S.-j. Park, M. El-tanani, A. Grichener, and A. Brown, "Tuning in to RF MEMS," *IEEE Microwave Magazine*, vol. 10, no. 6, pp. 55–72, October 2009.

[56] Y. Zhu, R.W. Mao, and C.S. Tsai, "A Varactor and FMR-Tuned Wideband Band-Pass Filter Module with Versatile Frequency Tunability," *IEEE Transactions on Magnetics*, vol. 47, no. 2, pp. 284–288, February 2011.

[57] M. Sanchez-Renedo, R. Gomez-Garcia, J.I. Alonso, and C. Briso-Rodriguez, "Tunable Combline Filter with Continuous Control of Center Frequency and Bandwidth," *IEEE Transactions on Microwave Theory and Techniques*, vol. 53, no. 1, pp. 191–199, January 2005.

[58] J. Nath, D. Ghosh, J.-P. Maria, A.I. Kingon,W. Fathelbab, P.D. Franzon, and M.B. Steer, "An Electronically Tunable Microstrip Bandpass Filter Using Thin-Film Barium-Strontium-Titanate (BST) Varactors," *IEEE Transactions on Microwave Theory and Techniques*, vol. 53, no. 9, pp. 2707–2712, September 2005.

[59] A. Vélez, F. Aznar, M. Durán-Sindreu, and J. Bonache, "Tunable Coplanar Waveguide Band-Stop and Band-Pass Filters Based on Open Split Ring Resonators and Open Complementary Split Ring Resonators," *IEEE Transaction on Antennas and Propagation*, Vol. 5, No. 3, pp. 277-281, February 2011.

[60] R. Bagheri, A. Mirzaei, S. Chehrazi, M. E. Heydari, M. Lee, M. Mikhemar, W. Tang, and A.A. Abidi, "An 800-MHz to 6-GHz Software-Defined Wireless Receiver in 90-nm CMOS," *IEEE Journal of Solid-State Circuits*, vol. 41, no. 12, pp. 2860–2876, November 2006.

[61] Z. Ru, N.A. Moseley, E. Klumperink, and B. Nauta, "Digitally Enhanced Software-Defined Radio Receiver Robust to Out-Of-Band Interference," *IEEE Journal of Solid-State Circuits*, vol. 44, no. 12, pp. 3359–3375, December 2009.

[62] J.A.Weldon, R.S. Narayanaswami, J.C. Rudell, L. Lin, M. Otsuka, S. Dedieu, L. Tee, K.-C. Tsai, C.-W. Lee, and P.R. Gray, "A 1.75-GHz Highly Integrated Narrow-Band CMOS Transmitter With Harmonic-Rejection Mixers," *IEEE Journal of Solid-State Circuits*, vol. 36, no. 12, pp. 2003–2015, December 2001.

[63] B. Razavi. "Cognitive Radio Design Challenges and Techniques," *IEEE Journal of Solid-State Circuits*, vol. 45, no. 8, pp. 1542–1553, August 2010.

[64] A. Acampora, A. Collado and A. Georgiadis, "Nonlinear Analysis and Optimization of a Distributed Voltage Controlled Oscillator for Cognitive Radio," *2010 IEEE International Microwave Workshop Series on RF Front-ends for Software Defined and Cognitive Radio Solutions (IMWS)*, pp. 1–4, 2010.

[65] J. Choi, K. Lim and J. Laskar, "A Ring VCO with Wide and Linear Tuning Characteristics for a Cognitive Radio System," *IEEE Radio Frequency Integrated Circuits Symposium (RFIC)*, pp. 395–398, 2008.

[66] S. Cui, B. Banerjee and V. Acharya, "A Linearized Current-Controlled Oscillator for Ultra-Low Power Wideband and Cognitive Radios," *2012 IEEE 55th International Midwest Symposium on Circuits and Systems (MWSCAS),* pp. 146–149, 2012.

[67] Ansoft HFSS, http://www.ansoft.com/products/hf/hfss

[68] "DVB-H implementation guidelines," *European Telecommunication Std.*, Rev. TR 102 377 V1.4.1, April 2009.

[69] Abdulhadi A. E. and R. Abhari, "Tunable Compact Printed Monopole Antenna for Passive UHF RFID Tags," *IEEE AP-S International Symposium on Antennas and Propagation 2012*, pp. 1-2, Chicago, 8-14 July 2012.

[70] National Instruments AWR Design Environment, http://www.awrcorp.com